BEHAVIOR OF CUMULUS TURRETS

IN ALBERTA STORMS

by

Michael William Balshaw

A Thesis submitted to the Faculty of Graduate
Studies and Research in partial fulfilment
of the requirements for the degree of
Master of Science

Department of Meteorology
McGill University
Montreal

September 1967

ACKNOWLEDGEMENTS

It is with pleasure that the author acknowledges the patient and diligent supervision of Professor R. H. Douglas. The author also expresses his appreciation to Dr. P. W. Summers of the Alberta Research Council and the staff of the Alberta Hail Studies Project at Penhold for their assistance in procuring the photographic cloud data; to Mrs. F. Blake who was most conscientious in her typing of the final drafts of the thesis; and to Mr. S. Lapczak who assisted in the drafting of the diagrams.

The author is indebted to the Director, Canadian Meteorological Service whose permission and financial support made this study possible.

ABSTRACT

A cloud stereophotogrammetry system was operated from June to September, 1966, as a part of the Alberta Hail Studies Project in central Alberta. Films taken under near optimum conditions are analysed providing data on the behavior of cumulus turrets. Two storms are described in detail with reference to the atmospheric processes influencing their turret behavior. The description includes detailed computations of vertical growth rate, horizontal velocity and radial growth for a total of nine turrets. The cloud turrets are related to initial radar echoes, and precipitation growth processes are considered. The volume growth of the turrets is used to compute updraft speeds for the turrets.

In view of the results an evaluation is made of the role of the cumulus turret as a fundamental mode of cloudy convection. The ability of various models of cloudy convection to depict cumulus turret behavior is discussed. Some suggestions are made for future studies in cumulus convection using photogrammetry and in dynamic modelling.

TABLE OF CONTENTS

TABLE OF CONTENTS

MATHEMATICAL SYMBOLS

A	area of turret base at the reference level
a	bearing of horizontal velocity
B	length of stereo camera baselines
F	frame number
H	height of turret top above ground
i	observation number
J	code number for baseline and quadrant of view
k	Priestley "interchange parameter"
M	vertical mass flux
m	cloud mass
m'	number of sampling intervals per cycle
n	time panel frame sequence number
R	range from centre site
R*	specific gas constant of air
r	radius of hemispherically-capped turret cylinder = $\frac{S}{2}$
$r_{m'}$	numerical filter response = ratio of smoothed amplitude to original amplitude
S	diameter of cloud turret top
T	temperature
t	time
U	area averaged updraft speed over a horizontal cross section
V	cloud volume above the reference level
v	horizontal speed of the turret top
w	vertical growth rate of turret top
z	height above ground (ground level taken as 0.91 km MSL)
α	angle subtended by the baseline at the cloud turret
β	angle subtended (at the camera) by the best fit semi-circle to the turret top
Γ	air parcel temperature lapse rate

Γ_E environmental temperature lapse rate

ϕ azimuth of cloud element from centre site

ρ air density

σ entrainment coefficient

θ elevation angle to cloud turret top above artificial horizon

LIST OF FIGURES

LIST OF FIGURES

LIST OF FIGURES

CHAPTER I

INTRODUCTION

Meteorology has always been confronted with the problem of obtaining observational data on which to build an understanding of nature. Scaled down laboratory experiments are not so suitable because the behavior of the atmospheric fluids is very dependent upon the scale of the motions that are taking place, and methods of extending laboratory findings to the real atmosphere are not readily available. The fields of synoptic meteorology and general circulation showed great advances during the early twentieth century as regular surface and upper air observations became available. However, mesometeorology, and the study of convective storms in particular, did not receive a truly comprehensive observational treatment until the Thunderstorm Project of 1946-7, (Byers and Braham, 1949).

This project resulted in a qualitative but detailed description of convective storms consisting of cellular growth and decay. The scale of the cells was in the order of one hour and ten km. Since then many short term, comprehensive projects (e.g. Malkus, 1954, Fujita, 1963, Simpson, 1967) have attempted to obtain complete observational data on many varieties of convective phenomena, ranging from the small trade-wind cumulus to the hurricane. At the same time, advances were being made in the quantitative measurement of precipitation by radar, and in the development of new observational techniques, including doppler radar, aircraft instrumentation, satellite observations, and photogrammetry. Concurrently, there were increases in manpower for research in this field, and also the introduction of numerical techniques in data processing and in mathematical modelling. By 1963, the models of convective cloud development had become more sophisticated than the simple cell suggested

in 1949, and it appeared that mesoscale convection consisted of a spectrum of scales of behavior. These ranged from the small cumulus "bubbles" to the steady-state hail storms.

Atlas and Byers (1963) in the comprehensive review of this field "The Severe Local Storm", emphasized the need for expanded mesometeorological programs to further elucidate the structure and mechanisms of the convective storm. The general impression was that organization of cellular behavior, probably as the result of larger scale motion patterns or topographical features, was the link between the individual convective cells to the organized convective storm. So that although quantized buoyant convection is fundamental to all atmospheric cumulus development, in the giant cumulonimbus it may appear as impulses superimposed on an apparently steady circulation.

One difficult question which requires attention is the nature of the evolution of convective phenomena through this spectrum. If there are limiting sizes for the convective cells determined by the properties of the atmospheric fluid and the disturbing mechanisms, are they large enough under certain conditions to permit the giant cumulonimbus to be a single cell? If the answer is no, this would imply that the giant storm is a continuous, steady circulation only in a statistical sense. The individual events are obscured by the overall effect of many smaller scale events organized in space and time. If the answer is yes, then larger scale continuous circulations may be real identities and models which describe a large steady state structure may be adequate. Classical theories suggest that such limits exist but has not rigidly defined the limits in terms of the atmospheric properties. Observational approaches have not been able to fully resolve the question

but do suggest that large cumulonimbi are more an organization of pulsating cells rather than one large steady circulation.

This study deals with the behavior of cumulus clouds of transitional scale, larger than an isolated cumulus of the single "bubble" variety, but smaller than the giant cumulonimbus. Generally they appear as cumulus turrets, or towers, protruding from larger regions of convective cloud. Although they often occur in larger organized groups, the individual turrets have a scale of the order of 20 min and 2 km.

The behavior of such turrets was revealed by a stereo photogrammetry system operated at the Alberta Hail Studies Project based at Canadian Forces Base Penhold in central Alberta, (Figure 1), during the summer months of 1966. The Project, which was organized in 1956, is sponsored by the Research Council of Alberta, the National Research Council, the Department of Transport (Canada), and the Department of Meteorology, McGill University. The data were analysed and interpreted during the 1966-67 term at McGill University.

At the outset the author had two broad objectives. The first was to photograph and analyse developing storms, particularly those which occurred under optimum conditions, to study the detailed behavior of the individual cloud turrets. The second was to complement these observations with other types of data available for the same turrets, their environment and the associated precipitation. It was hoped that the results could then be related to some of the current models of convective growth and behavior.

Part I of this thesis deals with the background and technical operations of the systems used in this study, including a discussion of analysis techniques. Part II presents the detailed results of the analysis of two

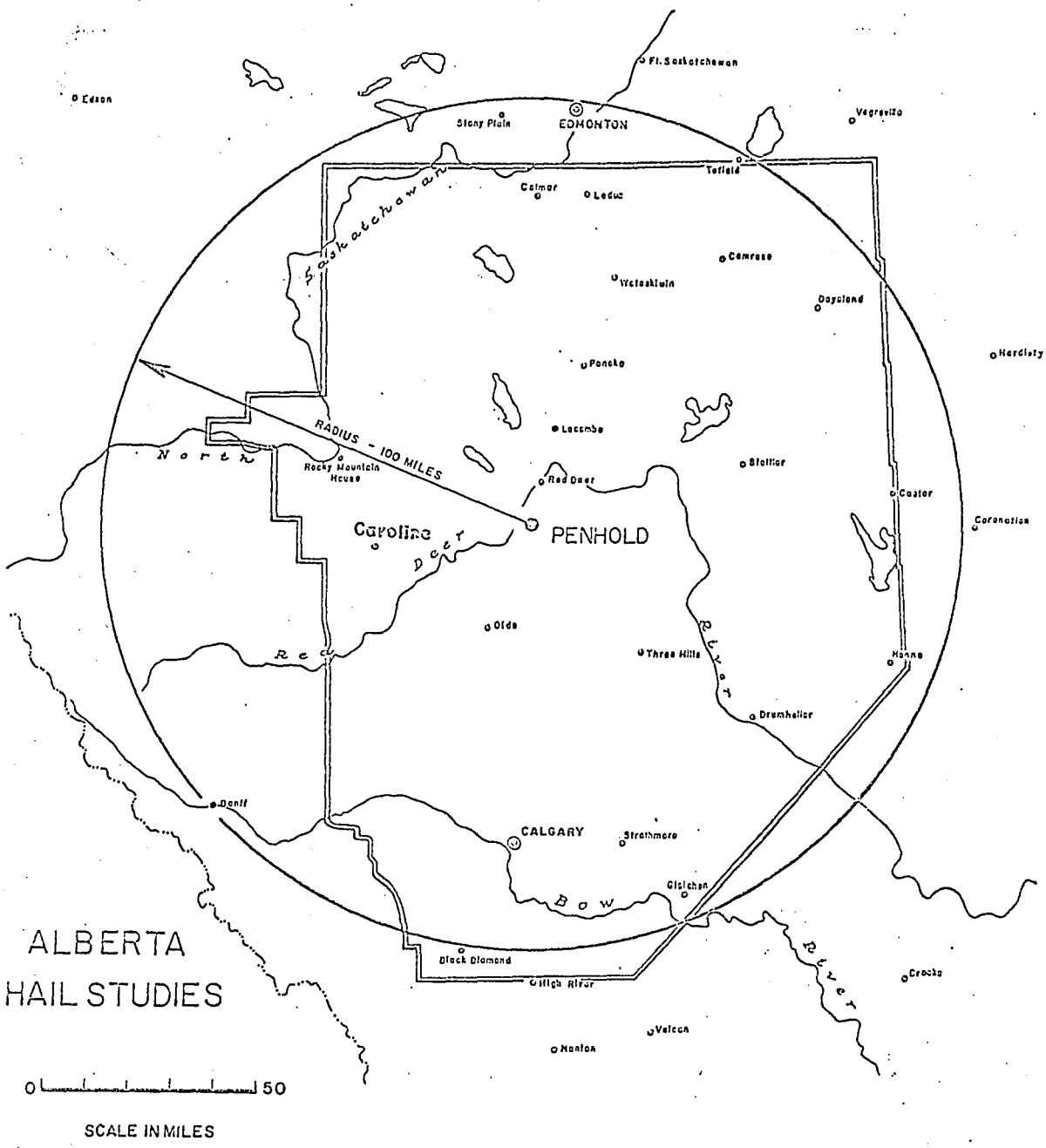

Figure 1: Project area - outlined by double boundary.

groups of turrets observed during the 1966 field program in Alberta. The turret behavior is related to the general environmental conditions that existed on the two days under study. Radar observations of these same turrets are presented and precipitation growth discussed. The scope of data is then extended. By modelling the airflow at the turret boundaries, indirect measurements of the updrafts within the turrets are made. These updrafts are compared with those measured by other authors. Finally, current models of cloudy convection are discussed, and an assessment is made of the ability of these models to depict the behavior that was observed in cumulus turrets.

PART I

A DESCRIPTION OF THE INSTRUMENTATION AND TECHNIQUES

CHAPTER II

THE STEREO ANALYSIS SYSTEM

A. Photogrammetry

The system by which the data were acquired for this study has been described in detail in an earlier M.Sc. thesis (Renick, 1966). Only changes in layout, equipment or procedures will be discussed in detail here.

It has been shown that the percentage uncertainty in the range measurement is inversely proportional to the length of the baseline between the two camera sites. However, the length of the baseline is limited in practice by the analyst's ability to identify the same cloud element in the two superimposed cloud pictures (without serious distortion due to differing optical points of view). Renick's experience in using the system indicated that a somewhat longer baseline than those used in 1965 would still permit unambiguous analysis, while reducing the percentage uncertainty in the range measurements. Hence, while the author retained the former East-West baseline of 8400 ft $\pm$ 0.5% (bearing 275.8 deg true $\pm$ 0.1 deg), he established a longer North-South baseline of 17,930 ft $\pm$ 0.6% (174.2 deg true $\pm$ 0.1 deg). The new camera site was surveyed into position using standard field survey techniques at a location on the south side of the town of Penhold, about 3 miles south of the centre site at C.F.B. Penhold (see Figures 1, page 4, and 2, page 13). Subsequent analysis of films taken from this baseline has shown that a 3 mile baseline did not present ambiguities even at ranges as short as 15 miles; the improved accuracy would seem worthwhile.

Increasing the length of the baseline also increased the maximum usable range for any given percentage uncertainty. Specifically, for an uncertainty of $\pm$ 5% the maximum usable range is 85 miles for the North-South

baseline and 47 miles for the shorter East-West baseline. Typically, at a range of 30 miles, viewing at 90 deg to the baseline, the percentage uncertainties are ± 2% for the North-South baseline and ± 4% for the East-West (see Figure 6 under Sec. C of this chapter).

Two new cameras were put into operation including new time lapse accessories. They are Bolex H16RX reflex 16 mm cameras. A custom-made, versatile 115 V a.c. time lapse attachment was used on the centre site camera, while a d.c. transistorized timer of the author's design was used on the remote site camera. A frame rate of 20 frames per min was used in order to retain a maximum time uncertainty of ± 1.5 sec between the two cameras. However, radio synchronization of the two cameras is recommended for the future. This would make possible a reduction in the frame rate by a factor 3 or 5, thus greatly reducing film consumption in operational use.

Kodachrome II colour film in 100 ft rolls was used with a Kodak #1 A skylight ultra-violet filter on the cameras to improve the sky-cloud contrast. A total of 120 hrs of stereo photography was shot during the months of June through September, 1966. This is equivalent to about 800 ft of film. Experience has shown that about 5% of the footage shot is suitable for detailed analysis of the type described in subsequent chapters.

The major problem in finding a suitable sequence is in maintaining visual contact with a particular turret group for at least 30 mins. Because of the close range and the use of the narrow 1-inch lens on the cameras, the turrets would often pass beyond the field of view. However, other groups at ranges between 30 and 50 miles range will now be measurable with less than 5% uncertainties and so will increase the usable footage. Turrets often

become obscured by other clouds intervening between the interesting turrets and the cameras, further reducing the usable footage of film. Since many cumulus developments are associated with widespread cloudiness, particularly when large scale vertical motion fields exist due to the synoptic circulation, this will always be a problem. However, other types of analysis could make additional use of the films. For example, by using small inactive cloud fragments as tracers of the environment wind, local circulations could be measured. Such investigations are to be encouraged.

It is important to photograph even apparently uninteresting cloud developments, as later time lapse viewing often reveals many events not obvious in real time. In order to get a few interesting sequences, all potentially interesting clouds must be photographed. A detailed record of all operations and events is most important. Stereo analysis requires an accurate knowledge of the true azimuths of the reference marker poles which surround each camera site at nominal 10 deg intervals and which appear in the bottom of each frame of the time lapse films. Hence the sites are resurveyed for their azimuth marker poles every 3 weeks so that corrections to their nominal values can be made at the time of analysis. Time synchronization of the photo data panel clock with the radar and pilot balloon clocks is vital.

Analysis projection techniques, as described by Renick (1966), were used. Care was taken to rephotograph the analysis projection grids for the 1-inch and 10 mm lenses using the new cameras. It was found that placing a red filter over the lens of one of the projectors, or flashing one of the images on the screen over the second, aided in the accurate superpositioning of the cloud images from the two projectors on the semi-transparent projection grid.

B. Data Processing

The analysis of the stereo films consists of three phases: data extraction from the projected images of the films on the projection grid in terms of angular measurements; conversion to positions in space in terms of range, azimuth height and turret diameter; and computation of the vertical velocities of the turret. The first phase is time-consuming, but no suitable means of automation has yet been devised. Although the second phase can be handled by means of tables, the final stage can not. A nomogram was devised by Renick (1966) for vertical speed computations, but this is not suitable for horizontal velocity computations.

Since velocities are computed from small differences in relatively large values of height and range, errors in the instantaneous velocities can become quite large.[1] As a result, rather large amplitude noise components may appear in the computed velocities. It would be unreasonable to consider that a turret's position at any instant in time is completely independent of its position at earlier or later instants. Hence there is a need to smooth before computing values of velocity.

Although graphical methods can be used to produce smoothed values, a numerical method is considered more suitable because, once established,

1 The visual lifetime of a typical turret top is about 15 mins and hence a one-min observing interval is considered necessary to get a detailed description of time variations. A vertical growth rate of 10 m sec^{-1} would result in a vertical displacement of only 600 meters in 1 min. With a typical 5% uncertainty, at 3 km the incremental uncertainty in each height measurement would be $\pm$ 150 meters, and at 6 km $\pm$ 300 meters. Hence the possible error in the vertical speed computed from the two independent height measurements would be as large as 100% at 6 km. A similar situation exists for the horizontal measurements.

the technique requires less time and is more efficient on an operational basis. Furthermore, numerical smoothing is objective and is consistent from one sequence to the next.

However, theoretical work on the effects of numerical smoothing on data is both difficult to understand and incomplete. Hamming (1962) cautions that smoothing (referred to mathematically as a filtering process) at an early stage of the computations may produce effects in the results which must not later be interpreted as physical effects. The spectrum of frequencies that are physically possible in the observed behavior, and the spectrum of frequencies that are probably measurement noise should be estimated theoretically. Then one may choose a filter to attenuate the noise and pass the frequencies that are characteristic of real behavior. For cumulus turrets a theoretical estimate of the shortest periods likely to occur for buoyant parcels is approximately 6 minutes (this value would apply to parcel penetrating into an isothermal layer in the environment (Priestley, 1954)). With a sampling interval of one min, the noise would most likely be concentrated at periods approaching two min (i.e. twice the sampling interval that is used when extracting the observational data). A number of measurements were made of the accelerations necessary to produce the observed short period fluctuations of 1-2 minute periods. Most gave values of an order of magnitude greater than the forces per unit mass due to buoyancy, loading, and momentum exchanges that are normally found to exist in cloudy convection. Hence, our choice of a filter was one which attenuates strongly at periods of 2 mins but has little attenuation above 6 minute periods. The particular filter chosen (which will be described on page 15) was one of the simplest ones. Future work should include a study

of the use of other types which may have sharper response curves (again see Hamming, 1962, or Brooks and Carruthers, 1953).

Hence computer data processing was instituted to carry out all of the computational phases of the analysis.

The data which are extracted from the superimposed images (see Figure 3) included: ϕ, azimuth of the geometrical centre of the turret top; α, the angle subtended by the baseline at the cloud (see Figures 2 and 3);[1] θ, the angular elevation to the cloud turret top with respect to the artificial horizon (a zero deg elevation marker surveyed onto each azimuth marker pole); β, the angle subtended by the semi-circle that best encases the cloud turret top; and F, the frame number. The frame numbering begins at zero at the time of the last data panel insertion preceding the sequence to be studied. Subsequent data panel frame numbers are recorded during the sequence with the exact times of insertion. Normally every 10th or 20th frame is analysed, depending upon the time resolution that suits the accuracy of the space measurements that are being made. This assures that as much detail as possible of the time variations in velocity will be detected.

Three types of computer input cards are used: mode cards, time cards and observation cards. The mode card feeds in the turret identification number, date, time, and number of observations in the sequence before each sequence begins. The time card feeds in the exact time and frame number

1 This angle equals the angular separation between a particular azimuth marker pole appearing in each of the two stereo pictures when a cloud turret's images are superimposed. Due allowance must be made for the errors in each pole's azimuth from its nominal 10 deg value as measured by the most recent survey of the sites.

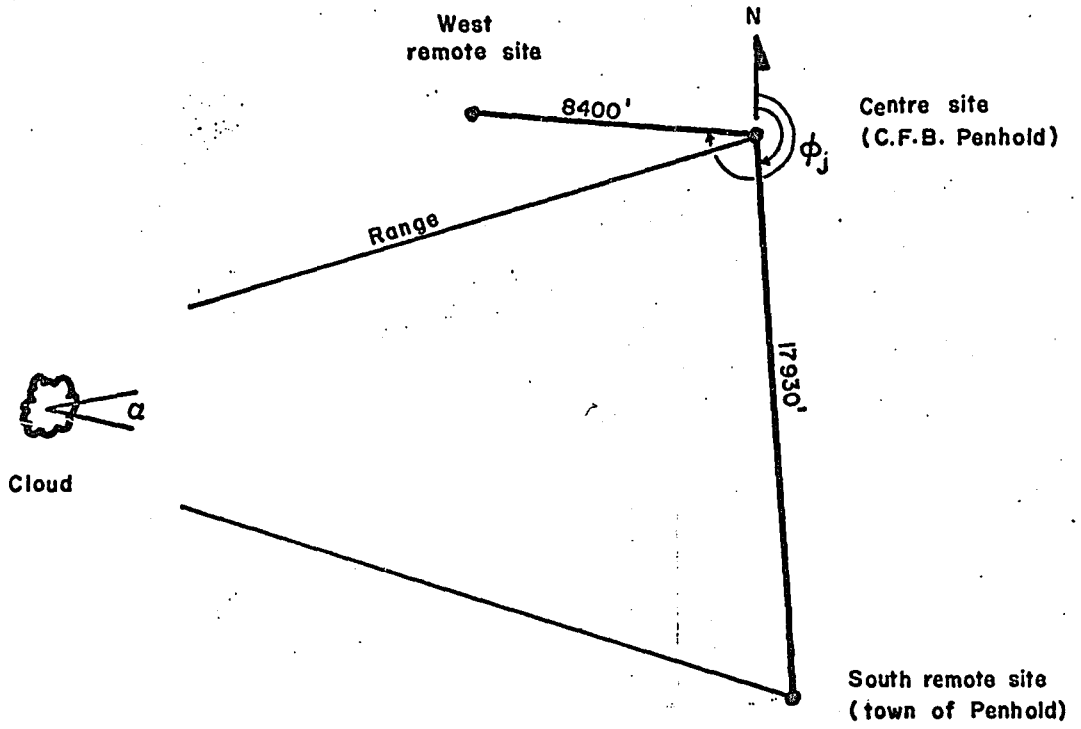

Figure 2: The arrangement of camera sites for the stereo-photogrammetry system. α, the angle subtended by the baseline at the cloud is shown for the North-South baseline. The length and bearing (ϕ_J) of the East-West and North-South baselines are also shown.

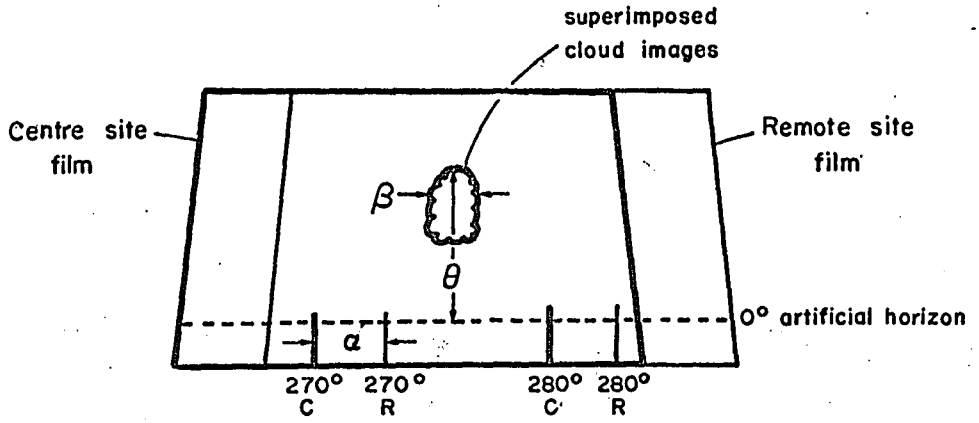

Figure 3: A superimposed stereo pair showing: α, the angle subtended by the baseline at the cloud; β, the angle subtended by the cloud diameter and θ, the elevation angle to cloud top. Azimuth marker poles appear in the bottom of each frame.

of the time panel insertion, usually every 10 mins. The observation card feeds in the frame number, F, ϕ, α, θ, β, and J, a baseline identification number.

In the processing, the following equations are applied to the data:

$$t_i = \left(\frac{t^{n+1} - t^n}{F^{n+1} - F^n}\right) F_i + t^n \qquad (1)$$

$$R_i = \frac{B(J) \sin\left(\alpha_i + (-1)^J(\phi_i - \phi_J)\right)}{\sin(\alpha_i)} \qquad (2)$$

$$H_i = \left[(R_e^2 + R_i^2)^{\frac{1}{2}} - R_e + R_i \tan\theta_i \cos\left(\frac{R_i}{R_e}\right)\right] C_1 \qquad (3)$$

$$S_i = 2R_i \sec\theta_i \tan\left(\frac{\beta_i}{2}\right) C_1 \qquad (4)$$

$$W_i = \left[\left(\frac{R_i}{R_e} + \tan\theta_i\right)\frac{\Delta R}{\Delta t} + R_i \sec^2(\theta_i)\frac{\Delta\theta}{\Delta t}\right] C_2 \qquad (5)$$

$$v_i = \left[R_i^2\left(\frac{\Delta\phi}{\Delta t}\right)^2 + \left(\frac{\Delta R}{\Delta t}\right)^2\right]^{\frac{1}{2}} C_2 \qquad (6)$$

$$a_i = \tan^{-1}\left[\frac{R_i \cos(\phi_i)\frac{\Delta\phi}{\Delta t} + \sin(\phi_i)\frac{\Delta R}{\Delta t}}{-R_i \sin(\phi_i)\frac{\Delta\phi}{\Delta t} + \cos(\phi_i)\frac{\Delta R}{\Delta t}}\right] \qquad (7)$$

where: t_i = time in minutes of the i^{th} observation.

t^n = time in minutes of the n^{th} data panel

F_i = frame number of the i^{th} observation

F^n = frame number of the n^{th} data panel

R_i = range in miles from centre site

J = baseline identification code

B(J) = length in miles of baseline J

α_i = angle subtended by the baseline at the cloud

ϕ_i = azimuth of geometrical centre of turret in deg true

ϕ_j = bearing of baseline J (see Figure 2) in deg true

H_i = height of turret top in km

R_e = radius of the earth at latitude 52N in miles

θ_i = elevation angle to turret top in deg

S_i = diameter of best fit semi-circle to turret top in km

β_i = angular diameter of turret top in deg

W_i = vertical growth rate of turret top in meters per sec

v_i = horizontal speed of turret in meters per sec

a_i = bearing <u>from</u> which the turret was moving in deg true

$\frac{\Delta(\ )}{\Delta t}$ = the numerical derivative $\frac{(\ )_{i+1} - (\ )_{i-1}}{t_{i+1} - t_{i-1}}$ at the i^{th} instant

C_1 = 1.609 km per mile

C_2 = 26.82 meter min per mile sec

The output consists of turret identification, date, time, ϕ, R, H, W, v, and a. In addition, Northward and Eastward components of range and horizontal velocity are computed. Then the observational data is smoothed and the computations are repeated giving smoothed velocities in the output. If further smoothing is necessary, this last step is repeated until the short period variations are removed. The smoothing or filtering equation is:

$$\bar{x}_i = \frac{x_{i+1} + x_{i-1} + 2x_i}{4} \qquad (8)$$

The response of such a filter is given by the expression:

$$r_m = \frac{\bar{x}_i}{x_i} = \frac{1 + \cos \frac{2\pi}{m}}{2} \qquad (9)$$

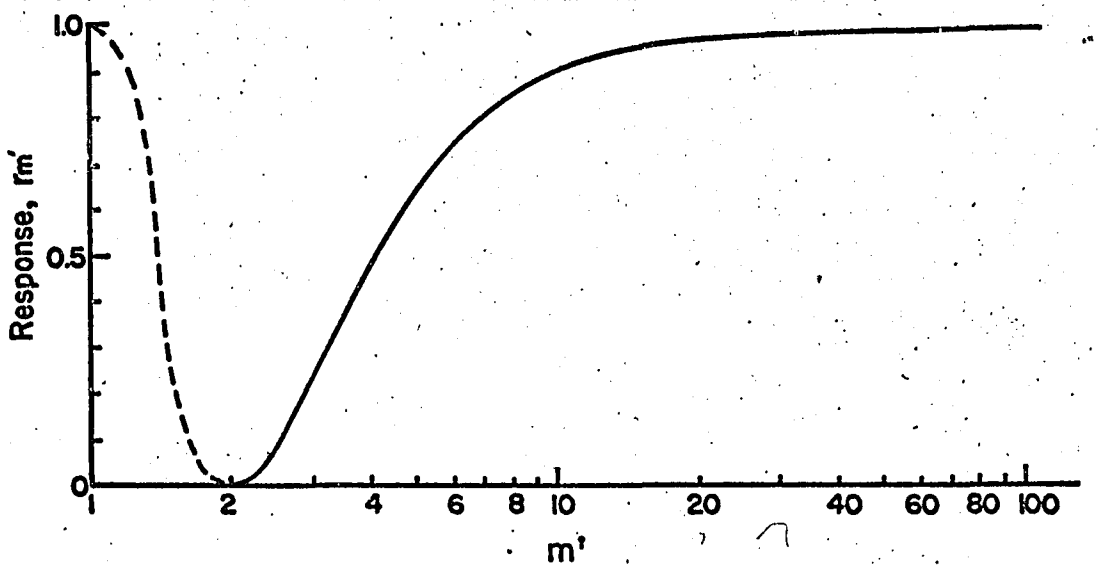

Figure 4: Response, $r_{m'}$, of the numerical filter as a function of m' the number of measurement intervals per cycle (= length of period of oscillation in data ÷ length of the measurement interval).

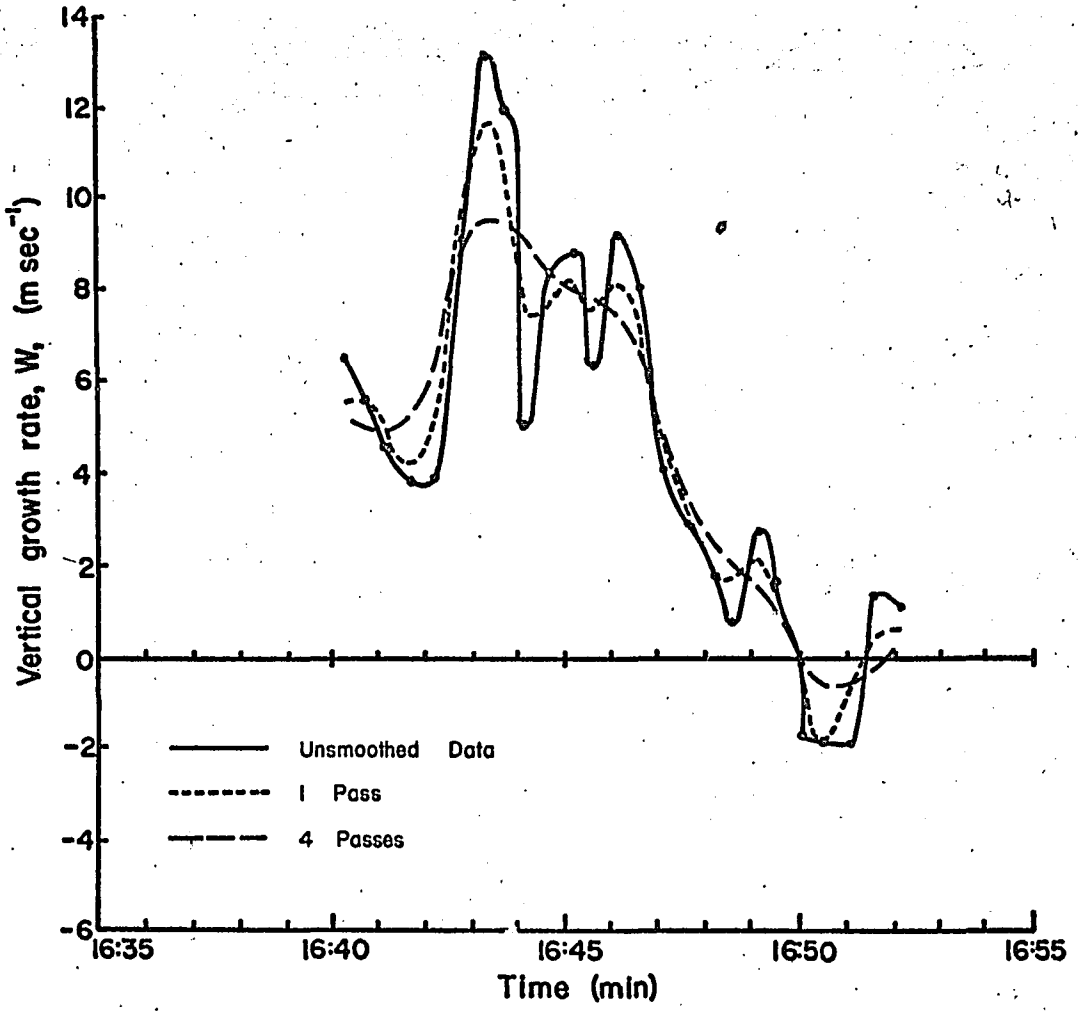

Figure 5: An example of the smoothing effects of the numerical filter on fluctuations in an observed vertical growth rate curve.

where $r_{m'}$ = the ratio of the filtered amplitude to the original amplitude for a certain component with a period equal to m measurement intervals

$\bar{x}_i$ = the smoothed value at the i^{th} instant

x_i = the original value at the i^{th} instant

Figure 4 is a plot of the response, $r_{m'}$, versus m', the number of measurement intervals per cycle. Up to four passes through the observational data were made in some instances, each pass resulting in further smoothing of the output. Figure 5 is an example of the vertical growth rate, W, as it appeared without smoothing, after smoothing using one pass, and after 4 passes.

C. Uncertainty Considerations

The fractional uncertainty in the values of range, height and diameter are computed from the expressions:

$$\frac{\partial R}{R} = \frac{\partial B}{B} + \frac{\partial \alpha}{\alpha} + \cot\left(\alpha \pm (\phi - \phi_J)\right)\left(\partial\phi + \partial\phi_J\right) \qquad (10)$$

$$\frac{\partial H}{H} = \frac{\partial R}{R} + \frac{2}{\sin(2\theta)}\,\partial\theta \qquad (11)$$

$$\frac{\partial S}{S} = \frac{\partial \beta}{\beta} + \frac{\partial R}{R} \qquad (12)$$

where $\partial(\ )$ = the incremental uncertainty in $(\ )$. For α, ϕ_J, θ, and β, these were estimated to be $\pm$ 0.1 deg, and for ϕ $\pm$ 0.5 deg.

Figures 6 and 7 give the percentage uncertainties in range to the turret and radius of the turret ($= \frac{S}{2}$) as a function of range. Figure 8 shows isopleths of percentage uncertainty in height as a function of height and range. These values apply to the North-South baseline using a 1-inch

lens. Values for the East-West baseline are approximately double those for the North-South baseline. Also the values using a 10 mm wide angle lens would be approximately double those indicated here.

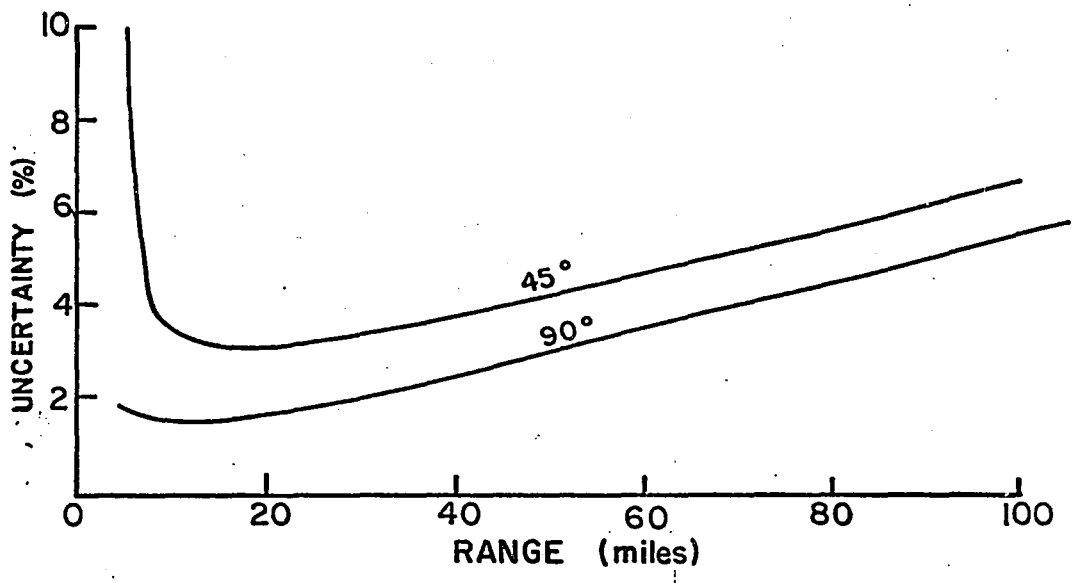

Figure 6: Percentage uncertainty in range as a function of range. Curve marked " 90° " refers to measurements made when cloud is perpendicular to baseline; curve marked " 45° " when cloud is at 45 deg to the baseline.

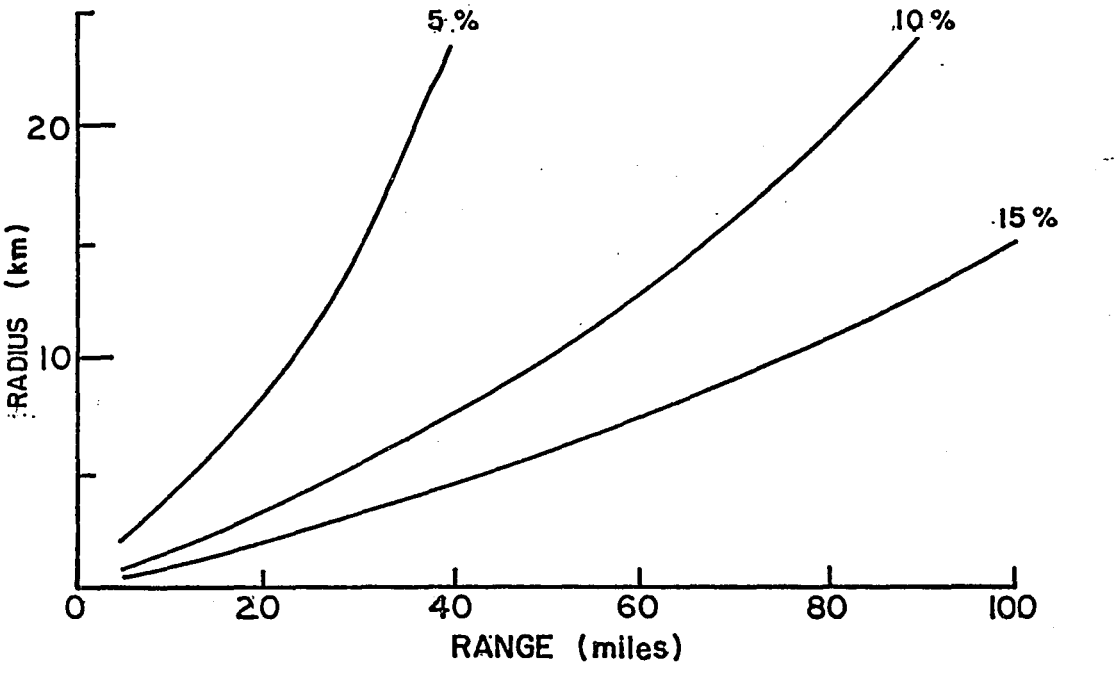

Figure 7: Isopleths of radius uncertainty as a function of radius and range.

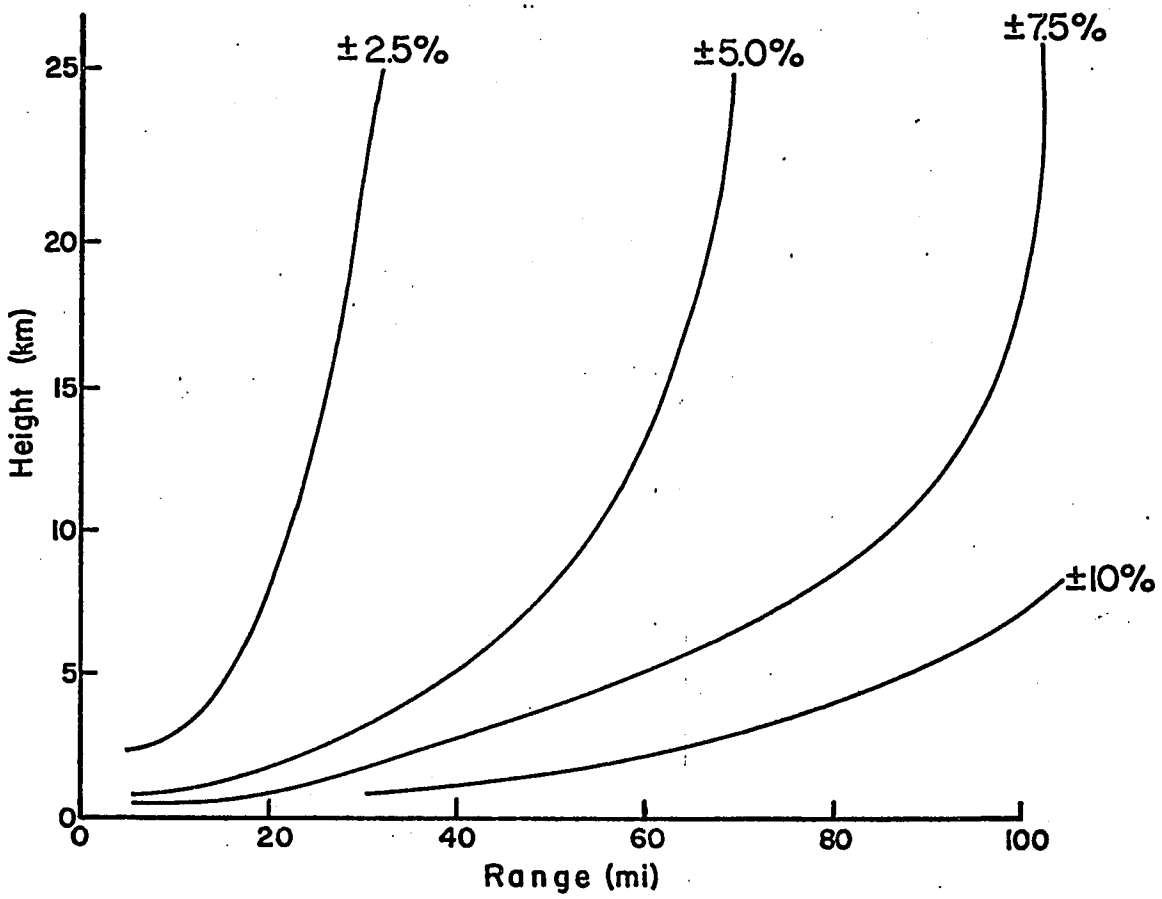

Figure 8: Isopleths of height uncertainty as a function of radius and range.

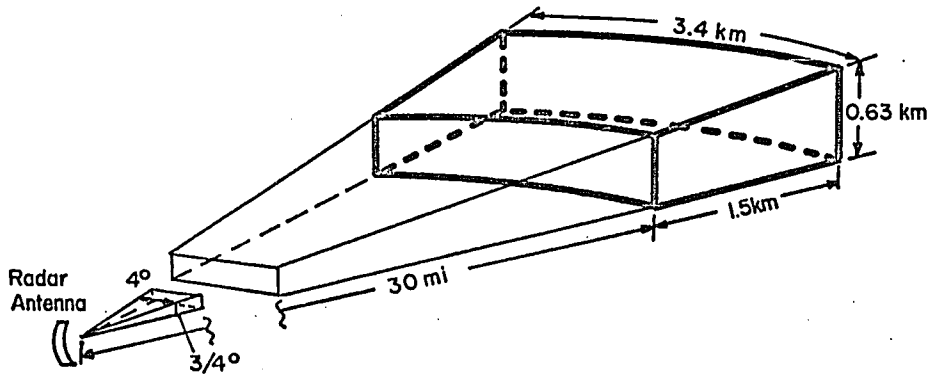

Figure 9: A representation of the radar pulse at 30 miles range when half power beam width is 3/4 in the vertical and 4 in the horizontal.

CHAPTER III

AUXILIARY SYSTEMS

A. The Radar

A Decca 3.2 cm radar unit was operated during the 1966 season at the Alberta Hail Studies Project. This is a low power unit, 30 kilowatts peak power, with a pulse length of 5 microsecs, and a pulse repetition frequency of 400 pulses per sec. The antenna has a half power beam width of 3/4 deg in the vertical and 4 deg in the horizontal. The dimensions of such a radar pulse at 30 miles range are shown in Figure 9, (see page 20).

The antenna is rotated at 20 rpm with an automatic tilting sequence of $\frac{1}{2}$ deg of elevation angle every 2 revolutions up to +20 deg elevation. The whole cycle requires approximately 4.3 min. The display is a PPI scope which is photographed on 16 mm film, one frame every 2 antenna rotations. A second display is regularly monitored and photographed with a Polaroid camera to provide on-the-spot radar observations to aid in the planning of stereo photography and hail-reporting network operations.

The low power and wide horizontal beam width result in a significant reduction in sensitivity beyond about 40 miles, so that light precipitation of small cores may not have been detected beyond 40 miles. Also attenuation of the signal in penetrating precipitation could be significant. This would result in "shadows" at ranges beyond the nearest strong echoes (Douglas and Hitschfeld, 1958).

The radar does provide good vertical resolution for determining echo tops, and a reasonable 3-dimensional depiction of the precipitation areas at the time when the first echo appears within about 40 miles range from the site. The uncertainties are estimated to be $\pm$ 1 deg in azimuth, $\pm$ 0.5 deg in elevation, and $\pm$ 1 mile in range, for ranges between 15-30 miles.

No adequate means of azimuth and range calibration exists for this unit. Such calibration is essential when individual echo cells of only a few miles' diameter are to be associated with observed cloud turrets of about the same size range at range of 15 to 30 miles. At least one standard radar target in each quadrant, at ranges 20 and 60 miles, would be desirable. However, the author was able to make some checks on the indicated azimuths and ranges by using the locations of known topographical features in the ground return echoes, which appear at zero and $\frac{1}{2}$ degree elevation scans. Two hills at 033.5 deg true, 19.7 miles and 032.5 deg true, 22.4 miles (approximately $3\frac{1}{2}$ miles Southeast of Lacombe, Alberta) were used to calibrate for the July 10, 1966, storm which occurred about 18 to 30 miles to the north of the radar and camera sites. A correction of -5.5° azimuth and +1.7 miles range was applied to the radar display's indicated values on this day. On July 7, 1966, it was found that the same correction was necessary when using the same hills as guides. But the positions of Mount Costigan (226.0 deg true, 85.5 miles), Devil's Head (230.5 deg true, 82.2 miles), and Limestone Mountain (256.0 deg true, 68.0 miles) on the radar scope showed little or no correction should have been necessary. The reason for this discrepancy is not certain, but mechanical maintenance was being performed on the rotating mechanism around this time. There were also indications that the antenna was not rotating at a constant speed within each rotation, possibly resulting in different corrections being necessary for different azimuths. Thus no correction was applied on July 7, 1966, to the observed echo positions, which were between 250 and 265 deg true at 20-30 miles. However, the reassurance of having artificial targets in known locations (and, if possible, of known equivalent reflectivity) would be very desirable in the future.

B. The Hail Reporting Network

A volunteer hail reporting program was first organized in a pilot project in the summer of 1956 (Douglas and Hitschfeld, 1958). It has been expanded each summer since then with mailed-in reports being augmented by field car surveys and telephone surveys of the regions lying in the wake of the more significant storms. Details of the hail reporting scheme are given by McBride (1964) and a summary of recent progress by Pell (1967).

Data on the time, character, and intensity of the hail and rain, and the size and estimated amounts of hail which fell from a storm were collected in this manner. However, the region of initial precipitation to reach the ground (presumably associated with first echoes) often was not surveyed in detail, leaving some doubt about the nature and time of occurrence of the first precipitation at the ground.

It is certainly desirable to have such information available to infer the nature of the precipitation which occurs in the first echo, and thus to estimate its effects on the dynamics of the developing turret. It is recommended that information on the first reported rain and hail be sought most diligently in the future. However, this may remain a difficult task over the western portion of Alberta because it is so sparsely settled, unless volunteer observations are supplemented with a network of recording rain and hail sensors.

PART II

THE RESULTS AND CONCLUSIONS

CHAPTER IV

GROWTH RATES AND MOTIONS OF TURRETS

A. Introduction

Two groups of turrets are studied in detail. The first group, designated 7/01 through 7/05, occurred as a part of a developing storm of considerable magnitude on July 7, 1966. The second, 10/01 through 10/04 occurred on July 10, 1966. These particular groups were chosen because they occurred at close enough range (within 40 miles) to permit near optimum measurement accuracies. An unobstructed view of the groups was possible for sufficient time to consider the complete visual history of a number of turrets in each group. Also good radar data and a limited amount of survey information were available. Unfortunately these were not days on which radiosonde ascents were taken right at Penhold, but ascents at Calgary (75 miles south) and Edmonton (90 miles north) were available.

Photogrammetric measurements were made at approximately one minute intervals on July 7 and at 30 sec intervals on July 10. Hence, values of height, vertical growth rate radius and horizontal velocity were computed at each one minute (or 30 sec) interval to construct the curves to be presented in the following sections. Both storms were within 18 to 32 miles of the sites and within 15 deg of being perpendicular to the baseline used for stereo photogrammetry.

B. The Storm of July 7

The general weather pattern differed considerably on the two days. On July 7 cumulus began forming over the foothills to the SW of Penhold by 12:00 MST (Mountain Standard Time) and a few cumulus congestus types were underflown in a light aircraft at 2.5 km above mean sea level (MSL) (approximately 1.5 km above terrain) in the vicinity of Caroline, about 40 miles

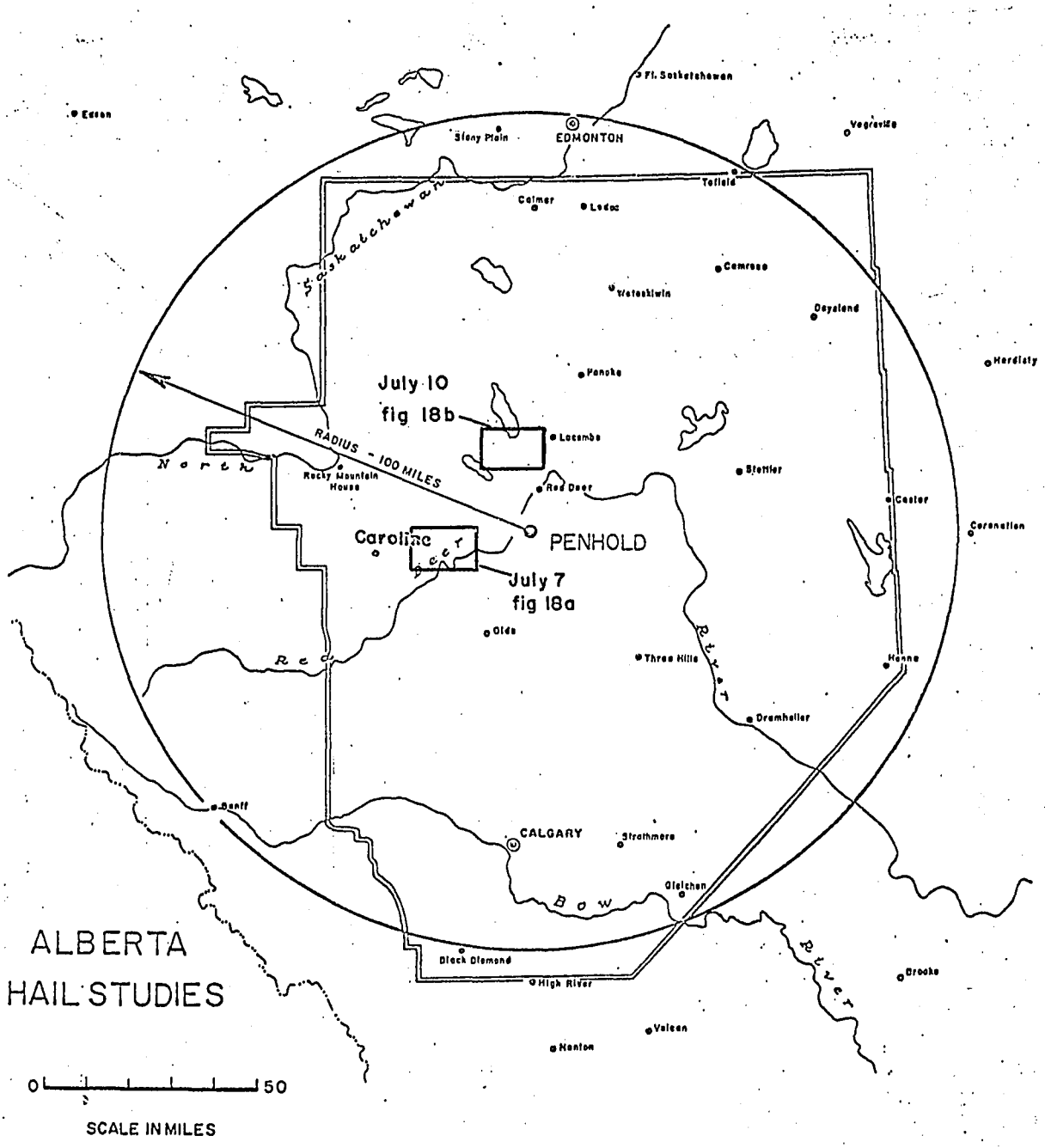

Figure 10: Map of central Alberta showing location of the two turret groups studied. The rectangles approximately outline the areas shown in the turret depictions of figures 18a and b.

west to west-south-west of Penhold at 13:15 MST (see map in Figure 10). Aircraft reconnaisance was carried out in a Piper Super Cruiser aircraft and considerable bumpiness was experienced in this area. A number of updrafts were encountered while flying below developing cumulus bases. A few of the stronger updrafts were estimated to have caused the aircraft to climb 300 to 400 ft in 5 to 10 secs even though the aircraft was at greatly reduced power. This would suggest vertical speeds of the order of 15 meters per sec. Some of the cloud tops were estimated to be about 5 km MSL (4 km above terrain). This whole region about 50-80 miles east of, and running parallel to, the main peaks of the Rocky Mountain Ranges, was scattered with developing cumulus clouds but the area to the east was still clear. In addition the presence of scattered alto-cumulus lenticularis suggested that gravity lee waves were established in the region south-west of Caroline.

Consideration of the flow aloft and the early sequences of the time lapse films suggests that this region just south of Caroline was the area from which the cloud group under consideration originated.

The surface flow on July 7 was light south-south-easterly while at 500 mb a cold trough extending from northern Alberta to a low off the west coast of the U.S.A. resulted in a 30 to 35 kt flow from the south-west over the area at upper levels. A weak surface trough was approaching the region of the storm from the north-west but did not pass through Penhold until 19:00 MST when the surface wind shifted to northerly (see Figures A2a and b in Appendix II for the surface and 500 mb charts).

A mean sounding of temperature and moisture was constructed from

the Calgary and Edmonton radiosondes for 17:00 MST (00:00Z) and the Penhold surface data for 14:00 MST (Figure A1). It shows a steep lapse rate from the surface to 3.8 km and between 6.5 km and 7.4 km.[1] The maximum relative humidity occurred in the layer between 3.2 and 3.8 km and was only 60%. The tropopause was at 10.3 km although a relatively stable layer extended down to 9.7 km. The convective condensation level was 1.2 km above ground with parcel instability above.

The turrets on this day seemed to protrude from a rather extensive region of cloud approaching from the south-west and obscuring much of the view of the lower reaches of the turrets. The top of this cloudy region initially was around 5.0 km and had the appearance of being the remains of earlier convective transports of moisture from lower levels to mid-levels, which was drifting in the flow and remaining relatively dormant.

Figure 11 is a frame from the analysed time lapse films at 14:37 MST on July 7. The view is toward the west-south-west; clouds are moving from the distant left of the frame to near right. The extensive cloudy region may be seen in the right foreground and again in the left background. The turrets studied are clustered closely together in the upper right quadrant of the picture. Each turret is designated with a dot and numbered in the margin.

1 All heights are heights above the C.F.B. Penhold radar and camera sites which are all at 0.91 $\pm$ 0.05 km above mean sea level, unless stated otherwise in the text. Within 40 miles of the sites, the height of terrain lies between 0.9 km and 1.1 km above mean sea level.

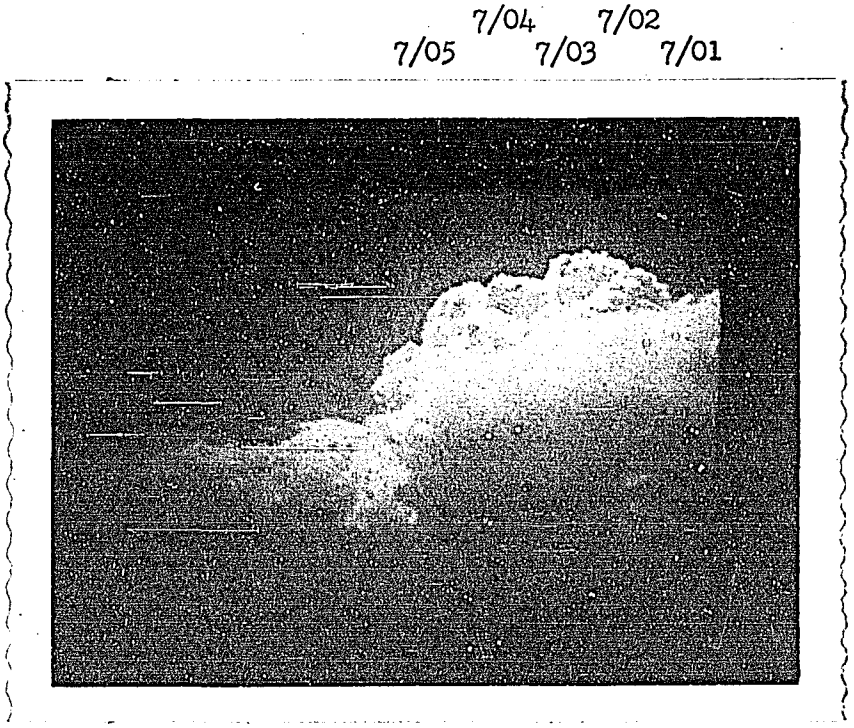

Figure 11: Photograph of the July 7 turret group from the centre site film at 14:35 MST. The individual turrets are identified by their numbers.

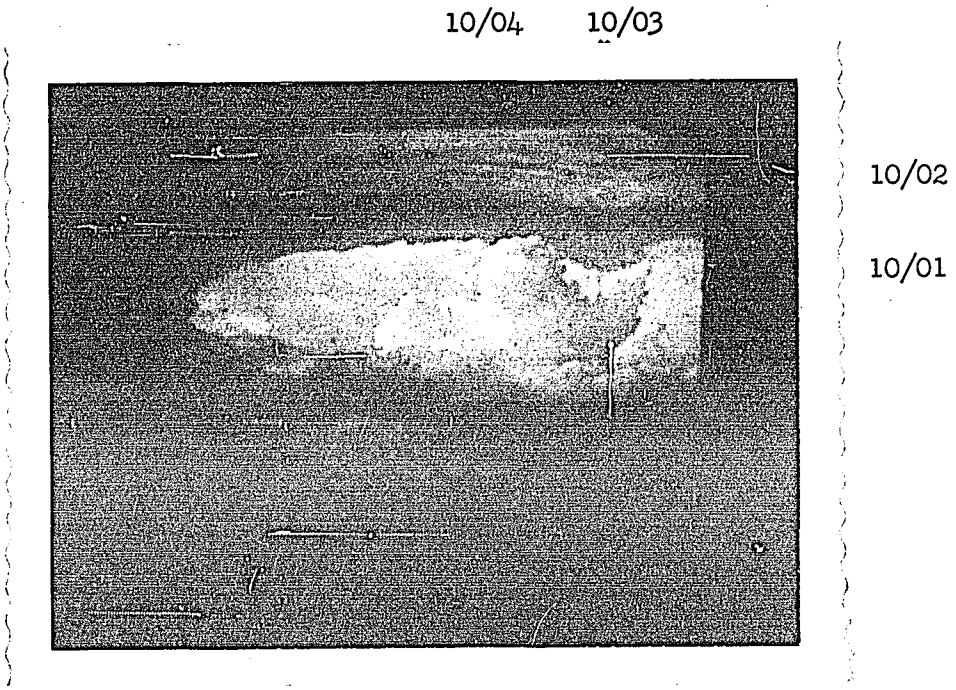

Figure 12: Photograph of the July 10 turret group from the centre site film at 16:45 MST. The individual turrets are identified by their numbers.

C. The Storm of July 10

The weather situation on July 10 was quite different from that on July 7. At 05:00 MST an inactive cold front lay to the north of Edmonton and Jasper and the flow was light northwesterly over the Penhold region. At 500 mb the cold trough still ran from northern Alberta to a low off the west coast of the U.S.A. However a short wave trough was moving out of the west coast trough position passing in the vicinity of Prince George, B.C. at 05:00 MST to lie through Edmonton by 17:00 MST (sfc and 500 mb charts appear in Figures A4a and b in Appendix II).

This trough developed a surface low pressure disturbance on the front during its passage over the front, resulting in an activation of the cold front behind it. Hence an active cold front swept through central Alberta from the northwest at about 25 kts, passing through Penhold at 17:05 MST. The winds shifted from calm at 17:00 MST to northwest at 30 kts at 17:05 MST. Between the hourly surface observations at 17:00 MST and 18:00 MST, the cloud cover went from scattered cumulus to broken cumulonimbus, the temperature fell 18 deg F, the dew point temperature fell 9 deg F and the msl pressure rose 2.7 mb. This very sharp and rapid moving cold front was most spectacular on time lapse films, showing the sudden increase in the winds with dust being whipped up behind the nose of the cold air, and convective "boiling" of the cold air as it surged over the much warmer ground resulting in broken bands of cumulus under the frontal inversion. Finally the violent eruption of cumulus congestus and cumulonimbus occurred as the cold air deepened over this area and presumably as prefrontal cooling of the warm air became sufficient to virtually eliminate the frontal inversion and permit the convection to continue up into mid-levels.

Figure 12 shows the development as it appeared at 16:45 MST on July 10. The view is toward the north-north-west (i.e. in the direction of deepening cold air). The surface front is just approaching the camera site and bands of shallow cumulus may be seen in the foreground. The cumulus congestus turrets appear in the midground of the picture at about 20 miles range, while a large cumulonimbus anvil is visible in the background at about 45 miles. Note how isolated the turrets are on this day compared with the group on July 7 (Figure 11).

In this case it was rather difficult to get a representative sounding of the atmosphere in the vicinity of the storm due to the presence of the front. Because Edmonton was already deep into the cold air by 17:00 MST (00:00Z), Calgary's sounding was considered to be more representative of the warmer air just ahead of the front into which these turrets were developing; this sounding is shown in Figure A3. It is seen that to release the potential parcel instability, a mechanism for heating the layer below 1 km, or for cooling the layer between 1 km and about 2.5 km would be necessary. Most probably the sharp trough associated with this very active cold front would have been sufficient to cause low level convergence and ascent of the warm air adequate to cool the mid-levels and release the potential instability.

As a first approximation to the modification brought about by such a dynamic process, the 850 mb and 500 mb levels were lifted adiabatically by 50 mb, and the 700 mb level by 100 mb.[1] The resulting sounding is shown

1 Such lifting is the result of assuming a profile of ascent rate for the warm air that was parabolic with height, having a maximum of 1 m sec^{-1} and acting for $\frac{1}{2}$ hour (Newton, 1963; Beebe and Bates, 1955).

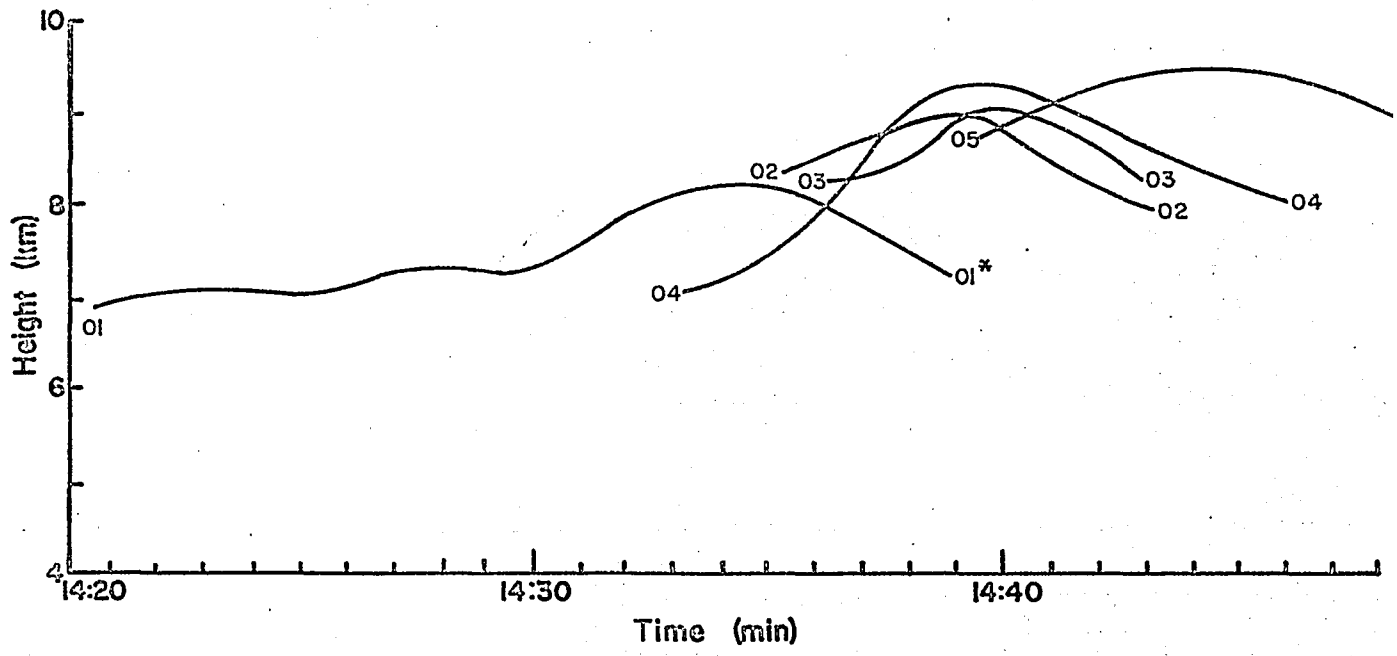

Figure 13a: Height of turret top as a function of time for the turrets observed on July 7, 1966.

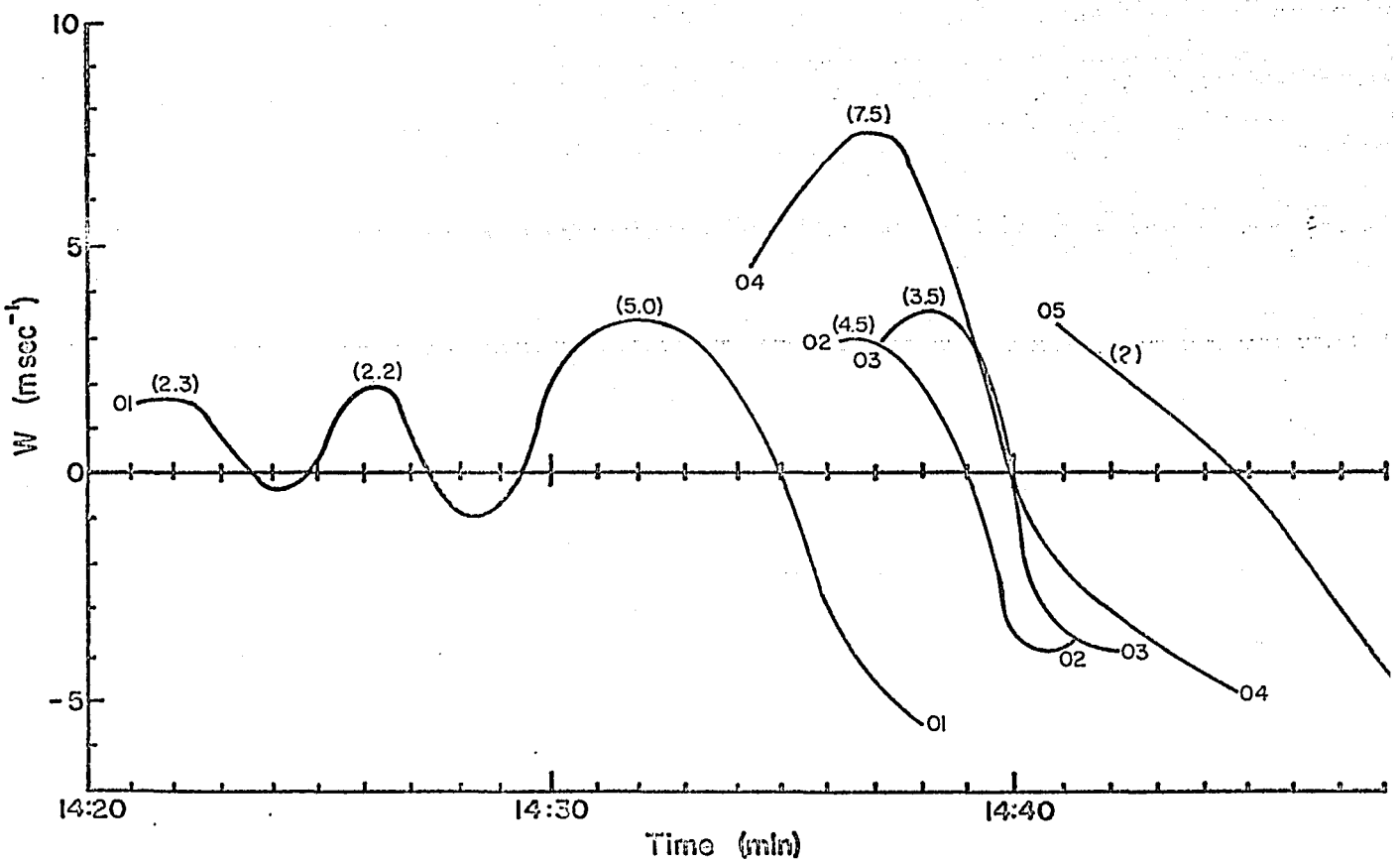

Figure 13b: Vertical growth rate, W, of the turret tops as a function of time for the turrets observed on July 7, 1966.

by the dashed curve in Figure A3. Parcel instability would then have been released in the rising air with a condensation level of 2.1 km and the environment would be near saturation from 3.1 to 5.6 km. The tropapause was at 9.1 km.

D. The Vertical Growth Behavior

The results of the stereo analysis of the five turrets viewed in the July 7th group are displayed in Figures 13a and 13b. Figure 13a is a plot of the turret top height above ground in km versus time of observation in minutes. Observations were made at one-minute intervals. Note that, with the exception of turret 7/04, the time of achieving maximum height progresses in time, each successive maximum being higher than the previous one. Turret 7/04 is only out of sequence in this regard by a minute or two. Turret 7/01 is somewhat unique in its length of duration. However its vertical growth appears to have been in three distinct pulsations.

It should be noted at this point that there is nothing of particular physical significance about the beginning or ending of an individual curve in Figure 13. In most cases it is the instant at which the turret comes into (or is lost from) view above the general cloud level that determines the beginning (or ending) of measurements. In a few cases the turret radius decreases to less than a few hundred meters and can no longer be analysed as a turret but rather is just a wisp of cloudy air. These cases are marked with a "*" on the height curves.

Figure 13b depicts the vertical growth rate of the turret top, W, derived from the numerically smoothed data. The numbers in brackets are the length in minutes of the half-period of the oscillations in the W curves.

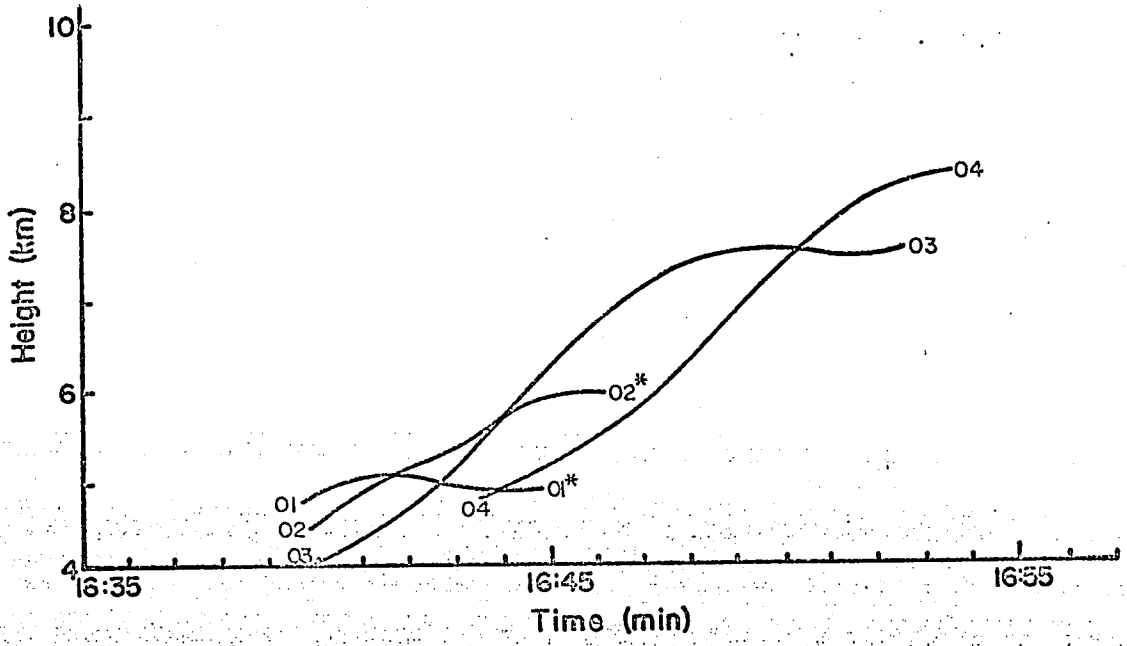

Figure 14a: Height of turret top as a function of time for the turrets observed on July 10, 1966.

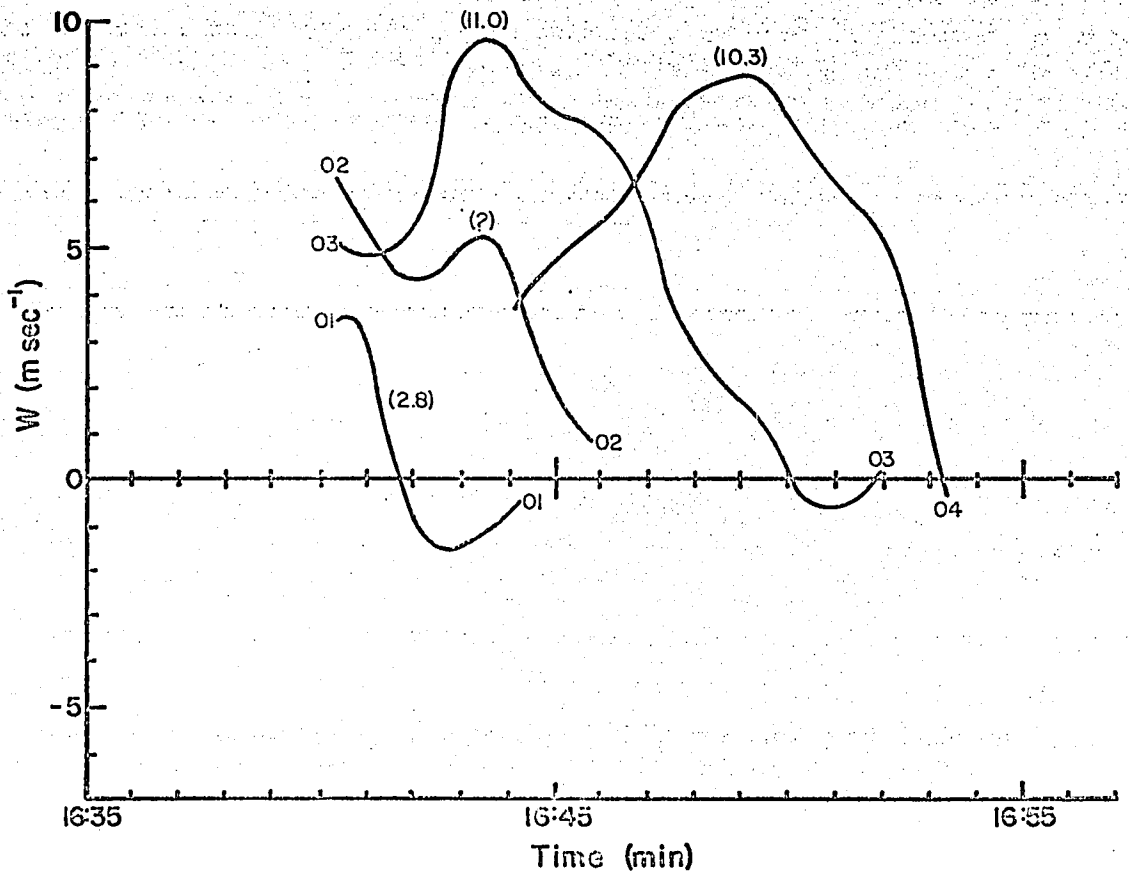

Figure 14b: Vertical growth rate, W, of the turret top as a function of time for the turrets observed on July 10, 1966.

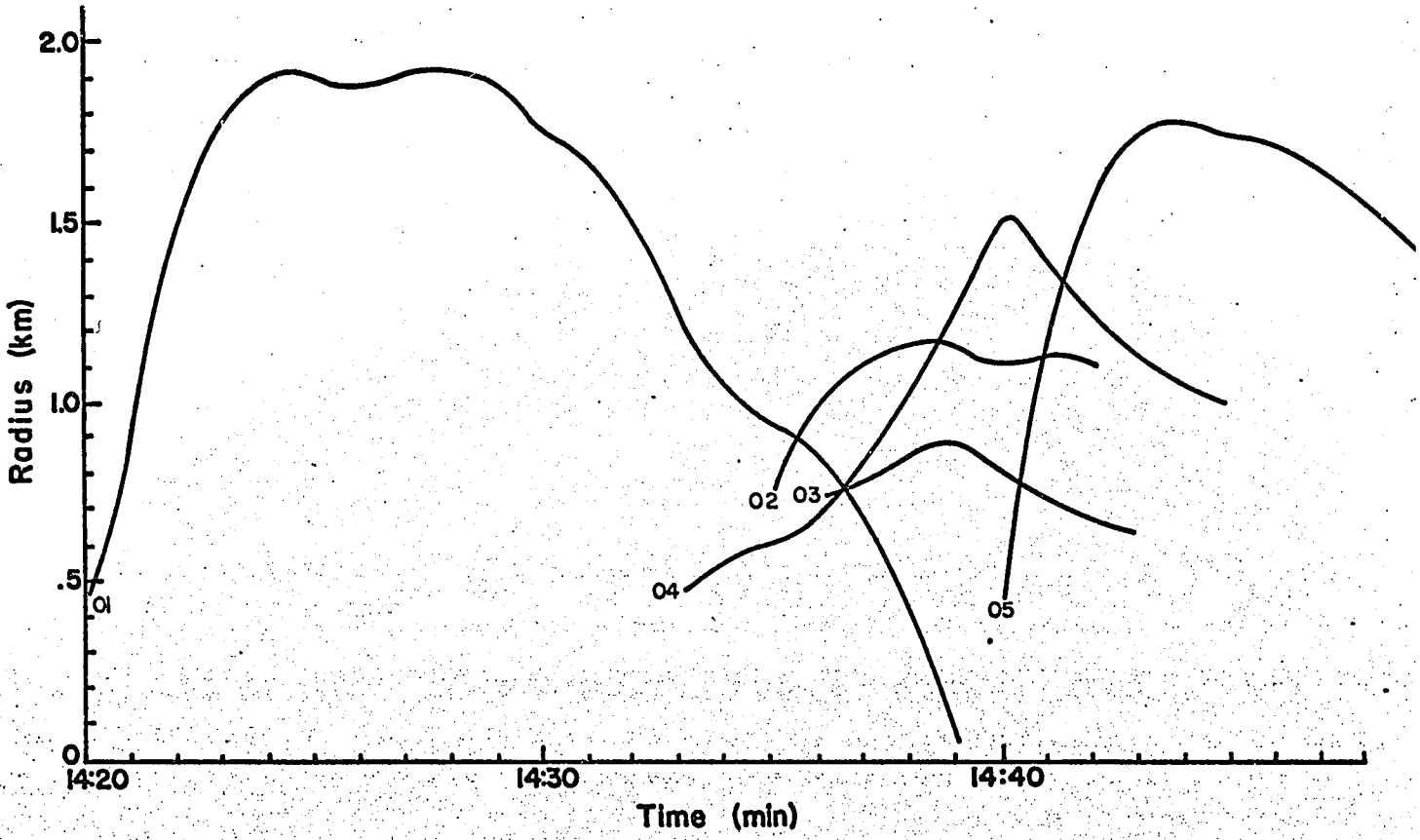

Figure 15a: Radius of cloud turret as a function of time for turrets observed on July 7, 1966.

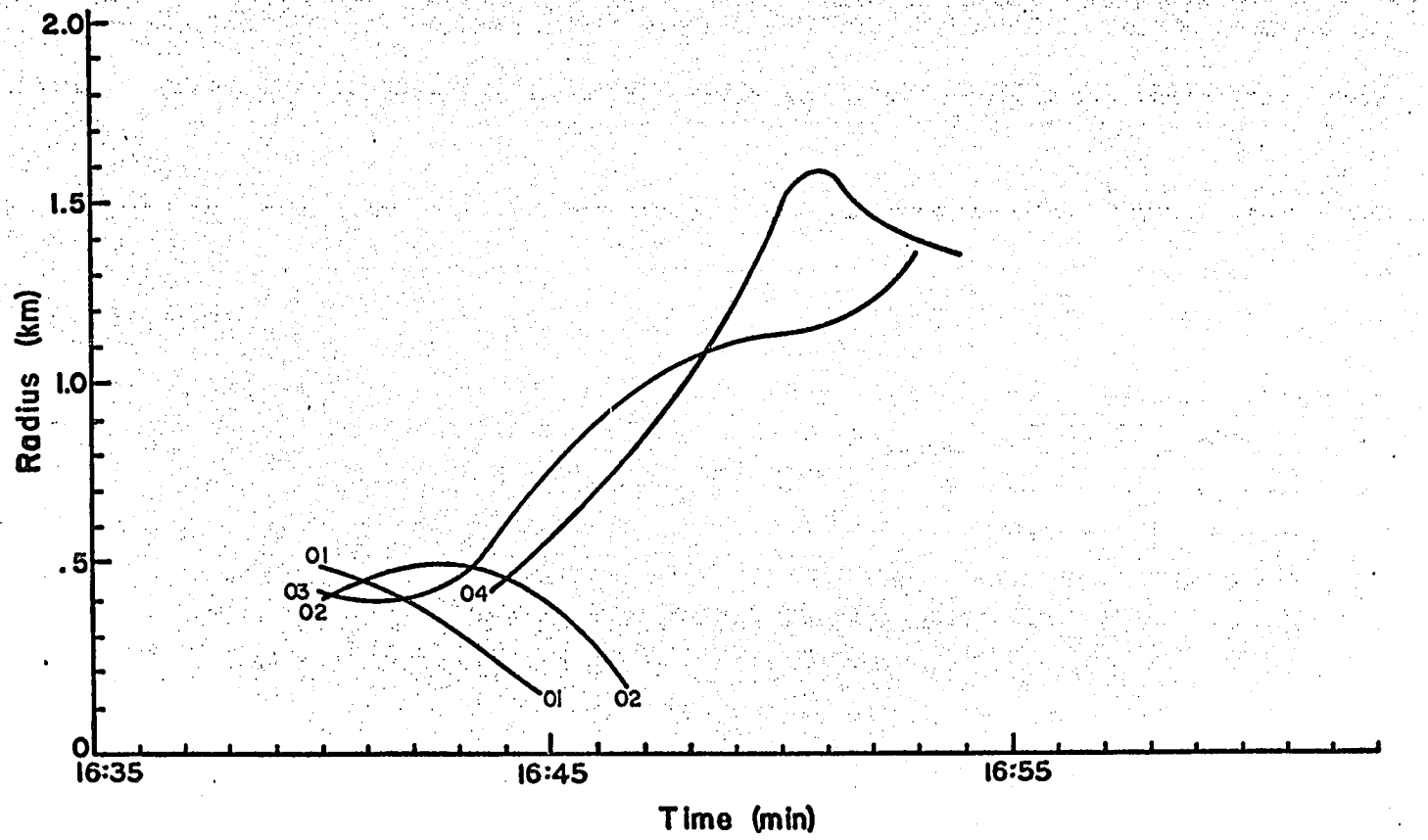

Figure 15b: Radius of cloud turret as a function of time for turrets observed on July 1(1966.

Turret 7/01 is considered as three separate pulses. Turret 7/05 was not viewed for sufficient time to estimate its half-period.

The results of stereo analysis for the July 10 group are displayed in Figures 14a and 14b. Once again the maximum height that each turret top achieves is higher than that of the preceding ones. In general, the vertical growth rates of these turrets reach larger values than on July 7. Maximum vertical growth rates of 8.9 and 9.6 m sec^{-1} are attained by turrets 10/04 and 10/03 respectively, compared with 7.5 m sec^{-1} for turret 7/04. Also the half-periods of the major turrets are somewhat longer on July 10.

E. Radial Growth of the Turrets

Figures 15a and 15b are plots of the measured radius of each cloud turret top in km versus time in minutes for July 7 and July 10 respectively. The radius was measured by fitting subjectively a semi-circle over the exposed turret top so that it most nearly represented the shape of the cloud top. This was found to be the most suitable simple representation of the form of the protruding turrets. For the tall, exposed turrets a hemispherically capped cylinder of that radius was still the best representation of the geometry of the turret.

Turret 7/01 (in Figure 15a) shows marked radial expansion during the first four minutes of growth. After a second weak pulse, a steady collapse sets in until it virtually shrinks out of existence by 14:30 MST. It is noteworthy that the rapid expansion is associated with the first impulse in the vertical growth rate, and the radial collapse with the third impulse in the vertical growth rate, the strongest of the three.

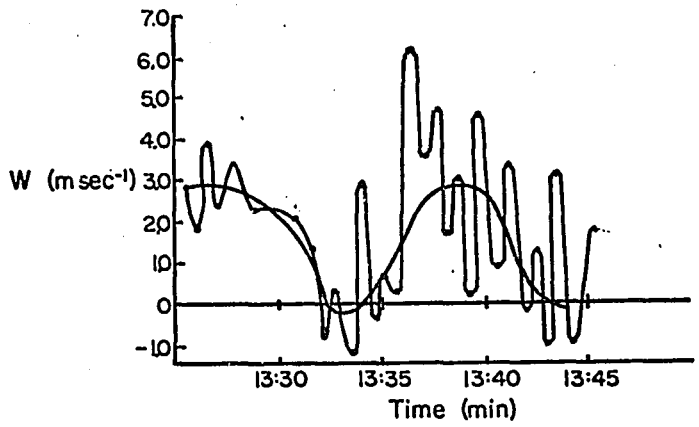

Figure 16: Vertical growth rate of a cloud turret top as observed by Anderson (1960).

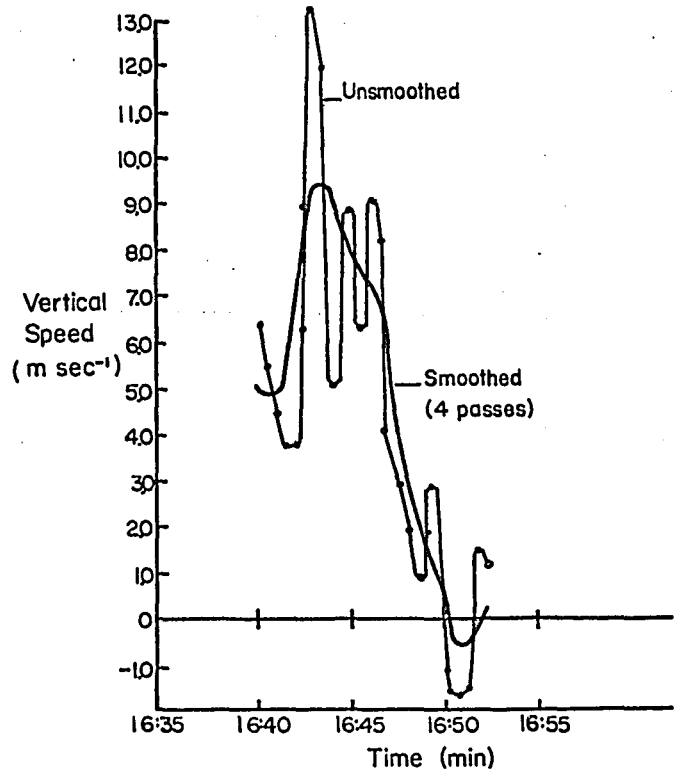

Figure 17: An example of vertical growth rate behavior for a cloud turret top from the present study (turret 10/03).

Turret 7/05 also shows rapid radial growth during the first 3 minutes after emerging, then quickly changes to a gradual decrease in size. The remaining turrets on this day also grew radially then shrank, but less rapidly than 7/01 and 7/05.

On July 10 (Figure 15b) it is seen that turrets 10/03 and 10/04 which show the largest vertical growth, also grow to the largest radial size. Turret 10/03 shows signs of renewed radial growth after 16:50 MST. A glance at the vertical growth curves (Figure 14) reveals an apparent rejuvenation in its vertical growth at about the same time. Turrets 10/01 and 10/02 both shrink out of existence although 10/02 does show some attempt at radial growth during the initial few minutes.

F. Discussion of Vertical and Radial Growth

The only published results of comparable detail on the behavior of cumulus turrets are by Anderson (1960). Figure 16 is from that article, and shows his measurements of vertical speed of a turret top in m sec^{-1} versus time in minutes. Anderson proposed a method of classifying turrets on the basis of the amplitude and frequencies present in these curves of vertical speed. The major frequency component in this, the only example given, had a half-period of 5.5 min, certainly within the range of values measured in this study (2.3 to 11.0 min). Anderson also interpreted the high frequency oscillations with half-periods of 0.51 min and 0.65 min as real fluctuations in vertical speed and suggested that these may be useful as additional criteria in classification. However these values are nearly equal to the sampling interval used by Anderson. Similar fluctuations also existed in the present author's computed vertical growth rates of turret tops (Figure 17 gives turret 10/03 as an example). For reasons discussed

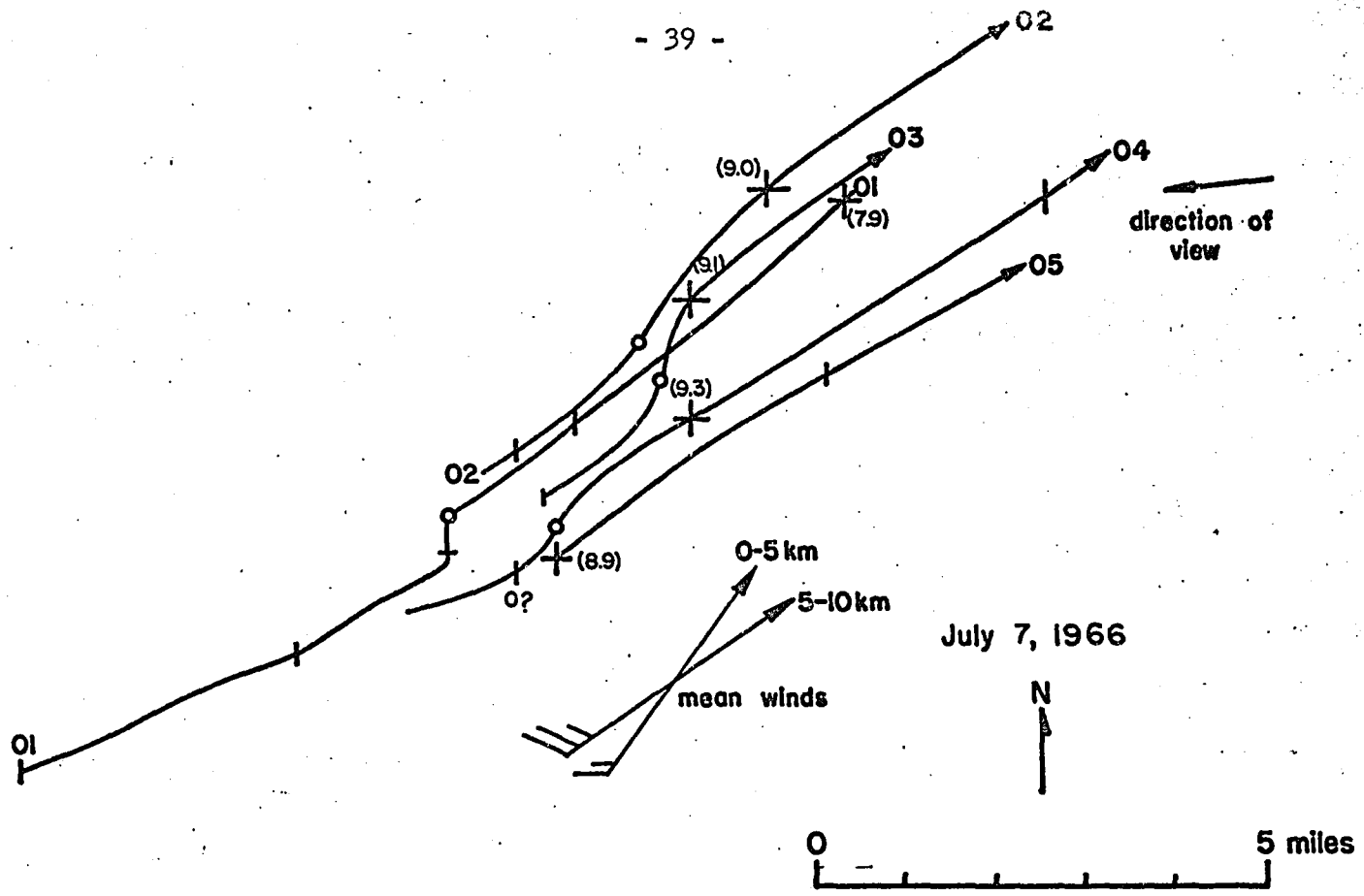

Figure 18a: Plan view map of turret tracks on July 7, 1966. "+" designates each turret's position at 14:40 MST; "o" a turret's position at time of peak upward speed.

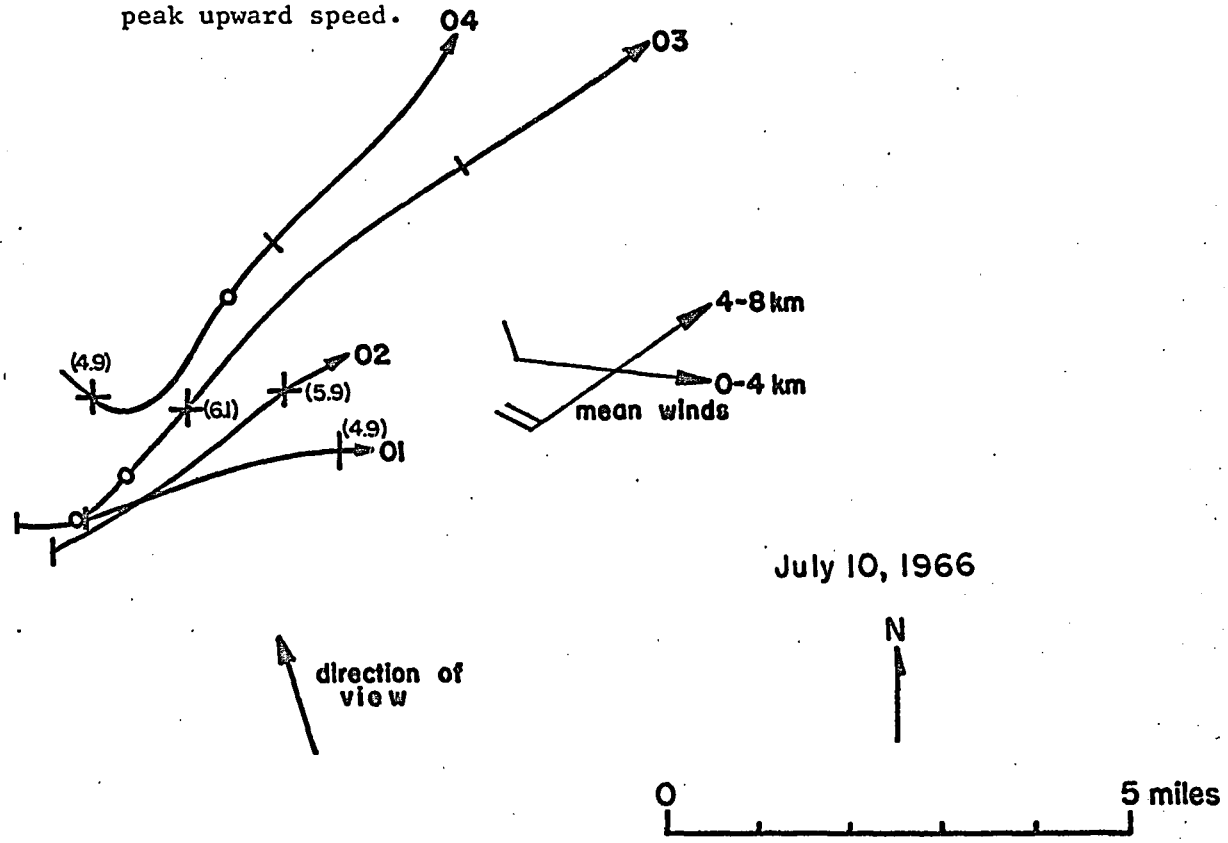

Figure 18b: Plan view map of turret tracks on July 10, 1966. "+" designates each turret's position at 16:45 MST. "o" designates a turret's position at time of peak upward speed of top.

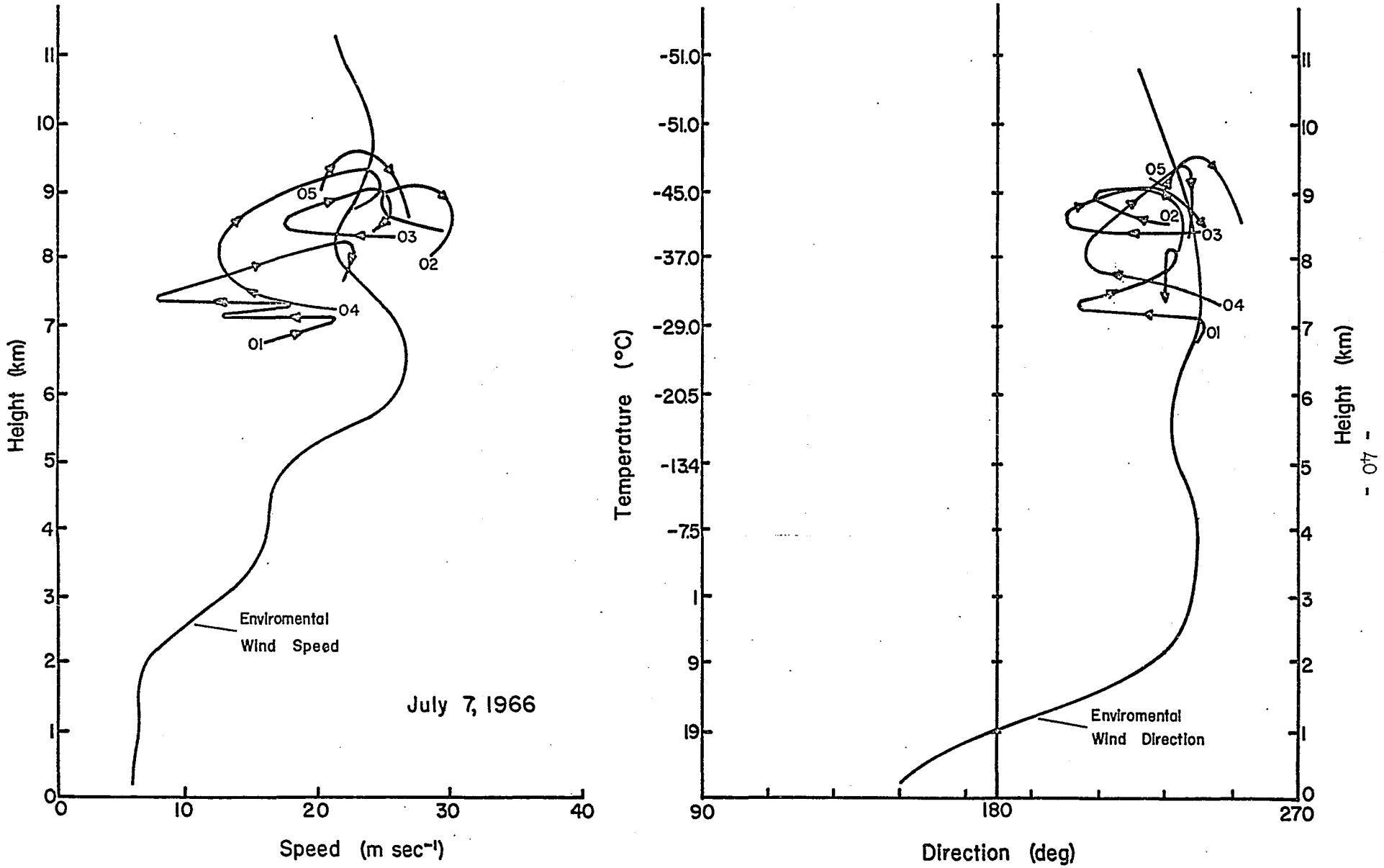

Figure 19: Horizontal speed and direction versus height for the turrets on July 7, 1966. Also shown is the enviromental wind speed and direction versus height. Enviromental temperature is shown on centre ordinate scale.

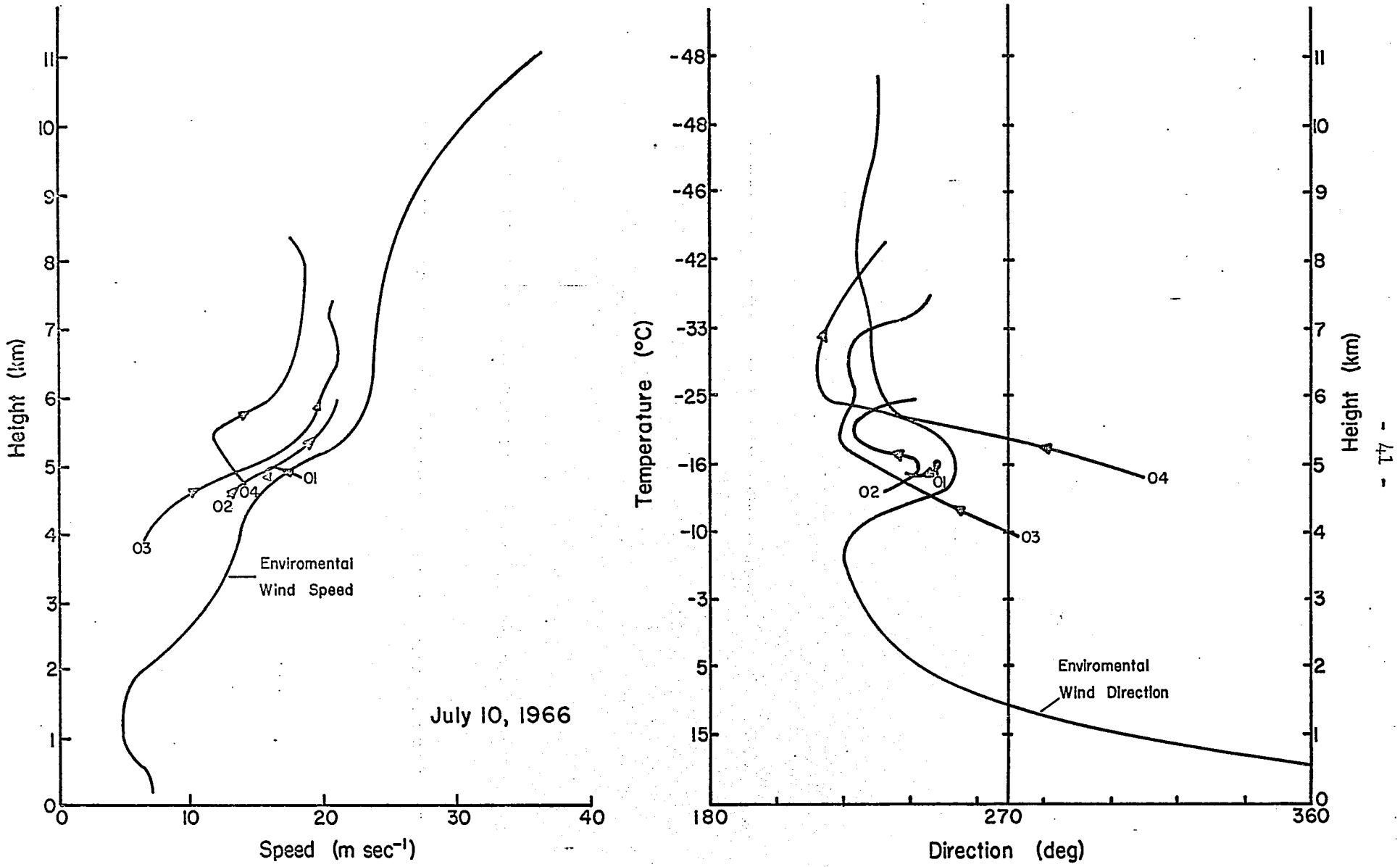

Figure 20: Horizontal speed and direction versus height for the turrets on July 10, 1966. Also shown is the enviromental wind speed and direction versus height. Enviromental temperature is shown on centre ordinate scale.

in Chapter II, Sec. B, fluctuations with half-periods similar to the sampling interval were interpreted as "noise" rather than real fluctuations and were filtered out. However, on July 10, when the sampling interval was approximately 30 sec, some high frequency components still remained even after four passes of the filter. The half-period of these is approximately 1 min and may be real fluctuations, indicative of the existence of behavior on a scale one order of magnitude smaller than that of the turrets themselves. However measurement of this new scale is almost beyond the sensitivity of the technique. Nevertheless, a detailed spectral analysis of data acquired under optimum conditions may reveal more information on such scales of behavior. They may well be indications of the arrival of individual eddies or parcels at the top of the turret.

More will be said about the radial growth of turrets in Chapter VII where models of convective cloud behavior are reviewed.

G. Horizontal Motions of Cloud Turrets

Figure 18a is a plan view of the tracks of the turrets on July 7. It may be thought of as a map of the turrets' positions in space as projected onto the ground. The position of each turret along its track is marked at 5 minute intervals, although measurements were made every minute on July 7 and every 30 seconds on July 10. A large "X" shows the positions of the turrets at 14:40 MST for July 7 and at 16:45 MST for July 10. The number in brackets is the height in km of that turret top above ground at those times. The "o" marks the position of a turret at which it achieved its maximum vertical growth rate. To give a general idea of the vertical wind shear in the environmental winds, the mean winds for a lower layer and an upper layer are shown by the wind arrows in m sec^{-1} (a full barb equals 10 m sec^{-1};

half barb 5 m sec^{-1}). The direction of view from the cameras is shown by the remaining arrow. To fit this map into perspective, the reader is referred to Figure 10 where the area of this turret map is shown as a rectangle on the map of the Project area.

Figure 19 is a detailed plot of the environmental wind speed and direction for July 7 (taken from the Edmonton and Calgary 17:00 MST radiosondes and adjusted for 11:00 MST pilot balloon data and Penhold afternoon pilot balloon ascents). These are plotted as a function of height above ground in km and are in m sec^{-1} and deg azimuth true (direction from which wind was blowing). The horizontal speed and direction of the individual turret tops as computed from the smoothed stereo analysis data is plotted on the same figures. The arrows indicate progress in time. It should be mentioned that a turret's position in space at each observation was taken to be the geometrical centre of the hemispheric cap which had been fitted to the turret top to determine its size.

Figure 18 b and Figure 20 are the corresponding diagrams for the turrets on July 10.

Some rather interesting behavior can be inferred from the results depicted in these diagrams. It is seen that the turrets were not always moving with the environmental wind velocity at their level of the atmosphere. They did ultimately acquire a velocity similar to the environment, but only after rather marked deviations.

For the July 7 group (Figure 19), there was a consistent tendency for a turret to acquire a direction of motion with a more southerly component and a speed of lower magnitude than the environmental winds of the layers

through which it was building. Its maximum deviations in this regard occurred at approximately the time of maximum vertical growth rate of the turret. It will be shown in Chapter VI that this time very nearly corresponds to the time of maximum updraft velocity within the turret. On July 10 (Figure 20) analogous behavior appeared, only this time the horizontal velocities of the turrets, during their periods of increasing vertical growth rate, deviated to a more northwesterly direction and a slower speed than their environment. On both days the deviations were toward the direction of the environmental winds of lower levels in the atmosphere. In five out of the nine cases the velocity of the turret at maximum deviation resembled that of the winds near or below the cloud base.

It is also interesting to note the behavior of turret 7/03 (Figure 18a). It started its vertical growth within 3/4 of a mile of the already established turret 7/04. By 14:40, 7/03 had veered off northward, thereby increasing the spatial separation to more than $1\frac{1}{2}$ miles in the horizontal. A similar behavior is seen for turret 10/01 (Figure 18b), apparently in response to the more energetic turrets 10/02 and 10/03 developing nearby.

H. Summary of Cloud Turret Behavior

A detailed record of the three dimensional behavior of nine turrets has been given. The state of the environments in which they were developing has been described using radiosonde data from Edmonton and Calgary, and surface and 500 mb charts.

The growth of a turret group consisted of a sequence of turret eruptions, each successive turret achieving greater maximum height than its predecessors. Considerable individuality was noted in the vertical

growth rates of the turrets with regard to maximum rates and half-periods. In general though the longer the half-period, the greater was the maximum value of vertical growth rate.

It was observed that vertical growth of a turret was not always accompanied by radial growth.

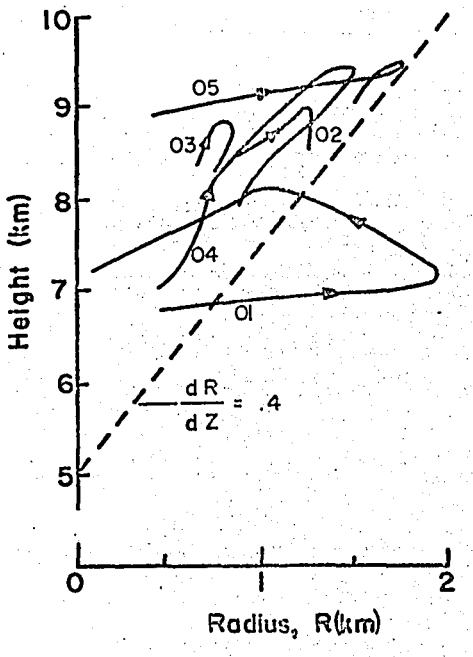

Figure 21a: Plot of turret radius versus height of turret top for July 7, 1966.

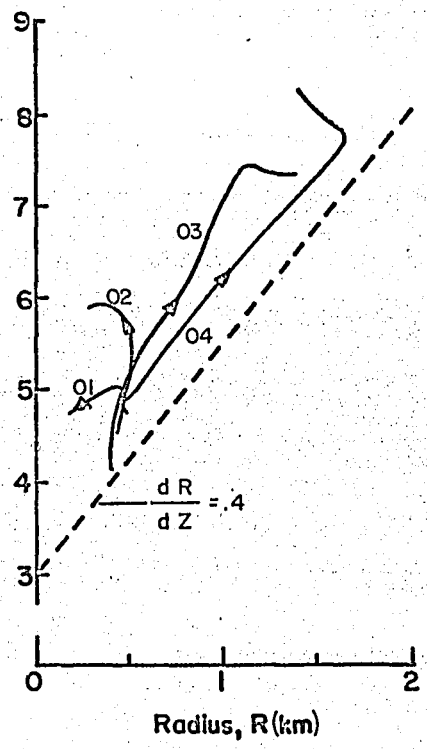

Figure 21b: Plot of turret radius versus height of turret top for July 10, 1966.

Figures 21a and 21b summarize the relations between radial and vertical growth. These are plots of height of turret top in km versus radius of the turret in km. Although initially all turrets show radial growth accompanying vertical growth, some subsequently deviate quite markedly. Turrets 7/01 and 7/05 show rapid radial growth for small vertical growth; 7/01 then changes its behavior radically, at about the time of the third impulse in its vertical growth rate, to radial collapse with vertical growth, and

finally collapse in all dimensions. The small turrets 10/01 and 10/02 appear to be unable to grow radially and finally shrink out of existence.

Essentially then, significant radial growth, initially at least, produces turrets which remain active for longer times and which are able to achieve greater height increments during their growth. The anomalous behavior of the third impulse in turret 7/01 will be discussed more fully in subsequent chapters.

From the present study it may be further concluded that the event of a turret achieving a certain level in the atmosphere results in subsequent nearby turrets surpassing that level with stronger growth rates through the levels previously traversed by the earlier turret. This may be due to the conditioning of a region adjacent to the earlier turret due to mixing between the environment air and the cloudy air of the earlier turret.

On July 10 there was evidence that of four initially co-existing turrets, only two grew into large turrets, possibly at the expense of the remaining two which were not able to produce significant radial growth. Exactly what determines whether or not a turret will continue to enlarge and to grow vertically remains to be clarified.

There was also evidence of nearby turrets interacting to produce anomalous deviations in the horizontal velocity of the smaller turrets.

The vertical acceleration of a turret top is accompanied by deviations in the horizontal motions of the turret top away from its environmental wind velocity toward a velocity more characteristic of those found at much lower levels. Byers and Braham (1949) were among the first to deal with

such behavior. In the simple case of constant wind direction, constant wind shear, and constant entrainment rate they were able to account for some of the observed deviations in echo cell velocity. They applied the law of the conservation of horizontal momentum to the rising air mixed with the entrained air as it rises through a sheared environment.

Their entrainment rate was assumed to be of the form $\frac{1}{M}\frac{dM}{dz}$ = constant, where M is vertical mass flux and z is height. This implies entrainment of the "dynamic" type resulting from the continuity demands of the updraft within the cell; and turbulent mixing at the boundaries, due to the horizontal shearing stress between the updraft and environment vertical speeds. (This latter term is sometimes modelled as being form drag). However, if the updraft is not steady state, it may become zero which means these entrainment terms become zero. Their formulation only explains vertical shear in the horizontal speed of an updraft that ultimately approaches the environmental wind shear, and which always has a horizontal speed less than the environment. Turbulent mixing which must have resulted from the horizontal shearing stress due to this difference in horizontal velocity was not taken into account. The rapid approach of the observed turrets' horizontal motions to near environmental velocities could be the result of such a mixing term, which would operate even when vertical motion has ceased. Since this term, and the term due to shearing stress between vertical motions are of a similar nature, the horizontal behavior offers a valuable clue to distinguishing and evaluating the relative roles of dynamic and turbulent mixing processes in damping turret growth. Hitschfeld (1960), Newton (1966) and Fujita and Grandoso (1966) have recognized this problem; in the latter two papers the authors attempt to evaluate such processes, and to include horizontal behavior in their storm models. Further work with photogrammetric and radar

measurements of horizontal behavior is encouraged, along with work on dynamic models which accept both forms of exchange processes and which include horizontal interactions.

CHAPTER V

RADAR ECHOES ASSOCIATED WITH THE CLOUD TURRETS

A. Introduction

The presence of precipitation size particles (50μ radius or greater) could play an important role in the dynamics of the cumulus cloud turret. Such drops, having a significant terminal velocity, may when associated with an appropriate updraft profile, result in storage of water content at certain levels within a developing cumulus turret. The accumulation must in turn influence the dynamics through loading, as well as influencing the subsequent precipitation growth. Consequently an attempt has been made to determine the nature of precipitation that may have existed within the turrets already discussed in Chapter IV. This will further complete the picture of their overall behavior.

Radar echoes observed with the Decca 3 cm radar located at Penhold, were studied. The limitations of this unit have already been discussed in Chapter III. However, very careful study of the development of initial echoes associated with the turret groups of July 7 and July 10 has permitted a qualitative analysis of a number of echo cells in relation to specific turrets in the groups.

The association between a given echo cell and a specific turret was not always obvious at first as the scale of these structures is only in the order of 1-2 miles, about the same or more than the distances separating the structures. Also the measurement uncertainties of the radar are of the same order. The decision to associate a given echo with a specific turret was made only after consideration of all of the data, including the three-dimensional spacial relationships, and the time relationships between turrets and initial radar echoes. In three cases this led to certain identification

of the echo associated with a particular turret. A fourth was ambiguous. The remainder apparently had no echo directly associated with them during their history.

These are displayed in Figures 22 through 25. These diagrams are vertical cross-sections of the cloud turret top and the associated radar echo as they appear when projected onto the vertical plane a-b shown in the plan view insertion in each figure. The insertion (upper corner of the figure) also shows the plan map of that particular turret's track and a schematic representation of the echo cell as it appeared at the time shown beside each echo. On a given day, each turret is projected onto the same plane a-b. The individual tracks are taken from the composites in Figure 18 of Chapter IV, Sec. F.

The vertical cross-sections show height above ground in km versus distance along line a-b in statute miles. The turret top is depicted in cross-section at one-minute intervals, the bold outlines designating the cloud top at the times approximately corresponding to the radar observations. Times are given in Mountain Standard Time in hours and minutes. In the cases having tall echoes, which required a significant amount of time (1-2 mins) to scan from base to top, the times at base and top are shown beside the echo profiles.

It should be noted that no attempt is made to remove the echo tilt due to the horizontal motion of the echo during the 1-2 minutes required for the radar to scan vertically through the height of the echo. The tilt that would have resulted from a uniform echo speed parallel to the direction a-b for speeds of 10 and 30 m sec^{-1} is indicated by the slope of the lines

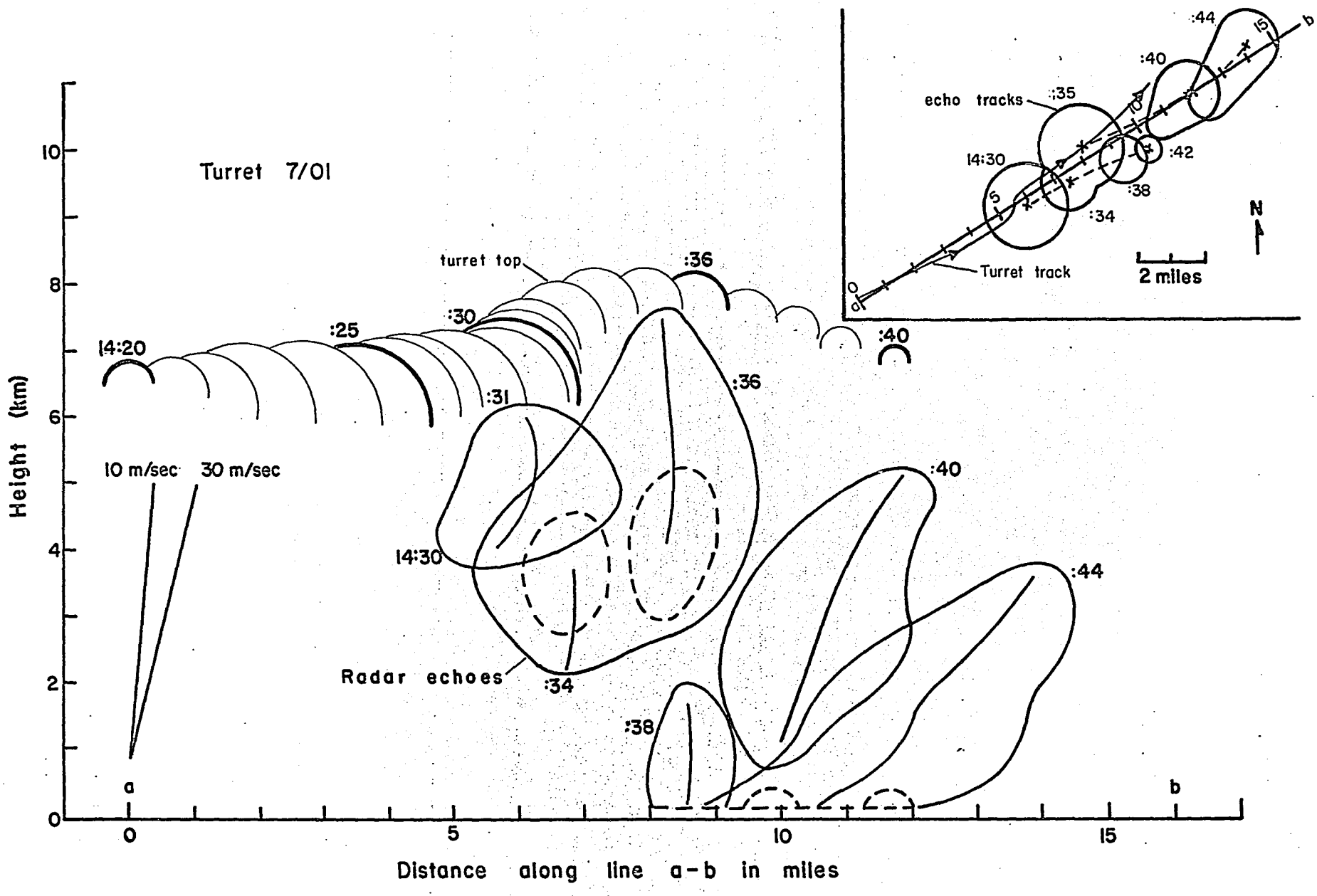

Figure 22: Vertical cross-section of cloud turret 7/01 and its associated radar echoes. Insert shows map of horizontal track of cloud turret and of radar echoes. See text for details of the format.

in the lower left corner of these figures. Since the motions were of this order, this suggests that some of the echoes may have been actually tilted up-wind at mid and upper levels, at least at the earlier stages of their development. Although not attempted here, techniques of computing particle sizes from trajectories in known vertical wind shears may give more information on the nature of the precipitation in the echoes. Or conversely, with assumptions as to particle size, an estimate of the internal shear may be made.

B. The Results

It was mentioned in Chapter IV that turret 7/01 on July 7 may have consisted of two or three separate events occurring very close together, resulting in the emergence of a new turret out of the top of another flattened turret. This complexity also appears in the radar echoes associated with it. In Figure 22 it is seen that what is initially a rather broad, shallow echo develops into two cores by 14:35 MST. These appear as though two cells may be present by this time. One could have developed during the first or second upsurge of the turret top; the larger cell developing in association with the third most vigorous upsurge of the cloud top. The initial echo appears between 3.8 and 6.2 km and is 1.2 km below the visual cloud top. The second cell spreads up to at least 7.6 km, only 0.6 km below the maximum height reached by the visual cloud top. It is during the stage of virtual collapse of the visual turret that the echo descends, resulting ultimately in precipitation reaching the ground by 13:38 MST.

Unfortunately the exact nature of the precipitation is unknown as reports from the volunteer survey network were incomplete in this area. The survey does indicate that areas of pea- and grape-size hail occurred about 30 miles further along the track of this storm.

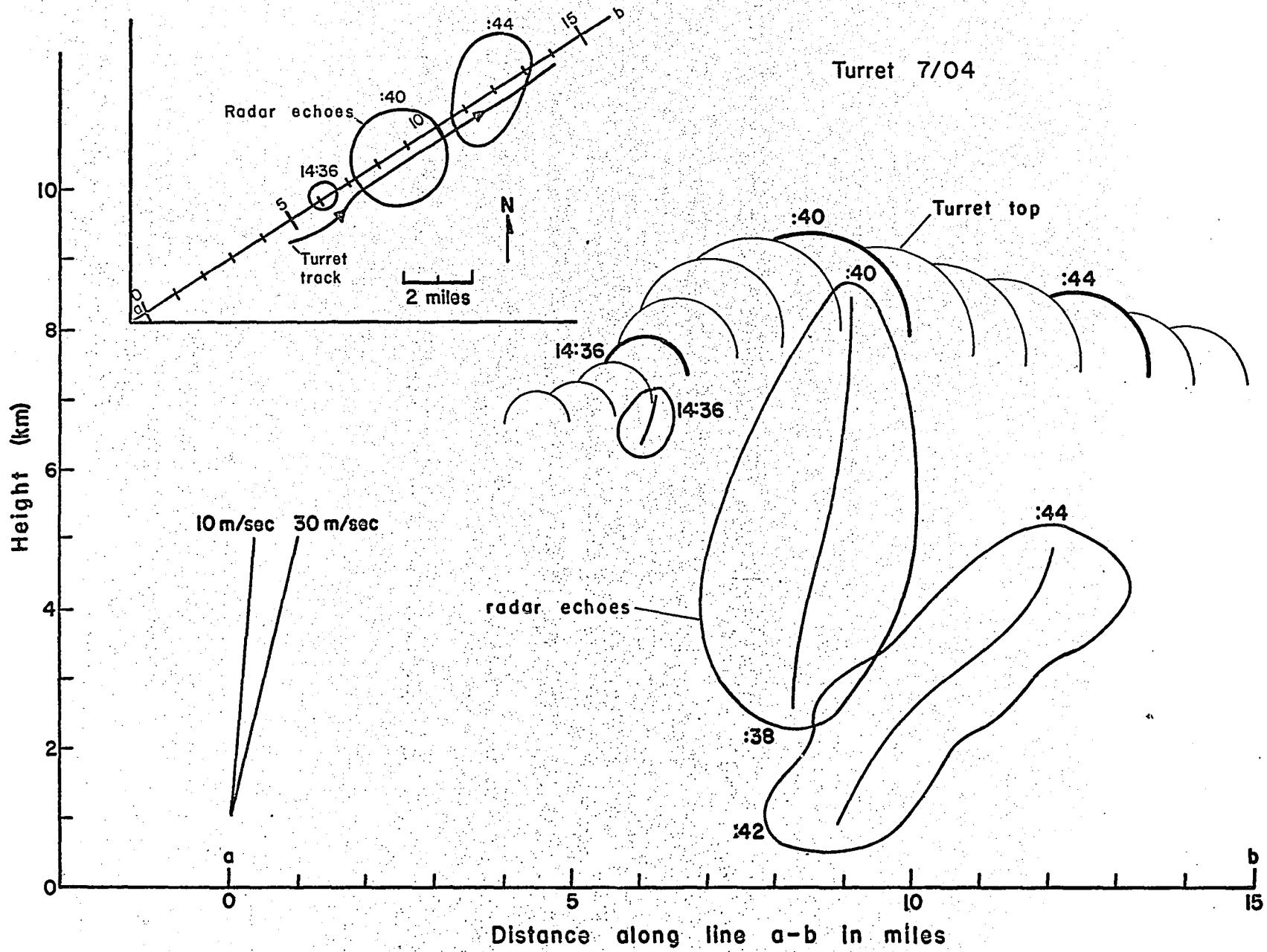

Figure 23: Vertical cross-section of cloud turret 7/04 and its associated radar echo. Insert shows map of horizontal tracks of cloud turret and radar echo. See text for details of format.

Turret 7/04, shown in Figure 23, appears as a single echo on the radar return. Initial echo develops between 6.2 and 7.2 km, and grows rapidly up, down and radially during, and subsequent to, the period of maximum vertical growth rate of the visual cloud turret. The visual turret does not collapse as rapidly as did 7/01 when the echo shows downward motion of its top. The echo top achieves at least 8.6 km which is 0.7 below the maximum height of the turret top.

The third echo cell on July 7 is associated with turret 7/05. This is shown in Figure 24. The echo makes its first appearance at 14:45 MST and is by this time already quite large, suggesting it may have started developing very shortly after 14:40 MST. Once again the echo develops during the time of vertical growth of the turret. Initial echo extends from 3.1 km to 6.9 km and was 2.6 km below the visual cloud top at that time. No subsequent positions are shown because by 14:49 MST the radar return was composed of too many echoes, too close together, to be resolved by a radar with a horizontal beam width of 4° (approximately 3 miles at these ranges).

Figure 25 is a similar display for the only radar echo which develops during the period of the photographic observations of the turret group on July 10. Turrets 10/01 - 10/04 have no echo associated with them. First echo appears late in the history of turret top 10/04. Initial echo appears between 4.3 and 5.8 km, but not until 16:58 MST, about five minutes after the turret 10/04 has started to shrink. Hence the association between the turret and the echo is not as clear in this case. It would seem to have developed along the track of 10/04, but the correspondence in time is not as observed for the July 7th examples. Possibly the echo was associated

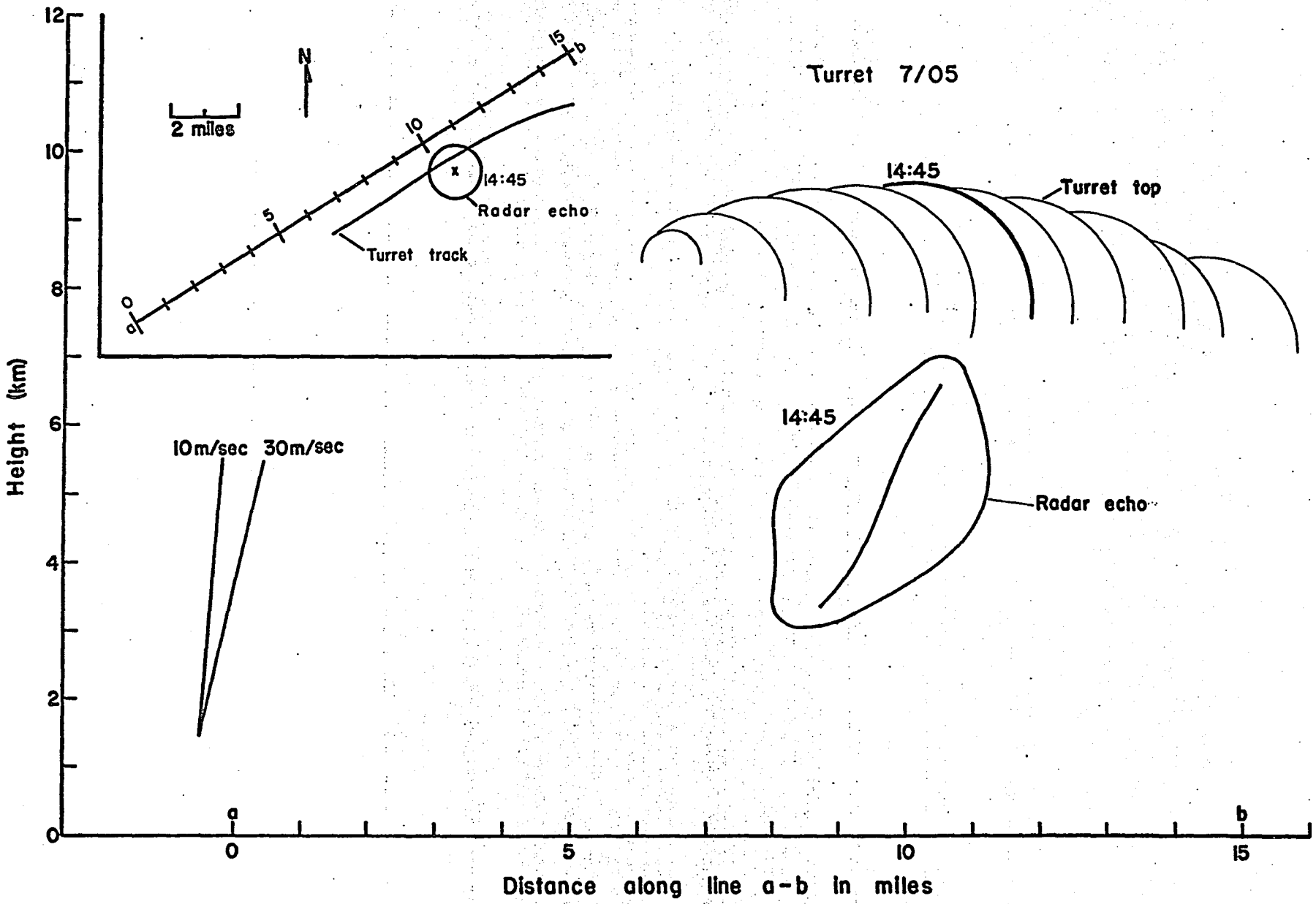

Figure 24: Vertical cross-section of cloud turret 7/05 and its associated radar echo. Insert shows map of horizontal tracks of cloud turret and echo. See text for details of the format.

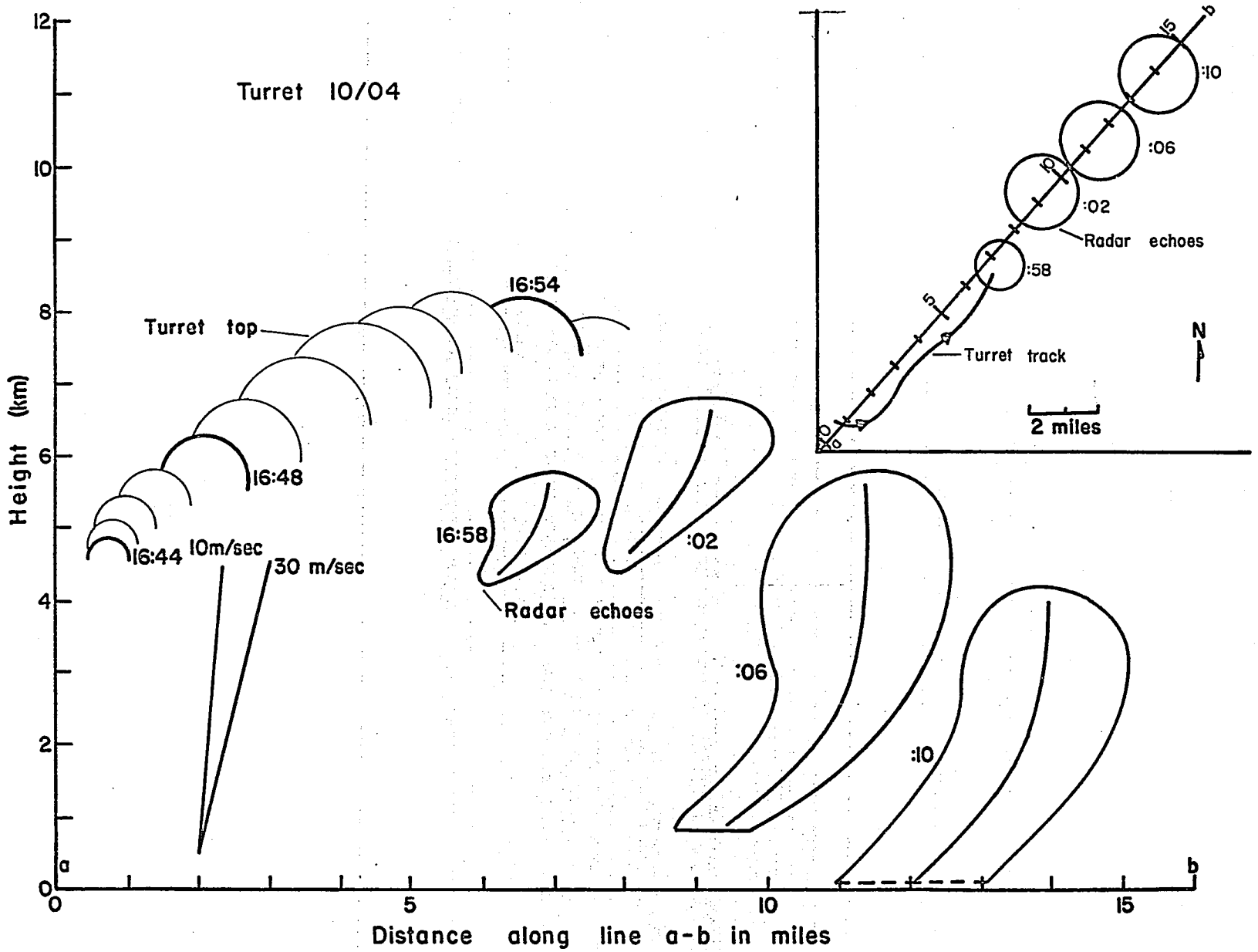

Figure 25: Vertical cross-section of cloud turret 10/04 and its associated radar echo. Insert shows map of horizontal tracks of cloud turret and echo. See text for details of format.

with another unseen turret developing after 10/04 but along a very similar track. On the other hand, this time lag may indicate a fundamental difference in echo development characteristics for this turret.

It is hoped that with the aid of better quality radar data, this type of analysis may be extended further into the life of a storm. Chisholm (1966) has already done a comprehensive study in the behavior of "high intensity cores" which he observed with 10 cm, narrow horizontal beam radar in Alberta storms. The scale of these cores, about 3-6 km and 10-30 min life span, suggests that they are similar to the cells observed in this study and would likely have had visual cloud turrets associated with them. Future work on relating first echoes and high intensity cores with visual turret behavior should be emphasized with a view to studying the detailed interactions between the development of precipitation cores and the dynamics of cloud turrets.

C. Discussion

Table I summarizes the conditions surrounding the occurrence of first echo with respect to the height of its top. Turret 01a refers to the small first echo in Figure 18, page 37; 01b to the second echo cell which protrudes out to the NE of 01a by 14:35 MST. "w_a" refers to the adiabatic liquid water content of a rising air parcel (computed from the representative tephigram in Figure A1 or A3, using a mean mixing ratio line between the surface and 700 mb to arrive at a convective condensation level). "Temp." refers to the cloud temperature also at the level of the echo top, and is taken from the tephigrams. "W_{max}" is the maximum vertical growth rate of the turret top and is taken as a first approximation of the updraft speeds that might have been associated with the turrets' growth

(but note that in Chapter VI it is found that this is generally less than the pseudo updrafts that are computed for other levels within the turret below its top). The figure in brackets under "Echo Top" is the distance of the top of first echo below the visual cloud turret top in km.

TABLE I

Turret	Echo Top (km)	W_a (gm kgm^{-1})	Temp (deg C)	W_{max} (m sec^{-1})
July 7				
01a	6.2 (1.3)	5.8	-21	1.5
01b	7.6 (0.6)	7.0	-34	3.4
04	7.1 (0.8)	6.7	-29	7.6
05	6.9 (2.6)	6.5	-27	4.2
July 10				
04	5.8 (2.0)	5.4	-23	8.9

T.W.R. East (1957) described an inherent precipitation mechanism in developing cumulus cloud in which condensation and coalescence occur simultaneously. He showed that the first 50μ droplets would appear at about the 6 gm kgm^{-1} level and detectable radar echo would develop soon afterwards. This was supported by observational evidence. He also predicted that the larger the magnitude of the updraft, the higher would be the adiabatic liquid water content at the level of first echo. With Easts's model in mind, the growth of the precipitation within these turrets may be discussed.

Turret 7/01a is probably the result of convection which reaches an equilibrium level below the top of the weak stable layer around 6.5 km. The associated updrafts would not have been too strong, but after two impulses and a radial spreading of the turret, the water contents at these levels would approach the adiabatic values, nearly 6 gm kgm^{-1} (Table I). Therefore precipitation size particles rapidly develop and the radar echo appears.

Recent experimental evidence exists (Vali, 1967) that, for samples of Alberta rain water, virtually all drops of 1 mm diameter or more could be frozen at temperatures below -15 to -20 deg C. The subsequent release of latent heat of fusion would raise the cloud air temperature by 0.3 deg C per gm kgm^{-1} of liquid water content frozen. This additional buoyancy, introduced into the cloudy air below 6.5 km, could have resulted in a new convective turret being set off, and surpassing the top of the weak stable layer at 6.5 km (see tephigram, Figure A1). Such a turret having little or no upward flux from lower levels would tend to collapse radially due to vertical divergence of the cloudy air, and then vertically after reaching its new limiting level. The original 1 mm drops, having a terminal velocity of about 4 m sec^{-1}, would fall out also decreasing the parcel loading and assisting vertical growth. Some of the original smaller droplets plus new growing ones would appear in the new turret as an echo. This could account for the complex behavior of turret 7/01 on July 7.

Turrets 7/04 and 7/05 on July 7, having more vigorous updrafts than 10/01a developed echoes at levels of higher liquid water contents. Rapid vertical spreading of these echoes (Figures 23 and 24) occurred. East (1957) was able to explain such behavior by assuming that some of the cloud droplets in a rising parcel become deposited on the way up and grow at these levels concurrently. Thus radar detectable droplets may appear in rapid succession at many levels and show up as a rapid vertical spreading of the radar echo. While the turrets on July 7 were very closely grouped, and rise from an extensive cloudy region extending up to 5 to 6 km, on July 10 the turrets were far more exposed (see Figure 12). Hence, while near-adiabatic values of liquid water content may have been possible on July 7, mixing could have reduced more significantly the liquid water

contents in the turrets on July 10. The development of precipitation in turret 10/04 on July 10 could have been arrested, resulting in echo appearing a while after the cloud turrets growth period, and at lower levels. Once precipitation had formed, freezing may have helped to initiate a new updraft within the remains of the old turret, explaining the rise seen in the echo between 16:58 and 17:02 MST in Figure 25.

Saunders and Ronne (1962) have compared radar echo tops with the visual cloud tower tops, as measured by theodolite and photogrammetry. Their observations of 37 cases with radar tops between 6 and 16 km show the height of the visible cloud to exceed the height of the echo top by 0.1 to 1 km. For cases with radar tops below 10 km (a sample more suitable for comparison with the turrets observed in this study) the difference never exceeds 0.6 km. Our observations show the echo top to not come within 0.6 km of the cloud top. Saunders and Ronne were using measurements from an R-scope display, of towers within 1-2 min of reaching their peak height, and were of storms in Florida. These Alberta measurements, made at fixed 4.3 min intervals from PPI displays, would have included at least some observations within 2 min of reaching peak height.

The radar used by Saunders and Ronne was a 10 cm, 500 kw unit with a half-power beam width of 1.0 deg in the horizontal and vertical. They computed the minimum detectable reflectivity to be 10^{-1} mm^6 m^{-3} at a range of 20 miles. Henry (1964) gives the minimum detectable reflectivity of the Alberta 3 cm Decca radar as 5.5×10^2 mm^6 m^{-3} at this range. Thus, while the measurement uncertainties in height of echo top of approximately $\pm$ 0.5 deg elevation ($\pm$ 300 m at 30 miles range) are

comparable for these two units, the sensitivities are not.

With their more sensitive radar Saunders and Ronne were able to conclude that, in the upper 0.15 to 0.45 km of cloud turrets, the average equivalent reflectivities range from a few tenths to a few $mm^6 m^{-3}$. Undoubtedly such low reflectivities were not being detected by the Alberta radar and this may easily account for the larger differences between height of cloud top and radar echo top reported in the present study.

Since the vertical profiles of radar reflectivity for these Alberta cloud turrets are unknown, it is not possible to evaluate quantitatively how much greater an underestimate was made by the low power Decca radar of the height of echo tops. Reference is made to median reflectivity profiles for echo cores of New England storms as computed by Donaldson (1961). These suggest that a difference in mimimum detectable reflectivity of a factor 10^3 should represent a height difference of at least 3.6 km. Since the discrepancy between measurements made with radars whose sensitivities differed by more than a factor 10^3 was apparently much less than 3.6 km (and probably closer to about 0.5 km), it suggests that the vertical gradients of radar reflectivity in the upper reaches of individual echo cores are likely much larger than those indicated by Donaldson's "median" profiles.

In addition, the results of the present study indicate that the height of the radar echo top is not always a good estimate of the height of the cloud top. Even within a few minutes of the time of reaching maximum height the errors may range from a few tenths of a km for mature echoes within large undiluted turrets observed with a sensitive radar, (minimum detectable reflectivity 10^{-1} mm^6 m^{-3}) to a few km for initial

echoes[1] within smaller turrets observed with less sensitive radars.

In terms of quantitative precipitation measurements, such errors are relatively inconsequential because they occur at such low equivalent reflectivities (rainfall rates). However in terms of convective cloud behavior, radar echo dimensions or growth rates do not necessarily depict the total volume involved in cloudy convection. The errors are least serious when the echo achieves its maximum volume. Hence the total volume swept out by a sequence of instantaneous measurements of echo volume during a period of time, more nearly represents the volume involved in cloudy convection over that period than would any single measurement or average of measurements. The value of instantaneous measurements in this regard is questionable, although in a statistical sense the echo volume may consistently represent some determinable fraction of the total cloud volume.

1 A recent paper by Harrington (1967) gives values of cloud top height minus height of first echo which range from 0.3 km to 2.1 km for 10 cases. Minimum detectable reflectivities were approximately 5 x 10 mm^6 m^{-3} for the 3 cm height finding radar unit used to obtain the measurements. Values for the four cases in the present study range from 0.6 to 2.6 km.

CHAPTER VI

THE INDIRECT MEASUREMENT OF UPDRAFTS

A. The Method

The behavior of a number of cloud turrets has been discussed in detail. These results came from direct measurements of the dimensions and location in space of the turret top. The actual properties and behavior of the cloudy air within the turrets could not be observed. However an estimate of the updrafts within the turrets will now be made.

The air motions which take place within these turrets are inferred by modelling the air flow producing the visual turret. In this case it is assumed that changes in the visual dimensions due to evaporation were much less than those due to air motion. Also it is assumed that there is no net transport of air through the visual cloud boundaries of the turret. Finally the turret's geometry is modelled as being a cylinder of radius $\frac{S}{2}$, capped with a hemisphere of radius $\frac{S}{2}$. (This is consistent with the manner in which the size of the turret, S was measured, i.e. by fitting a semicircle over the cap of the cloud turret on the film.) Anderson (1960) used a similar model in his discussion of cumulus turrets. Figure 12 (page 29) shows two turrets which were well exposed, and it is seen that such a hemispherically capped cylinder is not a bad approximation to the geometry of such turrets.

Under these assumptions, the increase in cloud volume above a given level, z_o, is due only to a volume flux through the base of the

turret cylinder.[1] If V is the total cloud volume above level z_o as a function of time, then $\frac{dV}{dt}$ is the rate of increase of cloud volume above z_o; and the volume flux would equal $\frac{dV}{dt}$ divided by the horizontal area of the base πr^2, where r is the radius of the turret cylinder. But a volume flux through level z_o is equivalent to a mean updraft velocity, Uo, averaged over the cross-sectional area of the turret at level z_o.

The five largest turrets of the nine analysed were chosen for these computations; the maximum volumes above the initial levels of observation for the remaining four being considered too small to warrant this type of study. The level, z_o, was chosen in each case as the first even 500 m level below the height of the first observation. The volume, V, was computed at one minute intervals from the expressions:

$$V = \pi r^2(z - z_o) - \frac{\pi r^3}{3}$$

for $z - z_o > r$, a hemispherically capped cylinder; and

$$V = \pi(z - z_o)^2 r - \frac{\pi(z - z_o)^3}{3}$$

for $z - z_o < r$, a segment of a sphere where r is the radius of the turret and z is the height of the turret top.

1 The volume expansion of air parcels rising in the turret due to the decrease in the ambient pressure with the height is also neglected. The fractional rate of volume change due to this term would be approximately $\frac{-\overline{U}}{\overline{T}}$ ($g/R^* + \frac{\partial \overline{T}}{\partial Z}$) where $\overline{T}$ and $\overline{U}$ are a representative cloud temperature and updraft speed respectively. So this term is $-\overline{U}\,(10^{-4})$ sec^{-1} for typical values of $\overline{T} = -23°C$; $\frac{\partial \overline{T}}{\partial z} = 9°C\ km^{-1}$ Measured fractional rates of volume increase: $\frac{1}{V}\frac{dV}{dt} = \frac{UoAo}{V} \doteq \frac{2Uo}{r}$. r is generally less than 2 km. Hence: $\frac{1}{V}\frac{dV}{dt} > Uo(10^{-3})$. Also, we may take $\overline{U} \doteq \frac{Uo + W}{2} < U_o$. Therefore generally $\frac{1}{V}\frac{dV}{dt} >> \overline{U}(10^{-4})$.

B. Turret Growth in Terms of Cloud Volume

The results are displayed in Figure 26. This is a plot of cloud volume, V, in km^3 versus time in minutes from the time of the initial observation. It seems that three types of volume growth behavior were observed. Turret 10/03 showed a rapid increase in its volume growth rate (i.e. $\frac{dV}{dt}$, the slope of the curves in Figure 26) during the first 5 min, followed by decreasing growth rate. The volume became steady near 12.5 km^3 after about 10 min then increased again. The renewed growth of 10/03 during the last few minutes of its visual history was noted earlier in Chapter V. Turrets 7/04 and 10/04 behaved similarly during the first 5 min, but continued to increase their growth rate up to about minute 7, then rapidly changed to decreasing volume with time. The third type of behavior was exemplified by turrets 7/01 and 7/05. These volume curves are much flatter indicating generally smaller values of the volume growth rates during their history. The reversal from volume increasing with time to decreasing with time is much more gradual. It was suggested earlier that turrets 7/01 and 7/05 were associated with growth in the vicinity of more stable layers in the environment on July 7; one layer extending below 6.5 km and a thin layer between 8.3 and 8.5 km. Note that the levels of initial observation of 7/01 and 7/05 were 6.5 and 8.5 respectively, and of 7/04, 7.0 km.

Although more examples are necessary, first indications are that of the major turrets, those which have precipitation cells associated with them behave differently from those with no detectable echo in their vicinity. The time of occurrence of first echo associated with each turret is indicated on the volume curves in Figure 26 with a large X.

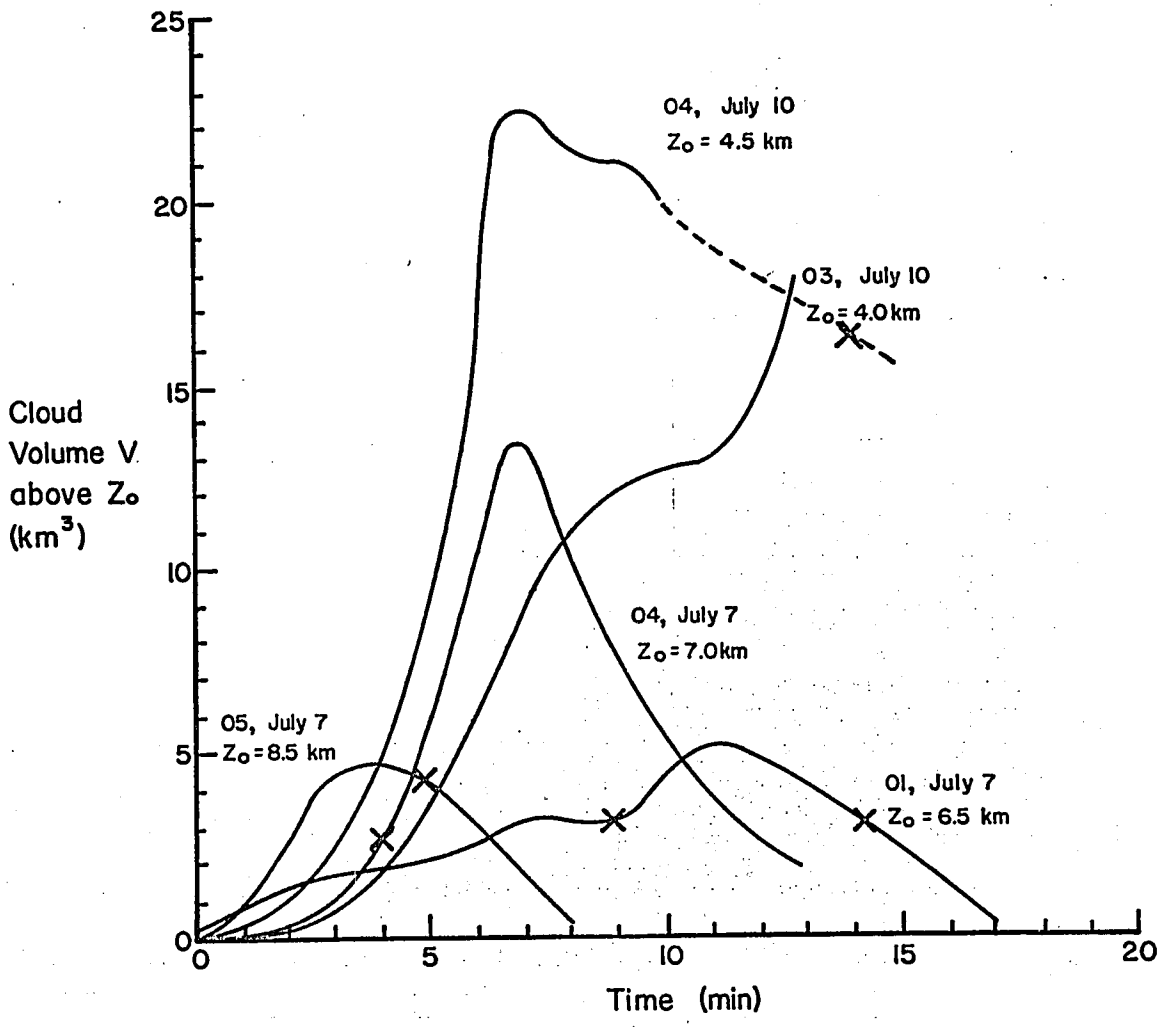

Figure 26: Volume of cloud turret above reference level z_o, versus time for the larger turrets on both July 7 and July 10, 1966. "X" designates the time of appearance of a radar echo cell in association with the cloud turret. Note that turret 03, on July 10, had no echo associated with it, and that the curve for turret 04, on July10, was extrapolated to the time of echo appearance.

Those with echo show a reversal in the volume growth rates, so that some of the cloud volume that is transported up, apparently is returned to lower levels. Alternatively a local sink for cloudy air could have developed in those turrets with developing echoes. This condition is not allowed for in the assumptions for the turret model. Turret 10/03, with no echo associated, showed renewed growth after 10 min rather than the decrease observed when echo was associated.

There were also indications that turrets, growing from levels in which the environment was more stable relative to other levels, showed a more gradual growth in cloud volume and achieved much lower values of maximum volume transport above the level of initial observation. It would seem that such turrets spread radially, and may play a vital role in the areal development of a storm. This radial spreading of moisture over a large area at mid-levels would mean that subsequent turrets are more likely to be growing through a nearly saturated, or conditioned, environment. This moist environment air, when entrained into subsequent turrets, would be less effective in diluting the buoyant cloudy air and hence permit them to maintain growth through this region.

C. Updraft Speeds

Having assumed no net loss or gain of cloudy air in a turret except that which passes through its base, it is possible to say that the volume growth of a turret above any level would be due entirely to an updraft through that level.

Values of this updraft, U_z, were computed not only at z_o, but also for the observed volume growths above successively higher levels up the

turret cylinder. Hence the variation with time of such a pseudo-updraft can be described for any level. Also the updraft's variation with height at any instant in time can be described (vertical updraft profiles).

Figures 27 through 31 are composite depictions of the time-height variations of this updraft, measured at 1 min time intervals and 500 m height intervals. The height scale in km appears on the left; the updraft scales in m sec^{-1} for each 500 m level on the right. The abscissa is time in minutes. The outline of the turret is shown at intervals to depict the manner in which the turret was growing in response to the updrafts within it. The dashed line is a plot of the height of the turret top versus time.

One of the main differences among the five turrets is in the time variation of the updraft at any level. Turret 10/03 (Figure 28) showed a rapid increase, changing to a gradual decrease in updraft speed. It did not develop a downdraft but rather showed rejuvenation near the end. Turrets 7/04 and 10/04 (Figures 27 and 29 respectively) showed more gradual increases, but steeper decreases in updraft after reaching a maximum; they did indeed achieve downdrafts. The maximum updraft speed at level z_o, the lowest level of observations, was 24 m sec^{-1} for 10/03, 18 m sec^{-1} for 10/04 and 16 m sec^{-1} for 7/04. The min values were 0.2, -3, and -7 m sec^{-1} respectively. Once again note that it was turret 10/03 which could not be associated with a radar echo, while the other two were. Hence it appears that the updrafts were showing a response to the development of precipitation within the turrets.

It should be mentioned that in one sense these pseudo-updrafts could be overestimates of the true values, as most researchers agree that

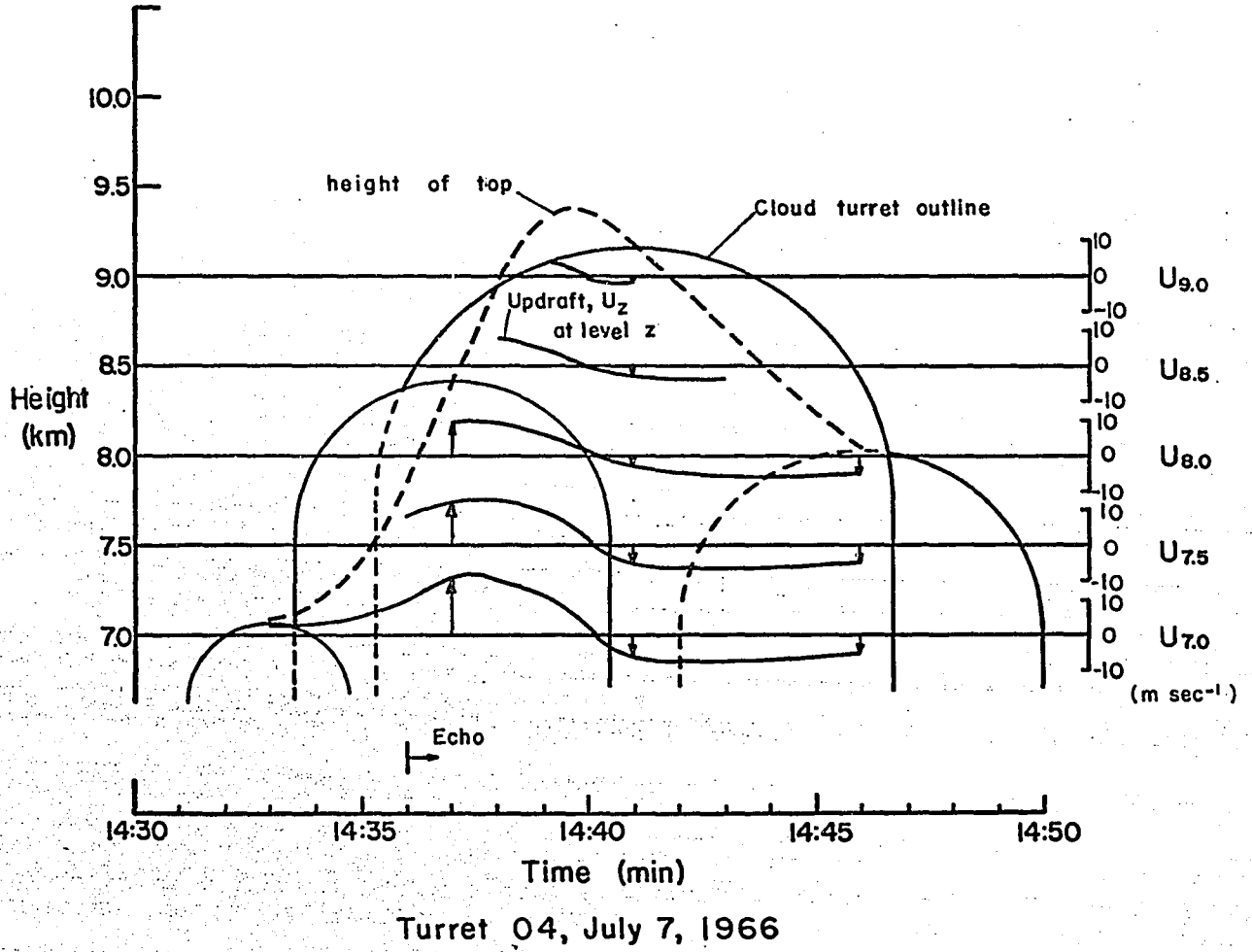

Figure 27: Composite diagram of computed updraft speeds at 0.5 km height intervals as a function of time for turret 04, July 7. The associated cloud turret is outlined at 4 min intervals. The time of echo appearance is also indicated.

Leaf 71 is not Missing

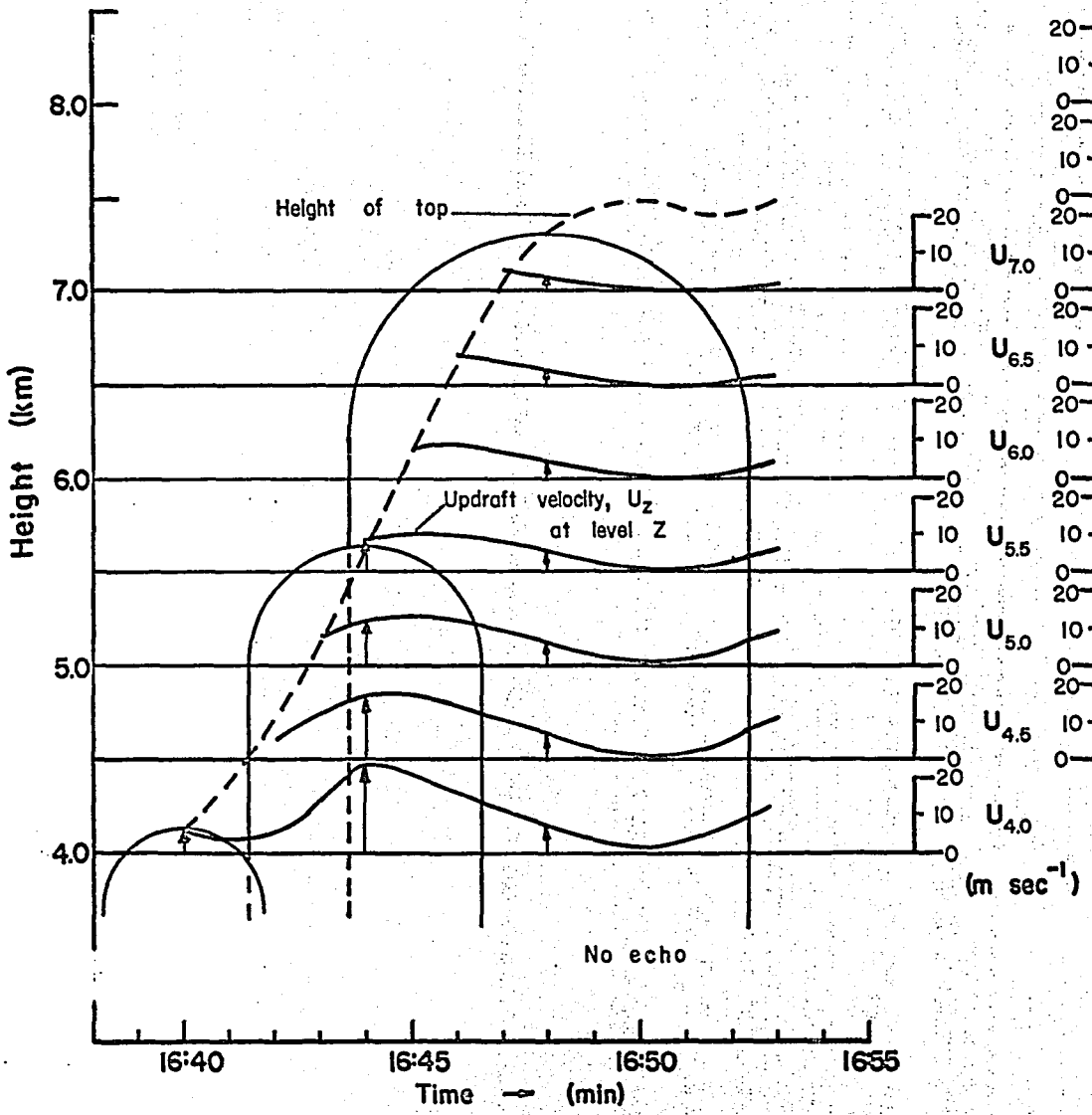

Figure 28: Computed updraft speeds at 0.5 km height intervals as a function of time for turret 03, July 10.

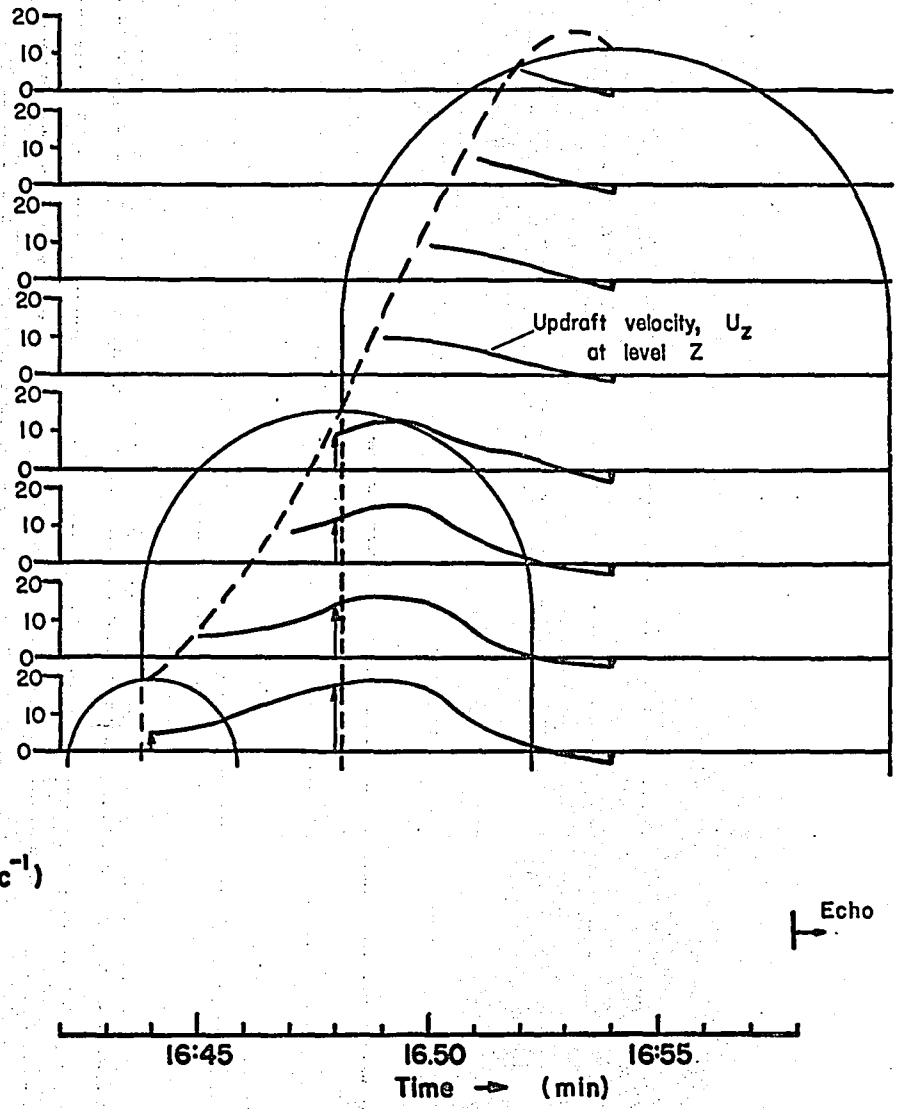

Figure 29: Computed updraft speeds at 0.5 km height intervals as a function of time for turret 04, July 10.

there would be a net entrainment into a developing convective cell (Byers and Braham, 1949, Scorer and Ludlum, 1953, Malkus, 1960). Hence some of the volume increase above a level could be due to a net influx through the sides, thus reducing the computed updrafts through the base. On the other hand, U_z is an areal mean over the base of the turret, and would be an underestimate of the maximum updraft speeds which might be found near the axes of the turrets. Generally speaking the walls of the turrets were observed to rise much less rapidly than the turret's tops, even subsiding in some cases.

Turret 7/01, shown in Figure 30, behaved quite differently. The maximum updraft speed at z_o, 6.5 km, was only 4.1 m sec^{-1}. The bulk of the turret volume growth was accomplished through radial expansion of the turret top, with only a small rise of the turret top during the first two impulses. The third impulse, which was the most vigorous in terms of the vertical motion of the turret top, was actually accompanied by the development of a strong downdraft within the turret. It started at lower levels, then spread upward. This resulted in a radial collapse of the turret at first, then vertical collapse as well.

For turret 7/05 (Figure 31) the maximum updraft was 17 m sec^{-1} at 8.5 km. Apparently the updraft developed while the turret was below this level as it was declining rapidly at the point of first observation. This resulted in a large radial growth and vertical growth during the first couple of minutes of observations. As with other turrets having echo associated, this rapid initial deceleration of the updraft is followed by the gradual development of a downdraft.

Leaf 74 is Total Missing

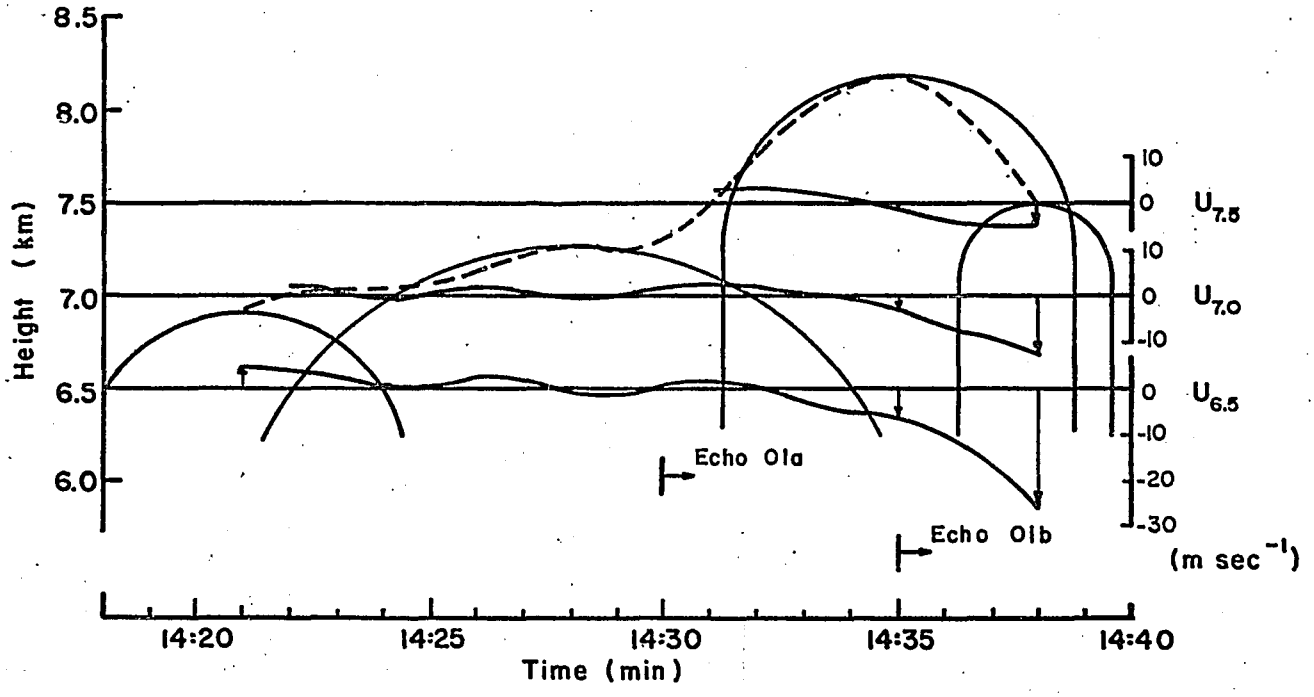

Turret 01, July 7, 1966

Figure 30: Computed updraft speeds at 0.5 km height intervals as a function of time for turret 01, July 7. The associated cloud turret is outlined at 7 min intervals. The time of appearance of the two associated radar echoes is also indicated.

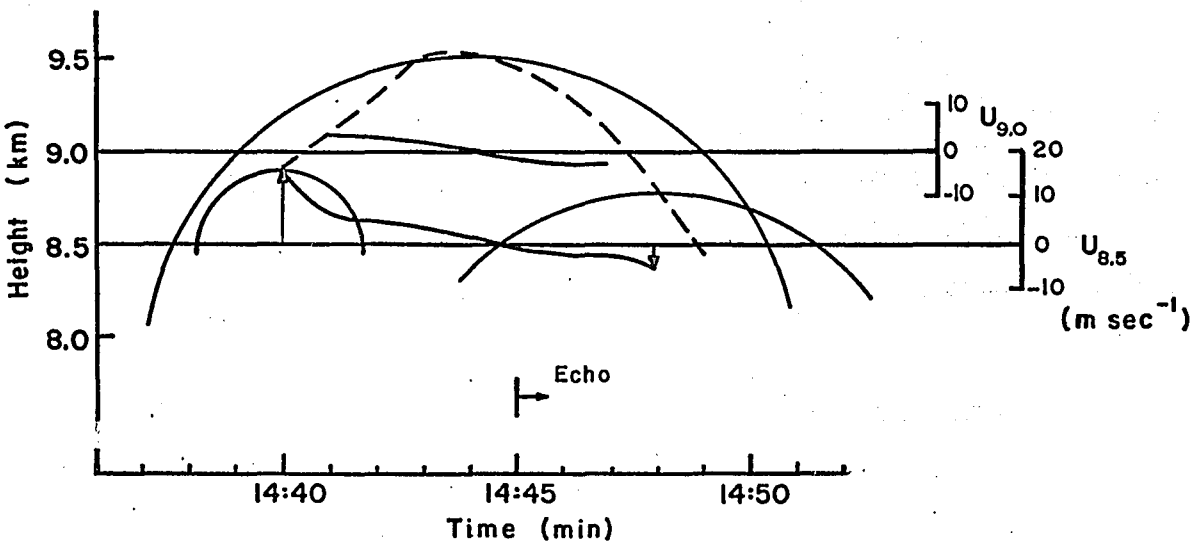

Turret 05, July 7, 1966

Figure 31: Computed updraft speeds at 0.5 km height intervals as a function of time for turret 05, July 7. The associated cloud turret is also outlined at 4 min intervals. The time of radar echo appearance is indicated.

D. Discussion of Updraft Behavior

Because modelling was used to compute the updrafts, it is desirable to compare the results with actual measurements of updraft speeds.

Byers and Braham (1949) measured updrafts within thunderstorms by aircraft penetration. Observations were made between 6.0 and 7.5 km on six summer days in Florida storms. Maximum updrafts ranged from 18 to 30 m sec^{-1}. Median values ranged from 6.5 to 9.8 m sec^{-1}. An earlier paper by Byers (1948), as summarized by Khrgian et al (1961) reported the most commonly measured updraft speeds in storm clouds to lie between 3 and 9 m sec^{-1} (68 out of 104 encounters). Values greater than 15.2 m sec^{-1} were reported in only 4 encounters out of 104. The distributions were similar at the 4.8, 6.3 and 7.8 levels. The maximum value reported was 26 m sec^{-1}.

Braham (1952) gave average conditions encountered during aircraft penetrations of Ohio storms. These are shown in Table II:

TABLE II

Height (km)	Updraft Radius (km)	Updraft Speed (m sec^{-1})	Downdraft Radius (km)	Downdraft Speed (m sec^{-1})
1.5	0.60	5.0	0.70	4.6
3.0	0.70	7.2	0.55	5.5
4.5	0.75	7.3	0.55	6.1
6.0	0.75	7.2	0.55	5.2
7.5	0.70	8.4	0.75	7.0

The size of the sample in the present study was not large enough to produce meaningful statistics on turret properties. But it would seem that the results of stereo photogrammetry and turret updraft computations

are in general agreement with measurements made by other authors by other techniques. The first impression is that these turrets are generally slightly larger than the average updrafts reported by Braham. However, this is not unexpected since at least a portion of the cloudy air near the turret boundaries would have properties of vertical speed more like the environment with which it is mixing, or may even have been subsiding slightly. Secondly, the updraft speeds would seem to have maximum values somewhat larger than the maximum values found by Byers in Florida. This is even more the case when we consider that other levels in the updraft profile of the turret may have values even larger than those measured at the observable levels (see Chapter VII, Figure 33). However these were peak values of a time variation within each cell, and Byers' chances of encountering a cell at the level of maximum updraft at the time of maximum updraft would be rather small. So spot encounters might give rather different maximum values than would continuous observations in space and time.

One important difference between these turrets and the cumulus cells envisaged by Byers and Braham is the time scale. Although time development proceeds in a similar manner to their model, Alberta turrets progress through a complete cycle in 5 to 20 min rather than the 45 to 90 min suggested by their observations. Although the whole storm composed of many cells may have a life cycle 45-90 mins or longer, it seems quite certain now that the individual convective cells have a much shorter life cycle.

E. Postscript

The assumption of no net entrainment through the sides of the turret in these computations could have resulted in larger values of updraft speed than were really occurring. The approximate magnitude of this over-estimate is derived in Appendix I. The over-estimate is computed for a typical entrainment rate of $\frac{1}{M}\frac{dM}{dz} = \frac{0.2}{r}\ km^{-1}$, where M is mass flux through a horizontal cross-section of the cloud, r is radius of cloud at level z (Srivastava, 1964). The magnitude of the over-estimate is approximately 40% when turrets are small (radius = 0.5 km) and cylindrical, becoming 80% when turrets are larger (radius = 2.0 km) and shaped more like a spherical segment. Thus if net entrainment had been taken into account, significant reductions in the computed updrafts would occur bringing our values more in line with updraft speeds observed by other authors using direct measurements.

If lateral entrainment is estimated using divergence patterns measured by balloons (Byers, 1949) in the vicinity of the developing turrets, or by comparing measured liquid water contents with the adiabatic values (Malkus, 1954) much better values of the actual updrafts could be computed by this indirect method.

CHAPTER VII

THE RESULTS AND CLOUD MODELS

A. Introduction

One of the best uses to which data on real cumulus behavior can be put is to relate them to current models of cumulus growth and precipitation development. A brief account of four such models will be given in this chapter, relating to the present results whenever possible.

The field of dynamic convective cloud models is somewhat argumentative. However, the author believes that diligent review of the models in the light of real cloud measurements will put sufficient quantitative restrictions on their behavior, to result in a model which is quantitatively precise and general enough to account for observed behavior on many scales. Such a model is certainly in demand, as once it is well and concisely formulated, it will permit researchers to discover the real controlling parameters in cumulus development. It will also permit precipitation researchers to put their models into more realistic dynamic environments. As a result, the interactions between dynamics, and precipitation growth and development will become more clearly understood.

B. Parcel Theory

Vertical velocity profiles of updraft speed versus height were computed using a simple parcel theory. In this parcel theory it was assumed that each unit parcel rises adiabatically and unmixed with no drag or viscous forces acting on it as it rises from cloud base to its limiting level (the level at which its vertical speed returns to zero).

Cloud base was taken as the convective condensation level (CCL) using a mean watervapour mixing ratio between the surface and 700 mb

(approximately 2 km), and the maximum surface temperature recorded at Penhold up to the time of the turret development that was observed. This made some allowance for turbulent mixing of the rising thermal below CCL, and yielded cloud bases that agreed with estimates made of cloud base heights by photogrammetry and surface observations. All of the liquid water condensed out was assumed to be carried along within the parcel. An adjustment for parcel loading due to this liquid water was made by reducing the buoyancy at any level (as given by the temperate difference between the rising parcel and the environment) by $\frac{1}{4}$°C per 1 gm 1 kg^{-1} of adiabatic liquid water at that level (Saunders, 1957).

The environmental temperature and moisture, and the parcel theory curves are shown on the Canadian Tephi-Grams in Figures A1 and A3 for July 7 and July 10, 1966, respectively. The corresponding vertical velocity profiles were computed from the positive and negative areas/energies appearing on these charts, and are displayed in Figures 32a and b respectively. Also shown are the adiabatic liquid water contents, assuming no mixing occurred above the condensation level (cloud base).

For comparison, vertical updraft profiles for turrets 10/03 and 10/04 on July 10 and 7/04 of July 7, 1966, were prepared using the pseudo-updrafts computed in Chapter VI and are shown in Figures 33a, b and c respectively. Only turrets for which observations were made through more than three levels are displayed. Neglecting for the moment the different times shown, and concentrating on the one time with the maximum vertical velocity in each diagram, we may compare with the parcel theory profiles of Figures 33a, b and c by the bold dashed curve. Note that the curves

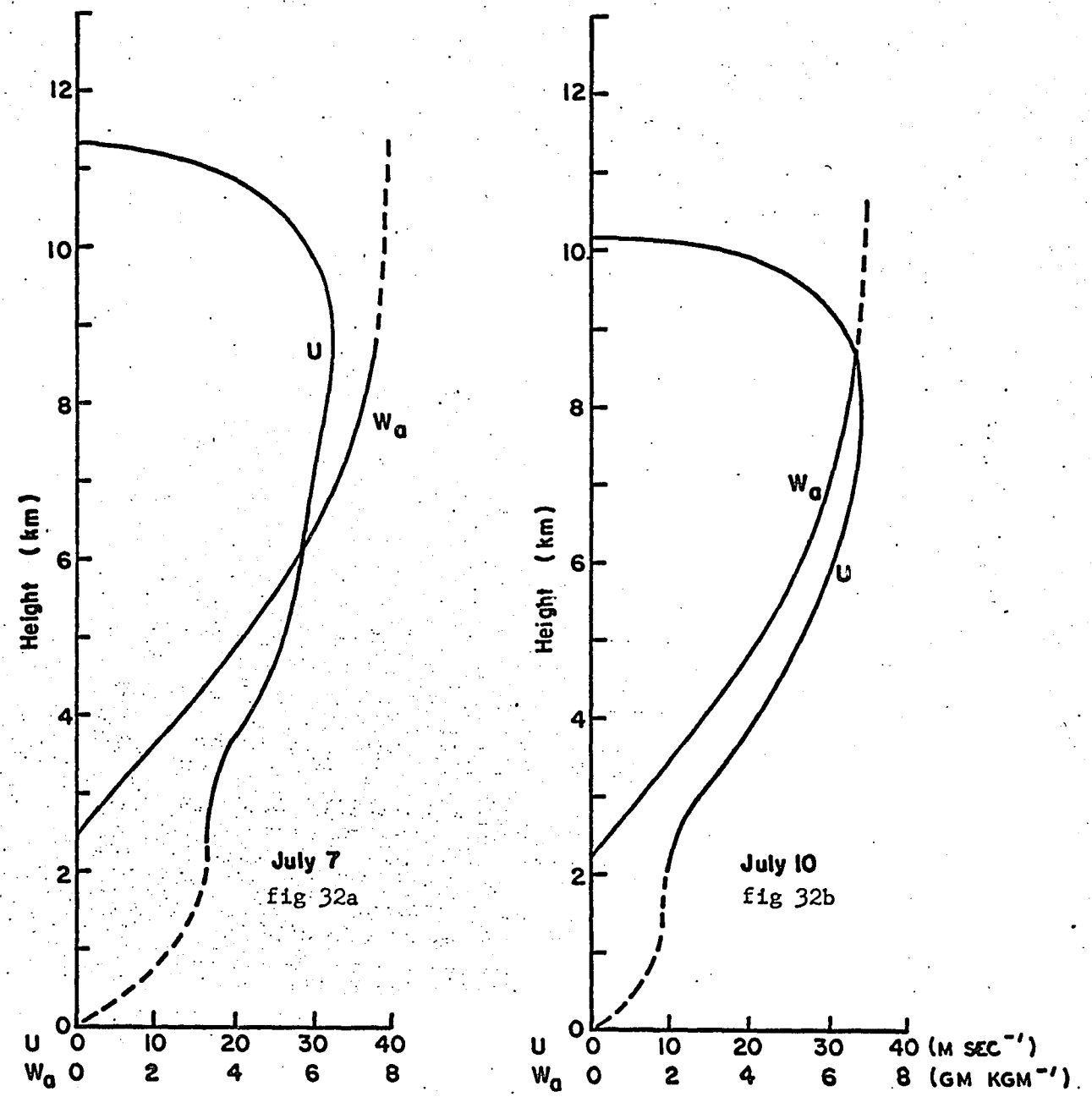

Figure 32a: Parcel theory updraft profiles and water content profiles for July 7, 1966. Values are computed as a function of height from the 17:00 MST sounding in fig A1.

Figure 32b: Parcel theory updraft profiles and water content profiles for July 10, 1966. Values are computed as a function of height from the 17:00 MST sounding in fig A3.

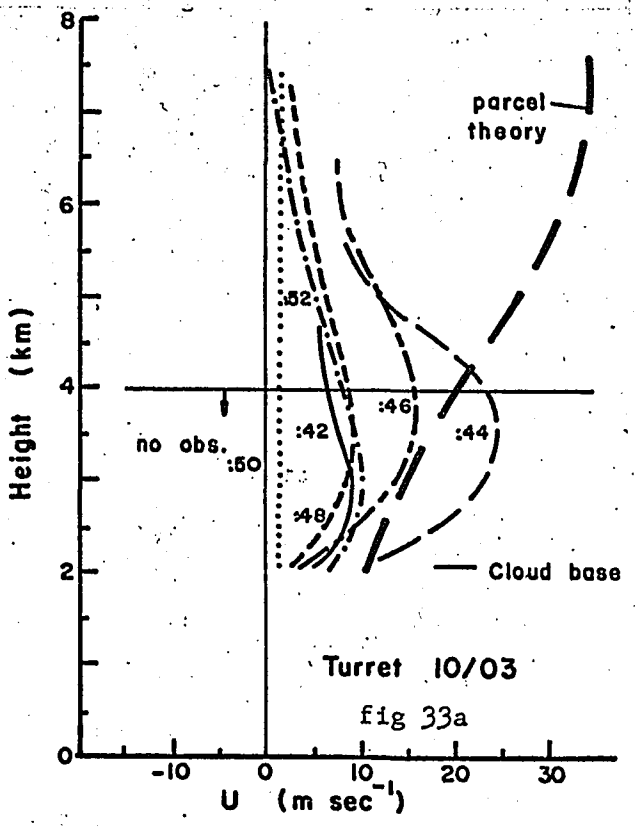

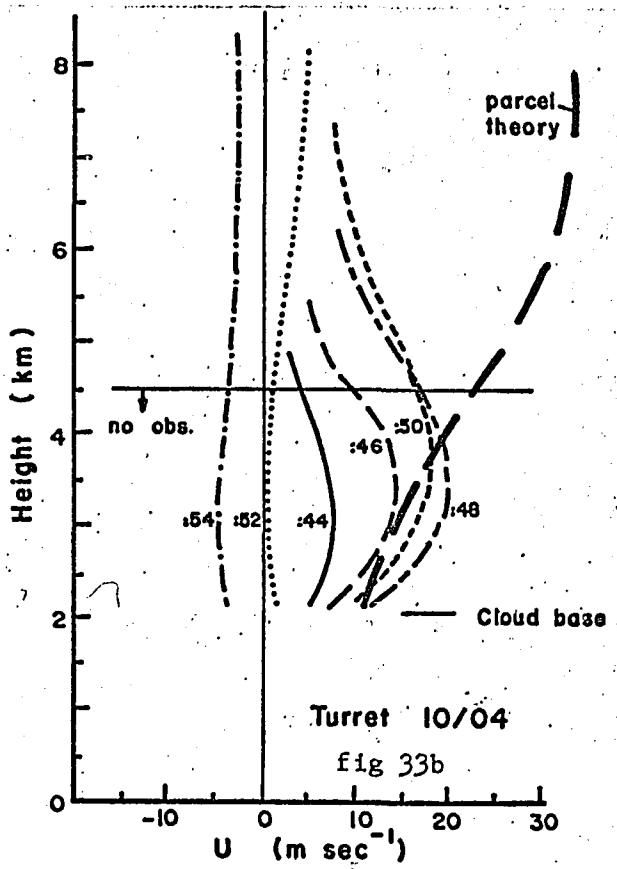

Figure 33a: Computed updraft profiles for turret 03, July 10, at 2 min intervals.
Figure 33b: Computed updraft profiles for turret 04, July 10, at 2 min intervals.
Figure 33c: Computed updraft profiles for turret 04, July 7, at 2 min intervals.

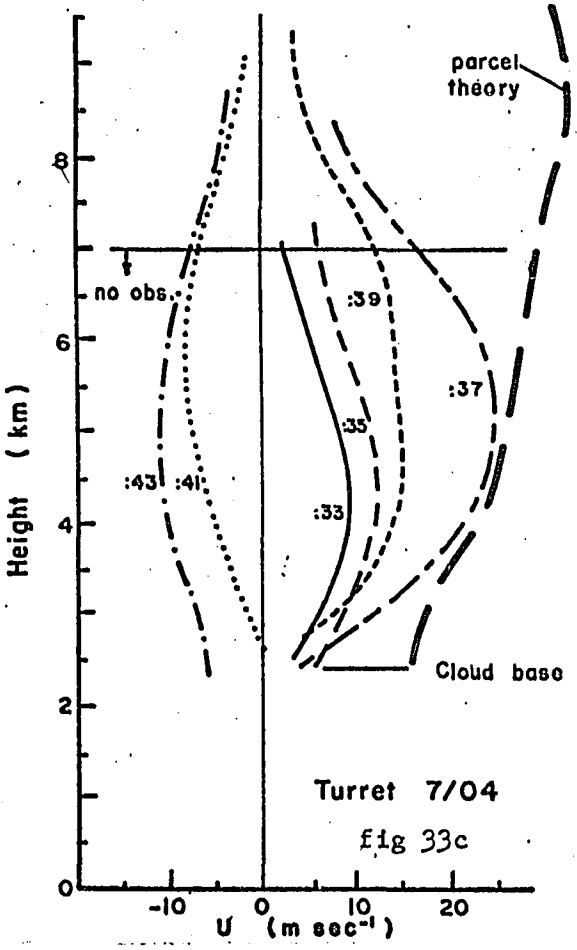

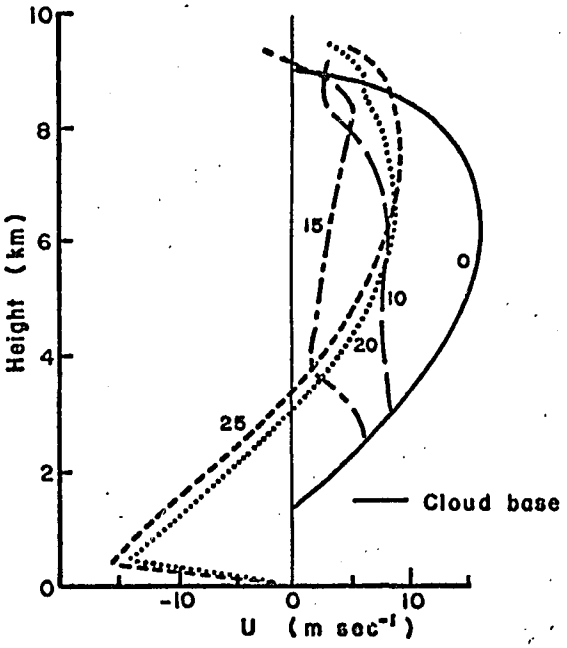

Figure 34: Example updraft profiles from Srivastava (1966). Note the longer time interval between profiles.

of measured updraft profiles were extended below the lowest level of observation in a purely schematic manner knowing that there would be a maximum below this level and that the updraft velocity at cloud base should be less than 10 m sec^{-1} (Byers and Braham, 1949; Malkus, 1954). The downward projection of these curves was done so that they would be consistent with the curvature of the portion of the curves based on real observations and with their time variations. Although both observed and parcel curves were computed assuming no net entrainment through the boundaries of the rising cloud, parcel theory further assumed no mixing whatsoever above the CCL, adiabatic ascent of the cloud parcels and no horizontal pressure difference between the parcel and environment. The parcel theory curves probably represent a maximum limit on the vertical speed of a cloudy parcel moving through any level.

The comparison reveals that maximum pseudo-updrafts measured in the observed turrets are, at lower levels, about 10 m sec^{-1} more than predicted by parcel theory, at mid-levels, 10-25 m sec^{-1} less than predicted, and the height of the maximum was about 4 km lower in the real clouds. However, since the parcel curves depict how the updrafts should appear at the centre of a very large, steady state storm cell, (so that the assumptions of adiabatic ascent become approximately valid), this discrepancy is not too surprising.

One of the first effects of mixing environment and parcel air would be to lower the predicted level at which the maximum vertical speed should be achieved. That is to say, the parcel curve would cross the environment curves in Figures A1 and A3 at a lower level. For example, the observed curves of July 10, (Figures 33a and b) imply an

equilibrium level of about 3.5 km. Taking the adjusted environment curve, and considering only the effects of mixing enthalpy, (in the manner suggested by Austin, 1948), it would require a mixing rate of the order of 400% per km to result in an equilibrium level at 3.5 km. The positive energy associated with such a mixed curve is also decreased, resulting in a maximum updraft velocity of approximately 15 m sec^{-1} at 3.5 km. Maximums on the projected observed profiles for this day were between 20 and 25 m sec^{-1}. However, once mixing is permitted, net entrainment into the observed cloud must be considered as possibly accounting for some of the cloud volume growth that is observed above any level.[1] This would probably reduce the computed updrafts for the observed clouds by at least a factor 2 and bring the updraft values back into line.

Observations of water content and horizontal momentum would further assist in arriving at an evaluation of the mixing processes that are taking place. Using the limits set by East (1957) on the liquid water contents necessary for the initial echo development, some inference may be made about the limits on the mixing of the cloud water with unsaturated environment air. As mentioned earlier, mixing of horizontal momentum at each level interacting with the vertical transport of horizontal momentum from other levels, in conditions of vertical shear, must account for the observed deviation of a turret's horizontal motion from its environmental winds (Malkus, 1954; Fujita, 1965). Evaluation of this process may provide a further method of measuring the magnitude of the mixing processes.

1 See Appendix I

C. Jet Models

Srivastava (1964) gave a detailed assessment of the entrainment problem from a theoretical point of view and presented a one-dimensional, jet type, numerical model from which vertical profiles of updrafts and liquid water content could be derived. Unfortunately, the assumptions necessary to arrive at a workable model do not permit a direct application of this model to developing turrets. Specifically, the assumptions of steady state and constant radius are not as observed for these turrets, but would be more valid for larger, anvilling cumulonimbus types of clouds. There is no indication in such a steady state model of how the updraft profile, within a cloud, evolves with time. The observed turrets contained updraft profiles which have a very significant evolution in time as may be seen in Figures 33a, b and c. Srivastava's model II has provision for updraft cores existing within a shell of cloudy air and hence is the type to be applied to turrets emerging from the top of cloudy regions, with the shell being extensive below the level of emergence, and rather thin around the emerging turret. It may be possible to investigate the time evolution of the updraft by permitting the radius of the core and shell to vary in time as a function of mass continuity considerations.

In a later paper, Srivastava (1966) removed the steady state conditions, included the growth of precipitation in his model, but did not include entrainment. This resulted in an updraft profile which evolved in time due to the loading effects of precipitation whose accumulation at upper levels and subsequent release produced coupled oscillations in the updrafts and precipitation, downdrafts in lower levels, and a pulsating rise of the cloud top. Figure 34 is an example of a

profile taken from this work. Some similarity to Figures 33a, b and c exists, although the time scale of the oscillations differs by about a factor 3 or 4. The lack of a downdraft at all levels in Srivastava's models may be related to the fact that no entrainment effects were included. Mixing with drier environmental air reduces the wet bulb potential temperatures of the updraft air arriving at the upper reaches of the cloud, and this process is thought to be one explanation for the development of extensive and vigorous downdrafts once they are initiated, probably by precipitation loading. Turret 10/03 of July 10, (Figure 33a) evolved in time, even though no detectable echo developed. However, no downdraft developed, but rather renewed growth set in, apparently starting from lower levels. Turret 7/04 of July 7 (Figure 33c) developed the most vigorous downdraft, and was associated with higher liquid water contents. Judging from the areal extent and intensity of the echoes, and the subsequent hail reports from later in this storm's history, more intense precipitation could have been associated with this turret.

D. Bubble Models

Scorer and Ludlam (1953) regarded convection as occurring in bubble-like units rather than in a continuous current or jet. The bubble was considered to grow by entraining environmental air if it was unstable or neutrally stable with respect to its environment, and by detraining air when it was stable.

Laboratory experiments by Scorer and Ronne (1956), Scorer (1957), and Turner (1963) with buoyant bubbles, normally involving incompressible fluids, revealed that for bubbles with constant vertical speeds or with constant accelerations, the rate of volume growth of the rising bubble

is nearly constant. Hence for spherical bubbles $\frac{dr}{dz}$ was observed to lie between 0.18 and 0.28. Diameters and upward velocities of bubbles emerging from tops of cumulonimbus clouds have been measured (Saunders, 1961; Glass and Carlson, 1963) giving spreading coefficients, $\frac{dr}{dz}$, between 0.18 and 0.19. The radius of the turret tops observed in this study are plotted versus height in Figures 35a and b for July 7 and July 10 respectively.

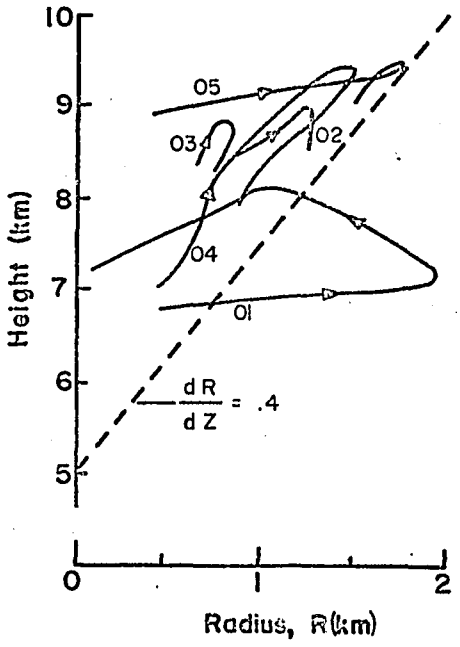

Figure 35a: Plot of turret radius versus height of turret top for July 7, 1966.

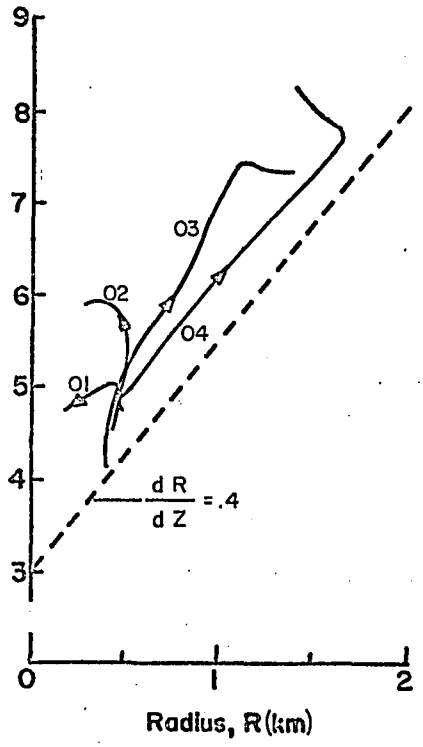

Figure 35b: Plot of turret radius versus height of turret top for July 10, 1966.

It is seen that the more vigorous turrets 7/04, 10/03 and 10/04 behaved somewhat like entraining laboratory bubbles, but the spreading coefficient was closer to 0.4 for the greatest portion of their visual history. Others, such as 7/01 and 7/05 had spreading coefficients one order of magnitude larger than reported by the laboratory experiments; though these may have been associated with growth in the vicinity of stable layers in the environment.

Priestley (1954) and Mason and Emig (1961) performed calculations for buoyant parcels, accounting for all of the effects due to mixing by means of a single parameter referred to as an "interchange coefficient" by Priestley, and a "damping factor" by Mason and Emig. Figure 36 shows curves which result from Priestley's formulation, indicating the various modes of behavior possible for the vertical speed of a rising parcel. These curves may be compared qualitatively to the rise of the observed cumulus tops in Figures 13 and 14 of Chapter IV. The behavior should be equivalent only if a real turret top consists of a single mixing parcel, and hence its height truly represents the trajectory of a single parcel.

It may be shown that the more stable the environmental lapse rate with respect to the cloudy parcel lapse rate, the shorter should be the period of oscillation about its equilibrium level. The amplitude is controlled by the magnitude of k, the damping factor. Looking at the July 7 tephigram (Figure A1) and the corresponding turrets, we may associate the shorter period oscillations of turrets 7/01 with the slightly more stable layer below 6.5 km and the longer period turret 7/04 with the less stable region above. The shorter period of 10/01 might be associated with

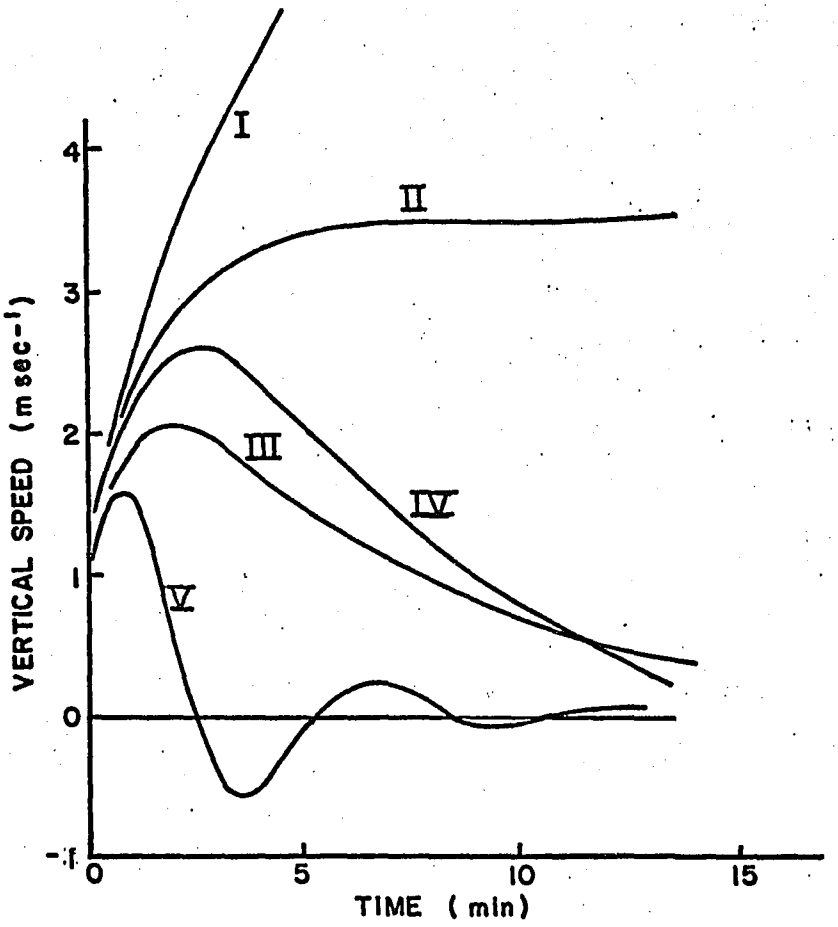

Figure 36: Modes of vertical speed behavior for a mixing parcel as described by Priestley (1954).

I - absolutely buoyant parcel $\Gamma < \Gamma_E$, k small.
II - buoyant parcel $\Gamma < \Gamma_E$, k large.
III - $\Gamma = \Gamma_E$
IV - asymptotic $\Gamma > \Gamma_E$, k large.
V - oscillatory $\Gamma > \Gamma_E$, k small.

where: Γ = lapse rate of temperature for parcel
Γ_E = lapse rate of temperature for enviroment
k = Priestley "interchangecoefficient"

the remains of the stable layer showing up at 4 km on the temperature sounding, considering the distance between the radiosonde stations and the turrets. But agreement with Priestley's model seems to end there, and the tendency for the turrets to take on large downward speeds was not predicted. However, in this formulation, no account was taken of the spatial variation of k (a function of parcel radius) and of $\Gamma - \Gamma_E$ (the difference between the cloud and environment lapse rates) that a parcel would naturally encounter as it rises, or of loading by water substance. This is because such spatial variations are not permitted when arriving at the analytical solution of Priestley's vertical motion equation, which describes the curves in Figure 36. Nor are the effects of loading by liquid water content permitted. In the course of the present study, a numerical integration including such spatial variations was performed using real data from the temperature soundings on July 7 and the radial behavior of the observed turrets. The resulting parcel trajectories showed good agreement with those of the cloud turret tops 7/01a and 7/04 up to the time when a significant downward motion sets in. Significant departures still existed at other times; hence initial conclusions on this type of formulation are that during a portion of a turret's lifetime, the turret top may depict the trajectory of a single mixing parcel. Further investigation should reveal whether the departures result from lack of a detailed knowledge of the spatial variations of k and $\Gamma - \Gamma_E$ (and also of freezing processes and realistic precipitation development), or from the fact that some turrets at least consist more of a circulation of cloudy parcels than they do a single parcel during their lifetime.

If the latter is true, we may be able to consider the turret to

be composed of a succession of such "Priestley parcels", the individual parcel velocities being some continuous combination of all the curves shown in Figure 35; different at different levels within the turret, depending on the relative stability of the cloudy parcel, its environment, and the appropriate value of k, for each level. The behavior of the total cloud volume at any instant would be a consequence of the individual parcels composing that cloud turret at that instant. Hence when we consider an updraft at any level within such a turret, we are simply determining the integrated effect of all parcels passing through that level. Vertical convergence of parcels implies radial divergence of the turret. The changes in the turret's size imply changes in the controlling parameter k and in the environment of subsequent parcels moving through the turret, and hence the feedback between space and time.

The full consequences of visualizing a turret as consisting of a variety of "Priestley parcels" originating at a variety of levels are not completely understood by the author, but it would seem to lead to a method of reconciling the duality of convective behavior (i.e. a jet composed of parcels) and may permit consideration of the continuous development of a convective storm from the small cumulus stage, resembling an individual eroding bubble, through to the giant cumulonimbus, resembling the steady state jet but composed of many circulating parcels.

It is understood that a complete integration in space and time of the primitive dynamic equations of motion, the equation of state, and the thermodynamic equation would be the ultimate approach. Some progress in this direction is being made (e.g. Ogura, 1963a). He emphasizes the need to examine the results of numerical experiments in the light of observed cloud behavior in order to evaluate the errors introduced by simplifying

the hydrodynamical equations, errors of numerical origin, and errors in the description of the initial conditions. Certainly the velocity and radial growth fields resulting from Ogura's experiment (Ogura, 1936b) display many of the properties and magnitudes observed here. Although the kinematic approaches discussed earlier are easier to manipulate and the necessary parameters easier to determine observationally, the generality of a hydrodynamic approach is most desirable. A full understanding of the nature of transition from small scale cumulus convection to large severe storms will likely come through advances in the hydrodynamic approach rather than from kinematic modelling.

E. Summary

As found by most observers, the simple parcel theory somewhat over-estimates the updrafts observed in these turrets. The Bubble model did not seem to give any consistent account of the behavior of turret tops, although it qualitatively predicts an oscillating behavior for the rising turrets in a stable environment. The radial spreading of laboratory bubbles was not consistent with the observed spreading of these turret tops, although the sample was rather small.

A promising approach would seem to lie in a more general form of a parcel type numerical model, integrated in space as well as time. Alternatively, a non-steady-state jet model which permits variations in radius and entrainment and includes the "shell-core" concept, precipitation growth and loading, and the release of latent heats of fusion and sublimation, should be considered.

Although the actual magnitudes of the pseudo-updrafts (computed assuming no net lateral entrainment) could be over-estimated by a factor

of 2 or 3, the time variations with periods in the order of 5-10 minutes, and the development of downdrafts in association with precipitation development remain quite conclusive.

CHAPTER VIII

SUMMARY AND CONCLUSIONS

In this chapter the author will summarize the conclusions reached from his observations of cumulus turret behavior. Recommendations for future studies will be made in the light of these conclusions.

On both of the days on which vigorous turret activity was observed, there was a southwesterly flow aloft and marked wind shear between the surface and mid-levels. Chisholm (1966) also noted such characteristics of the synoptic pattern in his study of two major Alberta storms in July, 1964.

Of the storms discussed in the present study, one was "air mass" (i.e. no strongly baroclinic zones in the region), the other definitely "frontal". The air mass storm (July 7, 1966) was characterized by the gradual development of a large storm, with vigorous turrets emerging from the top of an extensive area of convective cloud, transported into mid-levels by previous convection which had taken place upstream. The absence of fronts, surface troughs and upper level short wave troughs suggests the absence of significant large-scale vertical motion fields in the region of storm development. Under such conditions slightly stable layers can persist in mid- and upper levels of the troposphere, and may play a vital role in the areal development and organization of a storm. These stable layers seem to cause some of the earlier convective cells to spread radially at mid-levels. Such preconditioned mid-levels may be an essential first step for the development of a major storm.

Conversely, on July 10, 1966, a marked cold front resulted in cooling at mid-levels through the dynamically induced vertical motion associated with the strong baroclinic zone. This vertical motion would

have removed any slightly stable layers originally present at mid-levels as well as lead to the release of the instability itself. Convective cells in this environment grew unimpeded by stable layers at mid-levels and the gradual organization of a large areal storm through mid-level preconditioning was not evident. Rather each turret was more isolated and showed less tendency to spread radially at mid-levels than was observed on July 7.

Although precipitation cells developed on both days, the radar echoes on the air mass day tended to grow into large organized areas (of the order of 10 miles). Echoes on the frontal day remained smaller and more isolated. Both days produced rain showers and hail, but the air mass day was characterized by larger and more extensive hail than the frontal one.

This does <u>not</u> imply that an organized convective storm and significant hail may <u>not</u> be associated with fronts. The dynamic vertical motion fields accompanying an active front may well lead to the organization of a severe storm. Rather, these observations suggest that the organization and development of a major storm in non-frontal situations may be the result of the presence of apparently innocent-looking layers of mid-level and upper level stability in the troposphere. Future study is very necessary to further define the role of such layers.

A second major difference between the two days studied here was the character of the vertical wind shear. The July 7 storm was associated with veering winds between the surface and 3 km; slight backing above 8 km. The maximum wind was 27 m sec^{-1}. On July 10 the storm

followed the passage of a marked cold front which resulted in backing winds between the surface and about 4 km, veering to about 5 km, then backing to 8 km. The maximum wind was greater than 40 m sec^{-1}. The difference in storm character has already been discussed; a large organized storm on July 7 producing widespread rain and large hail, more isolated cells on July 10 producing scattered showers and small hail. Proppe (1965) has already found that for Alberta storms, strong wind shears hinder the development of most hail storms. Also conditions of veering winds below approximately 4.5 km and backing above, were most frequently associated with the occurrence of significant hail; and backing winds at all levels with showers. Hence the present study is consistent with Proppe's findings and suggests that further study of turret behavior, with particular attention to details of both wind and temperature soundings, may reveal the nature of the dynamic interactions between the clouds and their environment which produce the relationships.

From a consideration of the detailed observations of the vertical and radial growth behavior of these turrets, one may conclude that each exhibits a great deal of individuality. Some of this individuality was related semi-quantitatively to the thermal structure of the environment, and to the development of precipitation within the turret.

It appears that initial precipitation does not develop until the turret grows to levels at which the adiabatic liquid water contents approach 6 gm kgm^{-1}, as was predicted by East (1957). The precipitation echo spreads rapidly to other levels within the turret after the first echo appears. Indications are that the release of the latent heat of fusion from freezing precipitation within a turret may briefly enhance

a turret's updraft if it occurs while the turret is still building, or spawn a new protrusion which, lacking a flux from lower levels, soon expends itself. A downdraft developed whenever precipitation had formed, or was forming, within a turret.

Without further data on the wind fields surrounding a turret, or on its internal properties, it is not possible to separate the roles of vertical flux and lateral flux in producing the observed volume growth of a cloud turret. However pseudo-updrafts, computed assuming no net lateral flux into (or out of) a turret, show a rapid evolution in time. This evolution is more rapid than that suggested by current models of convective cloud growth. Major turrets complete an updraft cycle in approximately 10-20 min.

The overall behavior of these turrets suggests that, at least in the early stage of a storm's development, the convective cell with a lifetime of approximately 10-20 minutes and a size of 1-2 km must be considered to be the fundamental unit of convective storm growth. Even the large anvilled cumulonimbi of a severe storm show evidence of intermittent protrusions from the top of the anvil (Newton, 1966, and personal observations by the author of time lapse films). These protrusions strongly resemble convective turrets similar to those that were clearly visible at an earlier stage in the storm's development. Intermittency of rain and hail (Pell, 1965) and the behavior of high-intensity radar cores in major storms (Chisholm, 1966) further suggest such mechanisms as being a fundamental part of even the largest storms. Future work in dynamic modelling should concentrate on such convective cells and attempt to explain their evolution in time as well as space.

Such cells are probably best described as pulsating jets rather than either bubbles or steady state jets. Figure 37 is a schematic representation of the properties of such a model convective cell at 3-minute intervals in time, as inferred from the results of this study. The thin solid lines are isotachs of updraft velocity, the dashed line a particular air parcel trajectory. A uniform horizontal motion of 10 m sec^{-1} was assumed. The time of the emergence of the visual turret top is taken as zero min.

Interesting future studies in cumulus turret behavior might include the depiction of multiple parcel trajectories in a non-uniform field of horizontal motion. Such trajectories could then be modelled using a parcel theory model of the Priestley type but which includes parcel loading due to liquid water content, precipitation growth (and fallout), and freezing, along with parameters of mixing and instability that are variable in space. Horizontal motion may be treated on a momentum conservation basis. Cloud turret behavior would then be depicted by the relative positions of a variety of parcel trajectories at successive instants in time.

Many future uses of stereo photogrammetry suggest themselves in the present study. The pileus (or cap) cloud, or inactive cloud fragments in the vicinity of a developing turret, may be used as tracers of the local circulation. Also a detailed study of a complete storm, one which remains in total view for its whole history from small scale cumuli to large cumulonimbus, must be hoped for in the future. Such a study should include data on initial radar echoes, and subsequent high intensity cores as seen by a high resolution, quantitative radar system.

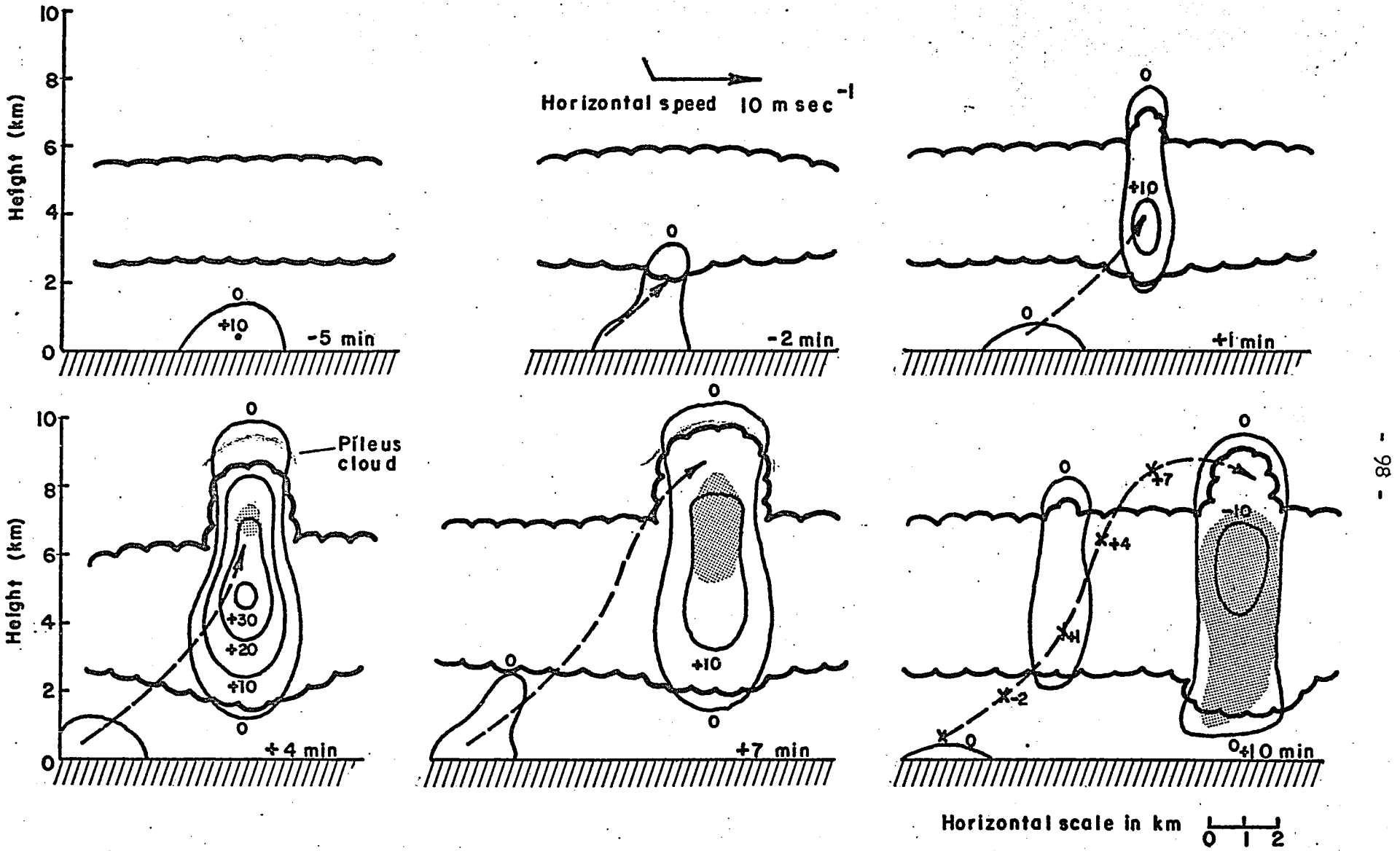

Figure 37: A pictorial representation of a cloud turret's life cycle viewed at 3 min intervals (minute zero taken as time of emergence). Isotachs of air parcel vertical speed are drawn at 10 m sec^{-1} intervals. A particular air parcel trajectory is shown by the dashed line, while precipitation exists in the stipled area.

Radiosonde soundings and pibal wind measurements taken within a few miles of the storm are essential for a complete analysis. A knowledge of all precipitation which ultimately reaches the ground will be helpful in interpreting the other data. With such an analysis in hand, the cloud and precipitation growth modellers will be able to continue with a better understanding of the reality they are attempting to model.

Overall, the author has found that stereo photogrammetric analysis under optimum conditions permits far more detailed description of the behavior of cumulus turrets in space and time than previously attempted. Such behavior is important in the evaluation of current models of cumulus dynamics and precipitation growth, and in achieving a fuller understanding of convective storms.

APPENDIX I

APPENDIX I

THE MAGNITUDE OF OVERESTIMATION IN PSEUDO-UPDRAFT COMPUTATIONS

Pseudo-updrafts have been computed in Chapter VI assuming no net lateral entrainment into the cloud turret. Also volume expansion of rising parcels due to decreasing ambient pressure with height was neglected. Hence the updraft through any reference level was assumed to account for all of the cloud volume growth which occurred above that level. This may be expressed:

$$Uo = \frac{dV}{dt} \Big/ Ao$$

where: Uo = the updraft speed through a reference level z_o averaged over the horizontal area of the turret Ao.

V is the total cloud volume above level z_o.

It would be better to say that the rate of change of total cloud mass above a reference level must equal the mass flux through its base plus the net entrainment of air through the sides over the entire turret's surface area. This may be expressed:

$$\frac{dm}{dt} = Mo + \int_{z_o}^{z_t} dM \qquad (A1)$$

where: m = total cloud turret mass above level z_o.

Mo = mass flux through the base at level z_o.

dM = incremental change in mass flux between level z and z + dz due to lateral entrainment.

z_T = height of top of cloud turret.

Srivastava (1964) after surveying many authors' observational and theoretical estimates of entrainment concluded that the fractional rate of change of mass flux with height may be expressed:

$$\frac{1}{M}\frac{dM}{dz} = \frac{\sigma}{r} = \mu \qquad (A2)$$

where: r = radius of the cloud element at level z.

σ = a coefficient having a value of 0.2.

Substituting for dM into equation (A1) from equation (A2),

$$\frac{dm}{dt} = Mo + \int_{z_o}^{z_T} \mu M \, dz \qquad (A3)$$

The entrainment term of equation (A3) may be written

$$\overline{\mu U} \int \rho A \, dz = \overline{\mu U} \, \bar{\rho} \, V$$

where

$$\overline{\mu U} \equiv \frac{\int \mu U A \rho \, dz}{\int \rho A \, dz}$$

$$\bar{\rho} \equiv \frac{1}{V}\int \rho \, dV = \frac{1}{V}\int \rho A \, dz$$

Then $\frac{1}{m}\frac{dm}{dt} = \frac{1}{\bar{\rho}} \frac{d\bar{\rho}}{dt} + \frac{1}{V}\frac{dV}{dt} = \frac{Mo}{\bar{\rho} V} + \overline{\mu U}$ (A4)

It may be shown that for typical values of atmospheric temperatures:

$$\frac{1}{\bar{\rho}} \frac{d\bar{\rho}}{dt} \doteqdot \frac{-\bar{U}}{\bar{T}} \left[g/R + \frac{\partial \bar{T}}{\partial z} \right]$$

Therefore: $$\frac{1}{\bar{\rho}} \frac{d\bar{\rho}}{dt} \doteqdot -\bar{U} \, (10^{-4}) \qquad (A5)$$

Since Mo is the mass flux through level z_o, $Uo^* = \frac{Mo}{\rho o \, Ao}$. Substituting this expression for Mo, (A1) and (A5) into (A4) and solving for Uo* we get:

$$Uo^* = \frac{\bar{\rho}}{\rho o} \left[Uo + \frac{V}{Ao} \left(\bar{U} \, 10^{-4} - \overline{\mu U} \right) \right] \qquad (A6)$$

Further simplifying, since $\frac{1}{\bar{\rho}} \frac{d\bar{\rho}}{dz} \doteqdot 10^{-4}$, $\frac{\bar{\rho}}{\rho_o} \doteqdot e^{-10^{-4} \frac{(z - z_o)}{2}}$.

It must also be assumed that $\overline{\mu U} \doteqdot \frac{\overline{\sigma U}}{r} \doteqdot \frac{\sigma \bar{U}}{\bar{r}}$. Then (A6) becomes:

$$Uo^* = e^{-10^{-4}\left(\frac{z - z_o}{2}\right)} Uo - \frac{V}{Ao}\,\overline{U}\,(10^{-4} + \frac{0.2}{r}) \qquad (A7)$$

In Figure 35, it was seen that two typical types of growth were observed; case I when $\frac{dr}{dz} \doteq 0.4$, $z - z_o > r$ (turrets 10/03, 10,04 and 7/04) and case II when $\frac{dr}{dz} \doteq 5$ (turrets 7/01 and 7/05). Within each case, the subcases a) and b) exist for r small (say = 0.5 km) and when r large (=2.0 km) respectively.

Case Ia) $Uo = 3\,W$, where $W = \frac{dz}{dt}$ = vertical growth rate of turret top.

$$\frac{V}{Ao} = 2.2\,r$$

$$\overline{r} \doteq r = 0.5 \text{ km}$$

Then $$\frac{Uo^* - Uo}{Uo} \doteq -0.37$$

Case Ib) $$\overline{r} \doteq r = 2.0 \text{ km}$$

Then $$\frac{Uo^* - Uo}{Uo} \doteq -0.66$$

Case IIa) $$Uo = 1.6\,W$$

$$\frac{V}{Ao} = 1.6\,r$$

$$\overline{r} \doteq \frac{r}{2} \doteq 0.25 \text{ km}$$

Then $$\frac{Uo^* - Uo}{Uo} = -0.58$$

Case IIb) $$\overline{r} \doteq \frac{r}{2} \doteq 1.0 \text{ km}$$

Then $$\frac{Uo^* - Uo}{Uo} \doteq -0.82$$

Hence, an overestimate of from 37% to 82% may exist in the pseudo-updrafts that were computed assuming no lateral entrainment and negligible volume expansion due to decreasing ambient pressure with height.

APPENDIX II

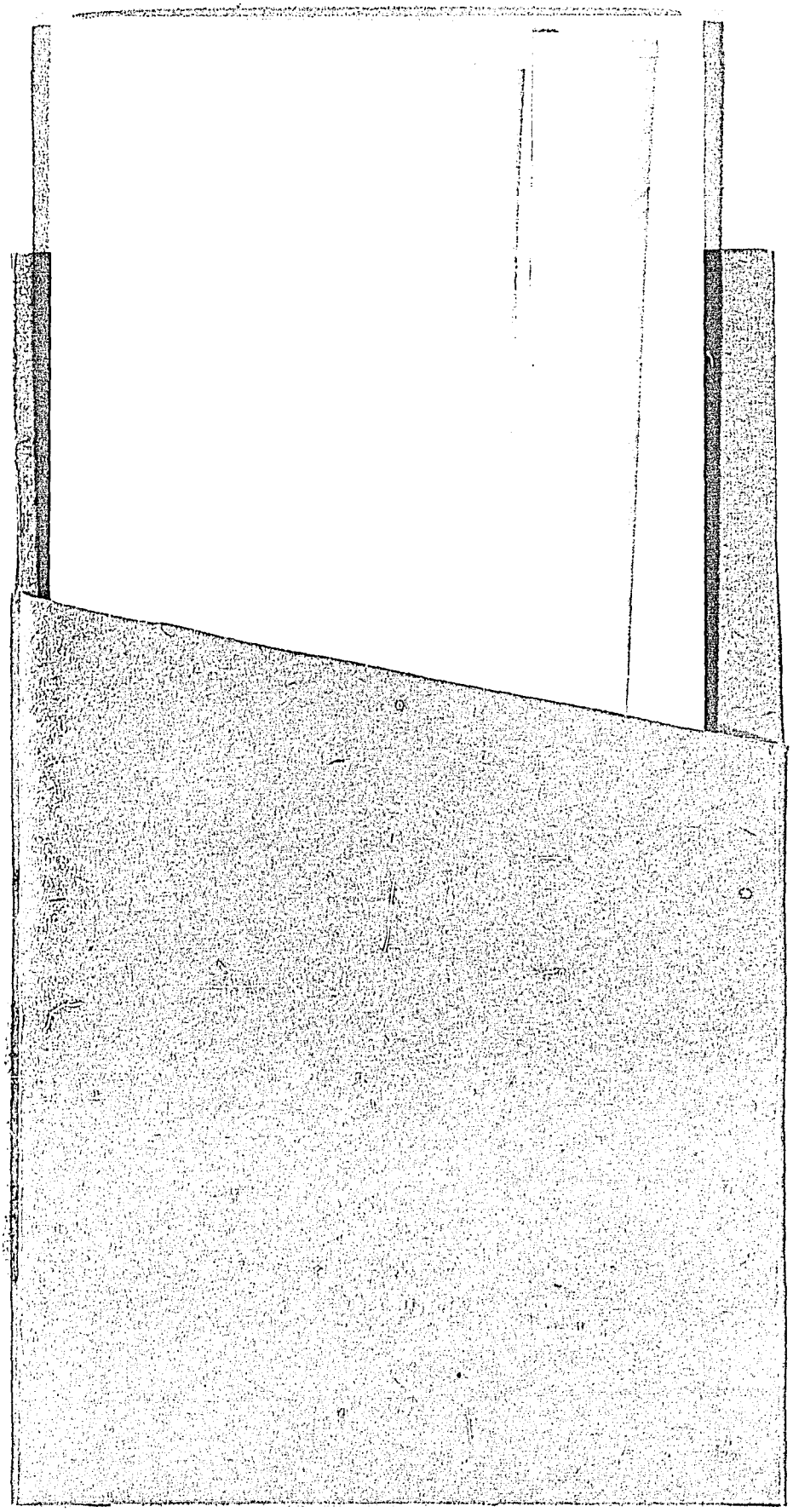

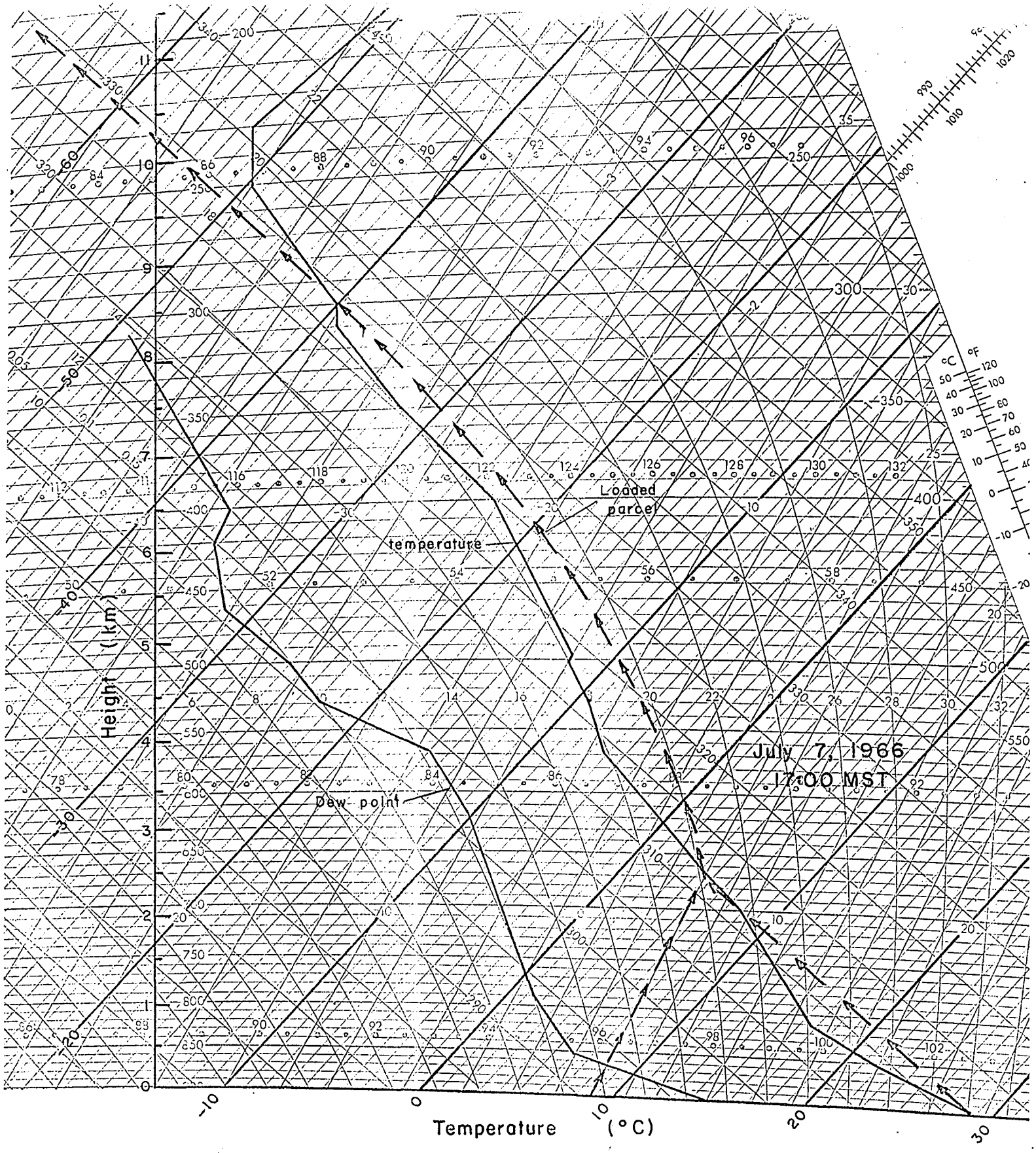

Figure A1: Temperature and moisture sounding for 17:00 MST, July 7, 1966. Data were taken from the Calgary and Edmonton radiosonde ascents and are displayed on the Canadian Tephigram. The arrowed curve indicates the effective temperature of a loaded parcel.

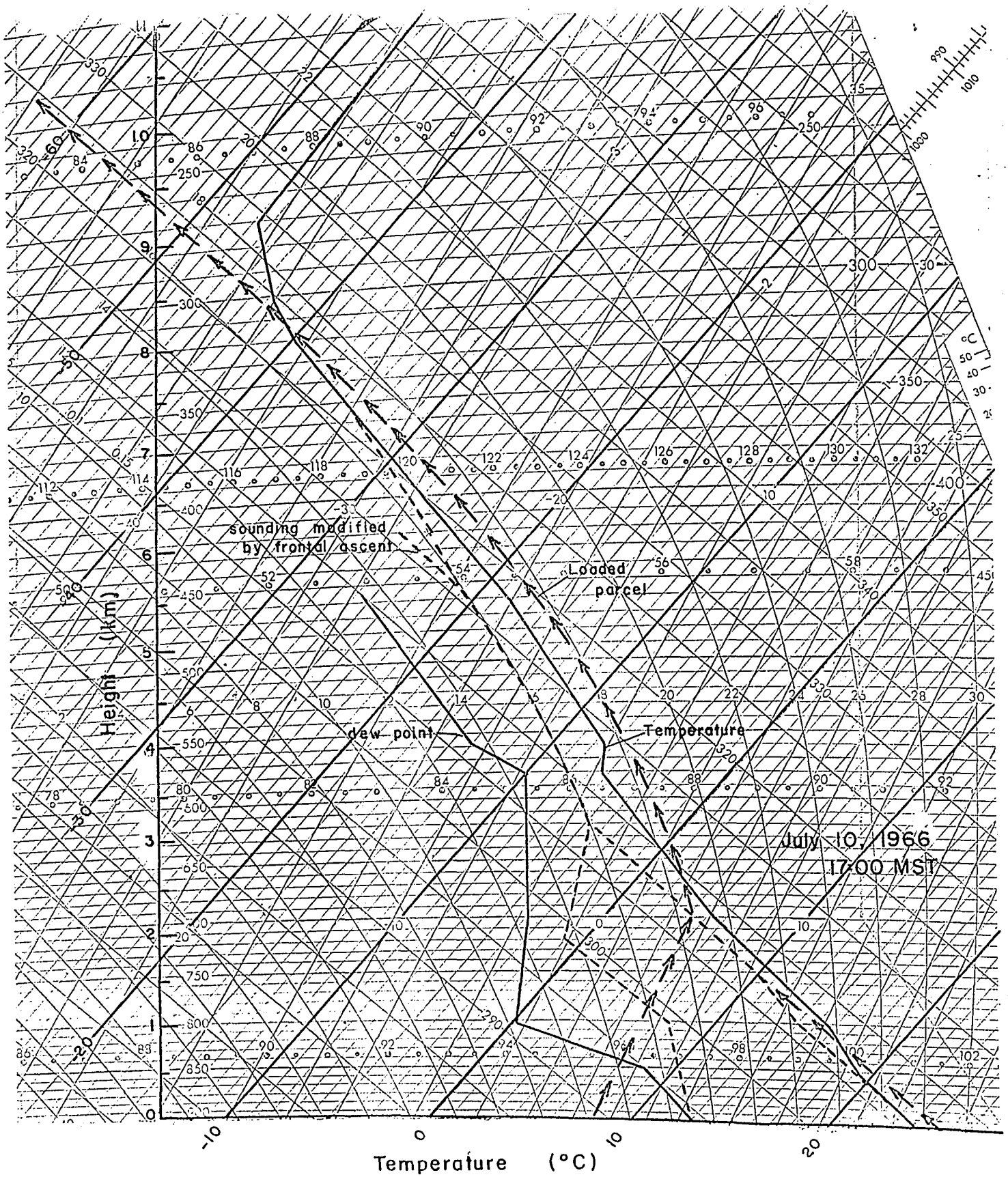

Figure A3: Temperature and moisture sounding for 17:00 MST July 10, 1966. Data were taken from the Calgary radiosonde ascent but were modified to account for cooling due to frontal ascent.(dashed curve - see text). Arrowed curve indicates effective temperature of a loaded parcel with no mixing.

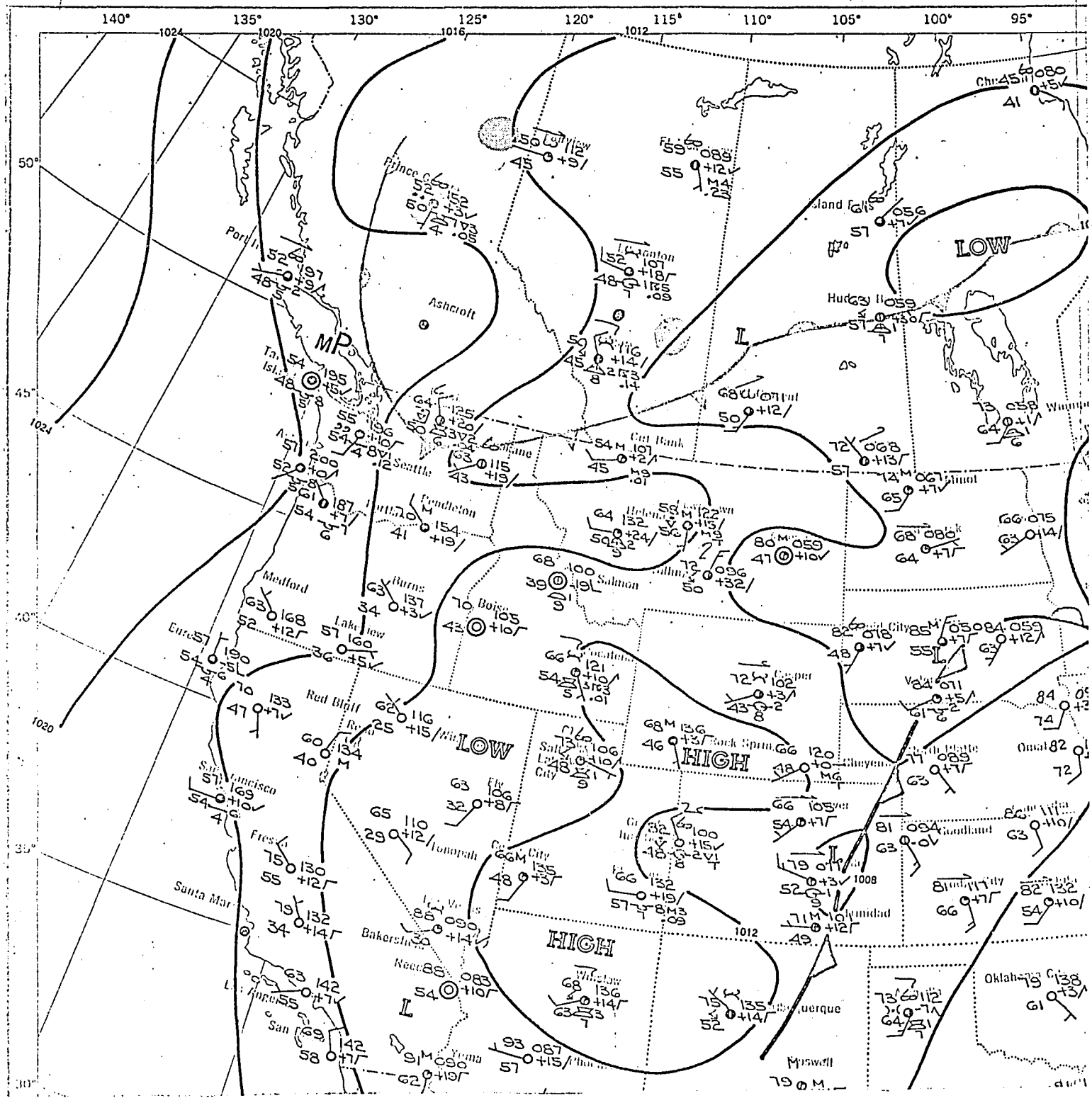

Figure A4a: Surface chart for 23:00 MST, July 10, 1966. (U. S. Dept. of Commerce Daily Weather Map)

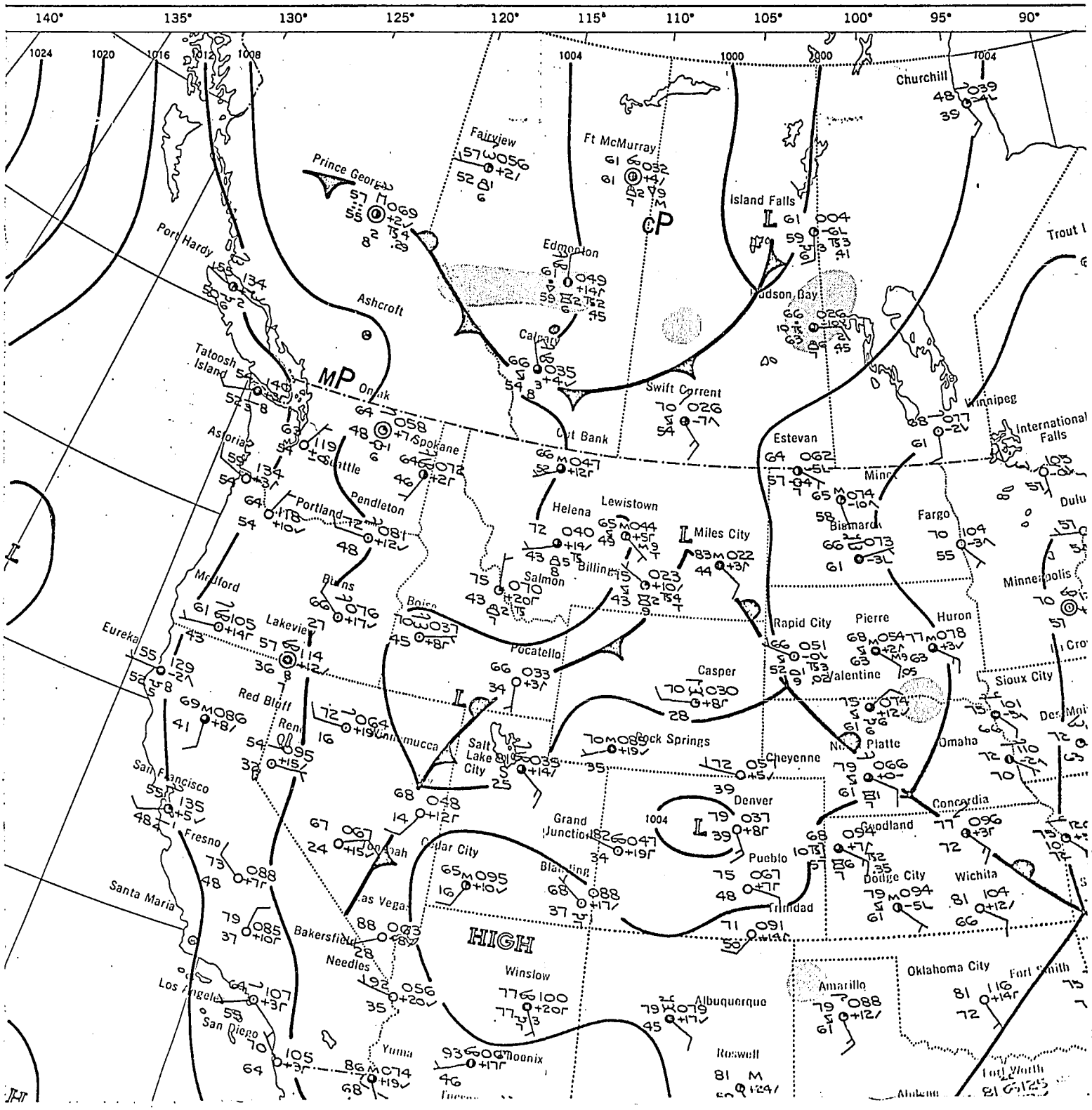

Figure A2a: Surface chart for 23:00 MST, July 7, 1966. (U.S. Dept. of Commerce Daily Weather Map).

REFERENCES

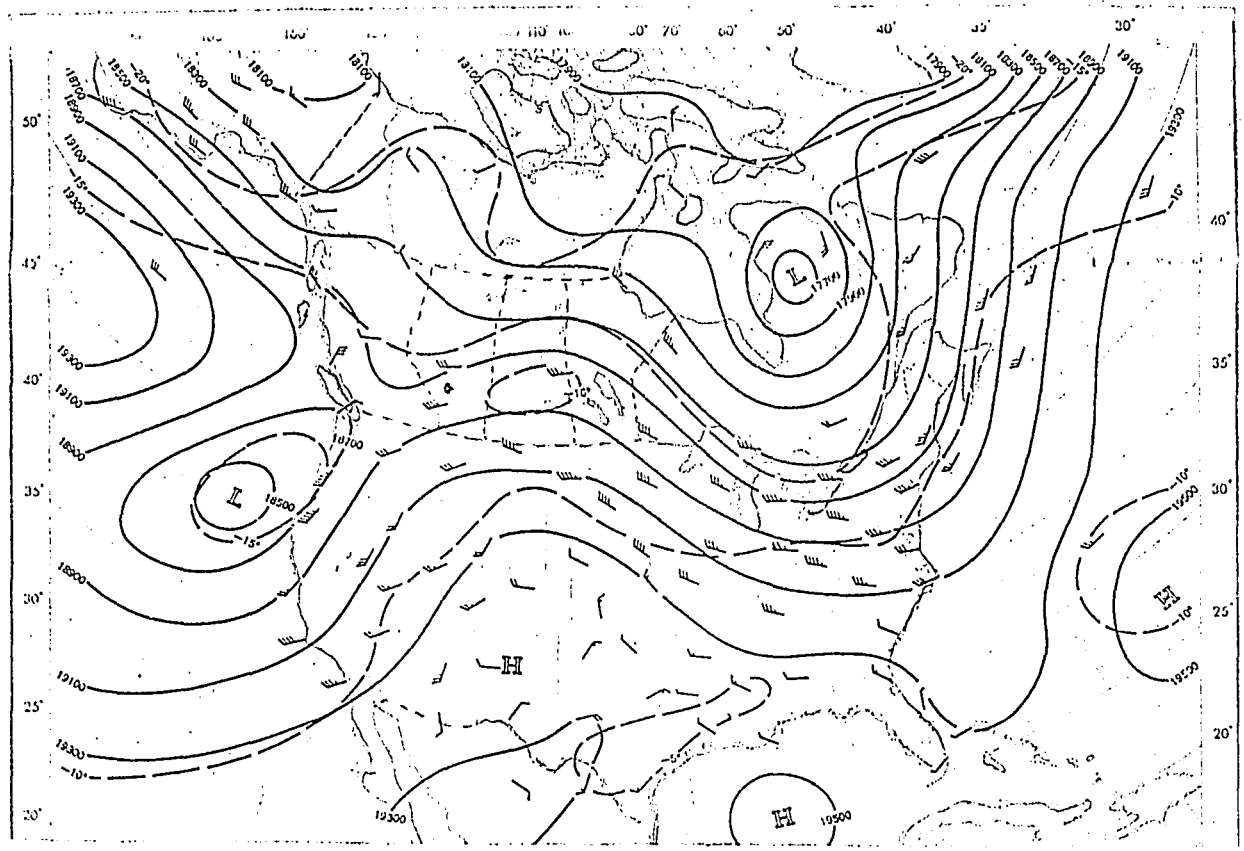

Figure A2b: 500 mb chart for 17:00 MST, July 7, 1966. (U. S. Dept. of Commerce Daily Weather Map)

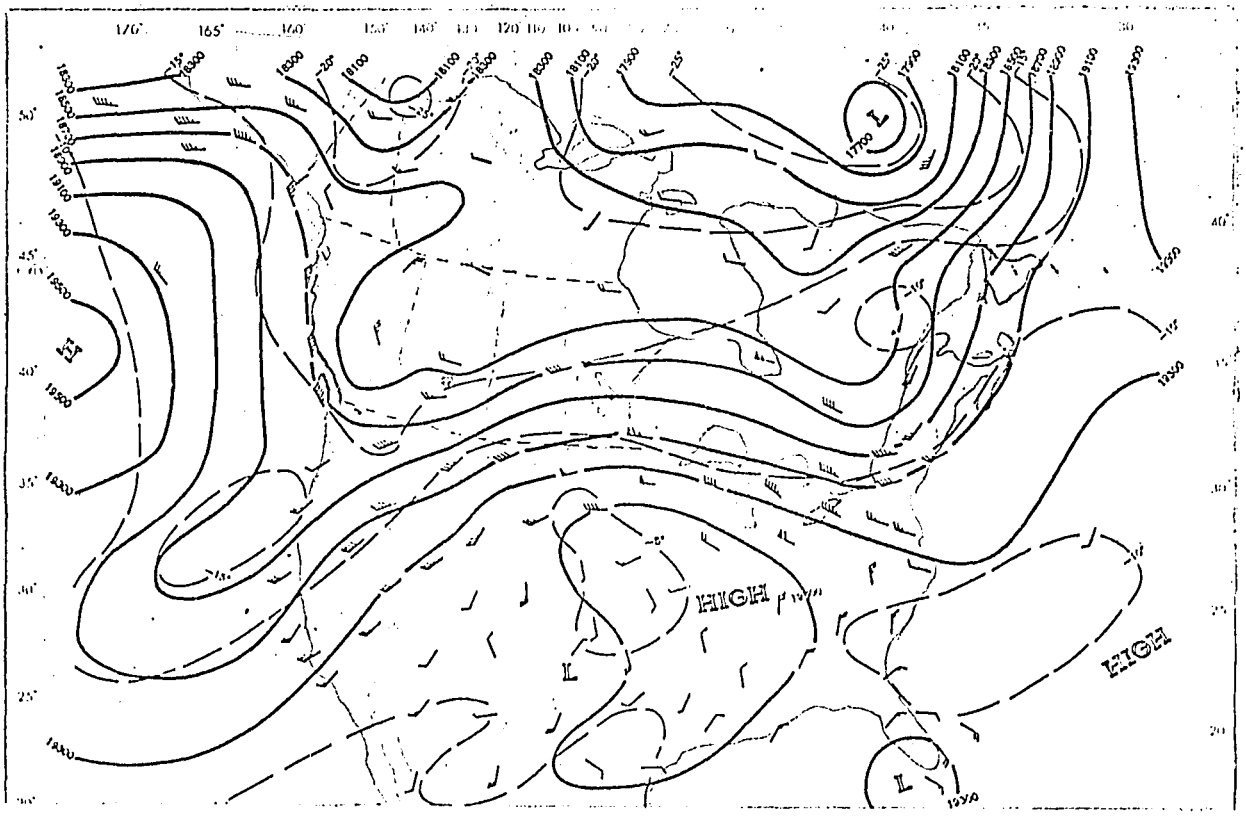

Figure A4b: 500 mb chart for 17:00 MST, July 10, 1966. (U. S. Dept of Commerce Daily Weather Map)

REFERENCES

American Society of Photogrammetry 1952: Manual of Photogrammetry, 2 ed. Wisconsin, George Banta Pub. Co.

Anderson, C.E. 1960: A Technique for Classifying Cumulus Clouds Based on Photogrammetry. Cumulus Dynamics, Pergamon Press, London, 50-59.

Atlas, D. and H.R. Byers 1963: Severe Local Storms in Retrospect. Meteor. Monographs, 5, 27, 242-247.

Austin, J.M. 1948: A Note on Cumulus Growth in a Nonsaturated Environment. J. Meteor., 5, 103-107.

Beebe, R.G. and F.C. Bates 1955: A Mechanism for Assisting in the Release of Convective Instability. Monthly Weather Rev., 83, 1-10.

Braham, R.R. Jr. 1952: The Water and Energy Budgets of the Thunderstorm and Their Relation to Thunderstorm Development. J. Meteor., 9, 227-242.

Brooks, C.E.P. and N. Carruthers 1953: Handbook of Statistical Methods in Meteorology. London, H.S.M.O.

Brown, R.A. 1966: Three Dimensional Growth Characteristics of an Orographic Thunderstorm System. SMRP Research Paper No. 61, University of Chicago.

Byers, H.R. and R.R. Braham 1949: The Thunderstorm. U.S. Department of Commerce, Washington.

Chisholm, A.J. 1966: Small Scale Radar Structure of Alberta Hailstorms. McGill University Thesis, Montreal.

Donaldson, R.J. Jr. 1961: Radar Reflectivity Profiles in Thunderstorms. J. Met., 18, 292-305.

Douglas, R.H. and W. Hitschfeld 1958: Studies of Alberta Hailstorms 1957. McGill University Stormy Weather Research Group Report MW 27.

East, T.W.R. 1957: An Inherent Precipitation Mechanism in Cumulus Clouds. Quart J.R. Meteor. Soc., 83, 61-76.

Fujita, T. 1963: Analytical Mesometeorology: A Review. Meteor. Monographs, 5, 27, 77-125.

_____ and H. Grandoso 1966: The Split of a Thunderstorm into Anticyclonic and Cyclonic Storms and Their Motion as Determined from Numerical Model Experiments. SMRP Research Paper No. 62, University of Chicago.

Glass, M. and T.N. Carlson 1963: The Growth Characteristics of Small Cumulus Clouds. J. Atmos. Sci., 20, 397-406.

Hamming, R.W. 1962: Numerical Methods for Scientists and Engineers. McGraw Hill Publishing Co., New York, 317.

Harrington, E.L. 1967: Depths and Temperatures of Continental Convective Clouds at the Time of Initial Precipitation Echo. Paper presented at the 268th National Meeting of the A.M.S., Washington.

Henry, C.D. 1964: High Radar Echoes from Alberta Thunderstorms. McGill University Thesis, Montreal, p. 11.

Hitschfeld, W. 1959: The Motion and Erosion of Convective Storms in Severe Vertical Wind Shear. J. Meteor., 17, 270-282.

Khrgian, A.K.L. et al 1961: Cloud Physics. Israel Program for Scientific Translations, Jerusalem, p. 166.

Malkus, J.S. 1954: Some Results of Trade Cumulus Cloud Investigation. J. Meteor., II, 220-237.

_____ 1960: Recent Developments in Studies of Penetrative Convection and an Application to Hurricane Cumulonimbus Towers. Cumulus Dynamics, Pergamon Press, New York, 64-84.

Mason, B.J. and R. Emig 1961: Calculations of the Ascent of a Saturated Parcel with Mixing. Quart. J. R. Meteor. Soc., 82, 212-222.

McBride, J.H. 1964: Small Scale Structure of Hail Swaths. McGill University Thesis, Montreal.

Newton, C.W. 1963: Dynamics of Severe Convective Storms. Meteor. Monographs, 5, 7, 33-58.

_____ 1966: Circulations in Large Sheared Cumulonimbus. Tellus, 18, 4, 699-713.

Ogura, Y. 1963a: A Review of Numerical Modelling Research on Small Scale Convection in the Atmosphere. Meteor. Monographs, 5, 27, 65-76.

_____ 1963b: The Evolution of a Moist Convective Element in a Shallow Conditionally Unstable Atmosphere. A Numerical Calculation, J. Atmos. Sci., 20, 407-423.

Pell, J. 1965: A Quantitative Hailstorm Study Using Broad Vertical Beam Radar. McGill University Thesis, Montreal.

_____ 1967: Continuity in Hail Production and Swaths: A Review. McGill Stormy Weather Group Report MW 49, Montreal, 27-53.

Proppe, H.W. 1965: The Influence of Wind Shear on Alberta Hail Storm Activity. McGill University Thesis, Montreal.

Priestley, C.H.B. 1954: Buoyant Motions and the Open Parcel. Meteor. Magazine, 83, 107-113.

Renick, J.H. 1966: Stereoscopic Cloud Photography and Measurements. McGill University Thesis, Montreal.

Saunders, P.M. 1957: The Thermodynamics of Saturated Air: A Contribution to the Classical Theory. Quart. J. R. Meteor. Soc., 83, 342-350.

_____ 1961: An Observational Study of Cumulus. J. Meteor., 18, 451-467.

_____ and F.C. Ronne 1962: A Comparison Between the Height of Cumulus Clouds and the Height of Radar Echoes Received From Them. J. Appl. Meteor., 1, 296 - 302.

Scorer, R.S. 1957: Experiments on Convection of Isolated Masses of Buoyant Fluid. J. Fluid Mech., 2, 583-592.

_____ and F.H. Ludlam 1953: The Bubble Theory of Penetrative Convection. Quart. J. Roy. Meteor. Soc., 79, 94-103.

_____ and C. Ronne 1956: Experiments with Convective Bubbles. Weather, 11, 151-154.

Simpson, J. 1967: An Experimental Approach to Cumulus Clouds and Hurricanes. Weather, 22, 3, 95-114.

Srivastava, R.C. 1964: A Model of Convection with Entrainment and Precipitation. McGill University Stormy Weather Research Group MW 38, Montreal.

_____ 1966: A Study of the Effect of Precipitation on Cumulus Dynamics. J. Atmos. Sci., 24, 1, 36-45.

Turner, J.S. 1963: Model Experiments Relating to Thermals with Increasing Buoyancy. Quart. J. Meteor. Soc., 89, 62-74.

Vali, G., 1967: Estimates of Initial Cloud Glaciation from Nucleation Experiments. Paper to be published in the Proceeding of the Conference on Severe Local Storms, St. Louis.